Politecnico di Milano

Department of Systems Engineering

School of Biomedical Engineering

Development and characterization of antibacterial treatments for titanium obtained by anodic spark deposition

Supervisors:

Prof. Roberto Chiesa

Prof. Matteo Santin

Ing. Cinzia Della Valle

Author:

Simone Panzuto

Matr. 740396

Academic Year: 2010-2011

Index

Summary

Introduction

The clinical practice based on biomaterials has undeniable advantages. Nevertheless, still remain some problems due to their use whose resolution is necessary to dull the failure rate and to reduce the social and health costs ensuing. Among the different causes of implants failure, the event of infections still represents the most serious and devastating complications that may involve biomaterial devices.

In the past decades, control of environmental and medical personnel contamination has been a principal target to cut down the rate of nosocomial and post-surgical infections. Although the introduction of strictly hygienic rules, the rising of antibiotic prophylaxis, the improvement of surgical techniques, the employ of materials more biocompatible have been reduced the infection rate, still remains a risk of infection with critical consequences.

Bacterial adhesion to biomaterials surface is the more critical aspect in the pathogenesis of infections and the initial step in microbial colonization [19]. Consequently, the most convenient way to contrast the bacterial infection is inhibit or avoid the microbial adhesion.

This purpose can be reached modifying the chemical-physical properties of implants surface or incorporating antibacterial agent such as antibiotics, antiseptics or inorganic agents with bactericidal properties (silver and gallium). Since in the last decades the antibiotiv resistance is dramatically increasing [27], is necessary develop new strategies to avoid the bacterial adhesion on biomaterials. The use of silver and gallium is promising [50, 57, 60].

Actually, titanium represents the first choice in applications involving hard tissues. Indeed it is widely used as implantable material in dental and orthopaedic field in order to restore impaired bone functions and simultaneously to promote the osteointegration. The anodic spark deposition technique (ASD) allows the modification of titanium oxide composition in order to optimizing the bone regeneration process and the osteointegration by favour at the same time a selective protein adhesion and the osteoblasts proliferation. Particularly, this electrochemical technique is able to produce oxide layers on titanium characterized by microporous morphology; at the same time, the ASD permits to embed in resulting oxide layer the chemical species present in electrolytic solution. Furthermore, since ASD technique directly performs a modification of the pre-existing oxide layer and don’t carry out a film deposition, it permits a better interaction between oxide and underlying substratum resulting in an increased mechanical stability of coating.

The aim of this work is to develop new biomimetic treatments on titanium characterized by antibacterial properties and an high osteointegrative potential.
Particularly, the purpose is to obtain antibacterial coatings using different antimicrobial agents such as silver and gallium which are widely known for their bactericidal properties. The technique chosen to reach this goal is the Anodic Spark Deposition (ASD) which allows to obtain homogeneous coatings characterized by a good stability.
The starting-point of this work is the ASD silicon-based osteointegrative treatment recently developed and patented by Politecnico di Milano [83, 84], which is nowadays used in clinical practice (dental field) with excellent results.

Materials and Methods

Materials

Samples preparation

All the samples were obtained from a plate of pure titanium grade 2; the samples used were either circular discs or rectangular plates. Before any treatment, they were cleaned by ultrasonic rinsing in acetone for 10 minutes and afterwards in water *Millipore* for further 10 minutes.

ASD treatments

The electrolytic solution (SUM) developed in the Politecnico di Milano thesis [84] (Na_2SiO_3*$2H_2O$ 0.03M, β-GP 0.1M, $C_4H_6CaO_4$*H_2O 0.3M, NaOH 0.036M) was enriched with silver nitrate or silver nanoparticles or gallium nitrate in order to embed these antibacterial agents in the resulting TiO_2 layer. To avoid the precipitation of silver and gallium salts, in some solutions was also added a chelating agent (L-cysteine or Oxalic Acid or EDTA). The resulting solutions were used to carry out the ASD treatments on the samples; per each solution, were used different process parameter (current intensity and final voltage) in order to direct the resulting morphology. All the treatments were performed in galvano-static conditions.
Samples obtained by the proper silicon-based ASD treatment [8] (ASD treatment with SUM solution and following alkali etching in NaOH) were used as material of control (label SUM Na).
After a preliminary screening, the treatment chosen for the characterization were: SUM AgNPs, SUM NITAG CIST, SUM NITGAL CIST and SUM NITGAL OSS. The labels refer to the antimicrobial agent and the chelant agent added.

Methods

Chemico-physical characterization

SEM: all the samples were analyzed by ZEISS-EVO 50 EP or Cambridge – Stereoscan 360 to assess the surface morphology.
EDS: the EDS analysis carried out on 500X and, in some cases, on 5kX magnification (Oxford, Inca energy 200) that correspond to micrometric surface (170μm x 230μm and 17μm x 23μm respectively) have permitted to assess the qualitative chemical composition until 2-3μm of oxide thickness.
XRD: to assess the crystallographic phases of oxide obtained were carried out

analysis with XRD diffractometer (Philips PW 1710) set to 40KV of voltage and 40mA of current intensity.

Profilometry: to study the surfaces roughness 3 measures per each sample were performed with laser profilometer (UBM Microfocus, 5600)

Contact angle: for each surface were performed 3 different water drop depositions at room temperature. The measurements were carried out by an optical device (Dataphysics Instruments Mod. OCA 15 plus) and a related software (32-bit software SCA20.

GD-OES: all the samples were analyzed by Horiba Jobin-Yvon RF-GDOES until a superficial depth of 20 μm.

ICP-OES: to assess the release of silver and silicon in PBS at 37°C from silver-containing samples and material control surfaces after 6h, 24h, 5days and 7days.

TiO_2 delamination tests: 3-point flexure tests with a flexion angle of 30°were carried out on rectangular plates samples previously anodized.

Biological characterization

Sample sterilization: the samples were disinfected three times per each side with 1 ml of pure ethanol and after sterilized with UV irradiation.

Cell types: the biocompatibility of all the samples was evaluated on 3T3 murine fibroblasts and Saos2 osteoblast-like cells from human osteosarcoma.

HPI staining: the viability and proliferation of 3T3 fibroblasts were assess after 24h and 48h of direct culture in samples with HPI staining. The response of Saos2 osteoblasts was evaluated after 48h and 72h of direct culture on all the different samples.

SEM: ZEISS-EVO LS-15 was used to evaluate Saos2 morphology and adhesion on all the surfaces after 48h and 72h of cell culture.

Phalloidin staining: Phalloidin-Rhodamine staining was used to evaluate Saos2 osteoblasts spreading on all the surfaces after 48 h and 72 h of culture

Results and Discussion

After SEM imaging, SUM Na has shown a more uniform morphology both in terms of distribution and average size of the pores in comparison to all the other surfaces. Contrary, SUM AgNPs SUM NITAG CIST and SUM NITGAL CIST showed zones with large pores emerging from an underlying substrate that was characterised by pores of smaller diameter. The EDS analyses show that the antibacterial species present in electrolytic solution are embedded in all the surfaces except for SUM NITAG CIST. However, the GDOES analysis confirms the presence of silver and gallium on all the surfaces.

The XRD analysis showed that on all the surfaces is present the anatase form of titanium oxide and, in the samples treated with cisteine, the anatase peaks are 2-fold higher than the titanium peaks. Even if the samples with antimicrobial purpose aren't post-treated with alkali etching, they show a roughness values near the minimal threshold perceptible from osteoblasts [91]. Among the coating with antibacterial purpose, the samples treated with cysteine have shown a roughness close to SUM Na value. All the surfaces

are hydrophilic since the static contact angle detected is under 90°. Hydrophilic surfaces enhance interactions with biological fluids, cells and tissues [95] and have a better resistance to bacterial adhesion [30].

All the coatings adhere perfectly on the substrates since there is no detectable oxide layer delaminations after the imposition of 30° flexion even if the oxide layers have a thickness of few micrometers. Particularly, the GDOES analysis has demonstrates that the cysteine present in electrolytic solution causes an increase in the oxide thickness resulting by ASD whereas the oxalic acid has a strong inhibiting action on its growth. Indeed both the SUM NITAG CIST and SUM NITGAL CIST samples have the thicker oxide in comparison with all the other samples.

Furthermore, the GDOES analysis has permitted to assess the concentration of antimicrobial agents in function of the depth in the oxide layers embedded with gallium and silver. Gallium is incorporating in the inner oxide matrix and not only in the superficial layer of SUM NITGAL CIST and SUM NITGAL OSS while the amount of silver in SUM AgNPs and SUM NITAG CIST is concentrated in the first 20nm of depth.

SUM NITGAL OSS and SUM AgNPs samples show the higher antimicrobial concentration in their oxide layers.

The silver release assessed by ICP confirms the results of GDOES: the release from both the silver-containing samples remains at similar levels at later experimental points but the release from SUM NITAG CIST is 5-fold less than SUM AgNPS. However, the amount of silver present on both the silver-containing surfaces and the amount of release are in the range recognised as sufficient to produce an antibacterial effect [54, 99].

The *in vitro* tests have shown that no-one of the analysed surfaces has cytotoxic effect neither on 3T3 fibroblasts neither on Saos2 osteoblasts. The presence of silver and gallium on the surfaces and their release are hence under the cytotoxic detection limit.

The osteoblasts viability rate on all the surfaces is around 90% at the both time points. Moreover, after 72 hours of osteoblasts culture, while SUM Na showed a cell proliferation rate slightly higher than the cell control (tissue culture plate), all the other samples have shown an increased cell proliferation in comparison with both cells in the control plate and on the SUM Na surface. In the case of SUM AgNPS and SUM NITAG CIST samples the proliferation increment is even around 50%-60% in comparison to the material control SUM Na rate.

Generally, in these surfaces the size of the pores is not uniform and the structures embedding the larger pores are deeper. Hence, the edge of the larger pores emerges more markedly from the underlying layer thus offering anchorage sites to the osteoblasts. Indeed, analysing the SEM micrographs of the osteoblasts cultures on SUM AgNPS, SUM NITAG CIST and SUM NITGAL CIST surfaces, it is clearly visible that the cells adhere strongly onto the surface by projecting their membranes towards and around the doughnut-like structures delimiting the pores. Rhodamine-phalloidin staining clearly show that the osteoblasts

cytoscheletons bind the edge of pores and, especially after 72 hours of culture on SUM AgNPS and SUM NITGAL CIST samples, cell-material and cell-to-cell interactions are established through filopodia and well defined focal points.

Conclusions

SUM AgNPs, SUM NITAG CIST and SUM NITGAL CIST samples have shown an increased osteointegration potential in comparison with SUM Na. Furthermore, the chemical characterizations have showed that on their surface are present the antimicrobial agents (Ag or Ga). The silicon-based ASD treatment modified with antibacterial agents has in conclusion allowed the production of titanium coatings characterized by enhanced osteintegrative potential and potential antimicrobial properties. However, microbiological tests performed with the bacterial species more relevant to the septic loosening of dental and orthopaedic implants will be necessary to confirm the antibacterial potential of the coatings developed in this work.

Sommario

La pratica clinica basata sui biomateriali ha dei vantaggi innegabili, tuttavia ad oggi resta la possibilita' di fallimento. Tra le diverse cause che comportano il fallimento di un impianto, l'evento di infezioni associate ai biomateriali e' ancora motivo di gravi e devastanti complicazioni.

Pertanto, negli ultimi decenni, il controllo della contaminazione ambientale e del personale medico è stato l'obiettivo principale e il mezzo più efficace per ridurre il tasso di infezioni nosocomiali e post-chirurgiche. Sebbene l'introduzione di norme igieniche rigorose, l'utilizzo di una profilassi antibiotica piu' efficace e il miglioramento delle tecniche chirurgiche abbiano permesso una notevole riduzione del tasso di infezione, l'adesione batterica alla superficie dei biomateriali rimane l'aspetto più critico nella patogenesi delle infezioni e il primo step nella colonizzazione microbica [19].

La strategia più efficacie per contrastare l'infezione batterica è quindi inibire o evitare l'adesione microbica sui biomateriali. Tale obiettivo può essere raggiunto modificando la proprietà chimico-fisiche della superficie degli impianti o incorporando agenti antibatterici come antibiotici, antisettici o agenti inorganici con proprietà battericide (ad esempio argento e gallio).

Tuttavia negli ultimi decenni la resistenza batterica agli antibiotici sta aumentando drasticamente [27] e pertanto è necessario sviluppare strategie innovative e piu' efficaci per impedire l'adesione batterica sui biomateriali. In tale direzione l'uso di argento e di gallio è promettente [50, 57, 60].

Alla luce della enorme popolazione di pazienti con protesi ortopediche, anche un rischio di infezione attualmente basso, stimato nel range di 0,5-5% per le protesi articolari, deve essere considerato molto rilevante per le sue gravi conseguenze [15].

Procedure di semplice pulizia chirirgica o la ritenzione della protesi con agenti chemioterapici o antibiotici sono trattamenti che non sono sempre efficaci sulle infezioni già in atto. A volte la rimozione della protesi e la sua sostituzione rappresentano l'unica opzione percorribile per sradicare definitivamente infezioni gravi. Questi drastici interventi hanno tuttavia ovvie implicazioni sulla psicologia dei pazienti e in termini di costi sanitari e sociali per la prolungata degenza ospedaliera che comportano (un singolo episodio di protesi infetta da rimuovere e sostituire costa in media $ 50.000 [16]).

Il titanio è considerato un biomateriale d'elezione nel campo delle applicazioni che coinvolgono i tessuti duri. Infatti viene ampiamente utilizzato come materiale impiantabile in ambito dentale ed ortopedico per ristabilire funzionalità ossee compromesse e nel contempo favorire l'osteointegrazione.

La tecnica denominata Anodic Spark Deposition (ASD) permette la modifica della composizione di ossido di titanio al fine di ottimizzare il processo di

rigenerazione ossea e l'osteointegrazione favorendo una adesione selettiva delle proteine e la proliferazione degli osteoblasti. In particolare, questa tecnica elettrochimica è in grado di produrre strati di ossido di titanio caratterizzati da morfologia microporosa e al contempo permette di inglobare al loro interno le specie chimiche presenti nella soluzione elettrolitica. Inoltre, poiché la tecnica ASD esegue direttamente una modifica del preesistente strato di ossido senza che ciò comporti una diretta deposizione di film, essa permette una migliore interazione tra
l'ossido e il substrato sottostante con una conseguente maggiore stabilità meccanica del rivestimento.
Lo scopo di questo lavoro è realizzare nuovi trattamenti biomimetici su titanio caratterizzati da proprietà antibatteriche e da un alto potenziale osteointegrativo.
In particolare, lo scopo è quello di ottenere rivestimenti antibatterici
In particolare, lo scopo è quello di ottenere rivestimenti antibatterici utilizza ndo diversiagenti antimicrobici come l'argento e gallio, che sono ampiamente conosciuti per le loro proprietà battericide.
La tecnica scelta per raggiungere questo obiettivo è la Anodic Spark Deposition (ASD) in quanto permette di ottenere rivestimenti omogenei e caratterizzati da una buona stabilità.
Il punto di partenza di questo lavoro è un trattamento ASD a base di silicio rentemente sviluppato e brevettato dal Politecnico di Milano [83, 84], che è oggi utilizzato nella pratica clinica (settore dentale) con ottimi risultati.

Materiali e Metodi

Materiali

Preparazione dei campioni

Tutti i campioni sono stati ottenuti da una piastra di titanio puro di grado 2; sono stati utilizzati principalmente dischetti circolari e lamine rettangolari. Prima di qualsiasi trattamento, tutti i campioni sono stati lavati con ultrasuoni per di 10 minuti in acetone e per ulteriori 10 minuti in acqua *Millipore*.

Trattamenti ASD

La soluzione elettrolitica (SUM) sviluppata nella tesi Politecnico di Milano [8] (Na2SiO3 * 2H2O 0.03M, b-GP 0,1 M, 0,3 M C4H6CaO4 * H2O, NaOH 0.036M) è stata arricchita con tre diversi agenti antibatterici, nitrato d'argento o nanoparticelle d'argento o nitrato di gallio, al fine di incorporarli nello strato di TiO2 risultante. Per evitare la precipitazione dei sali d'argento e di gallio, in alcune soluzioni è stato anche aggiunto un agente chelante (L-cisteina e acido ossalico o EDTA). Le soluzioni ottenute sono state utilizzate per effettuare i trattamenti ASD sui campioni; per ogni soluzione sono stati utilizzati diversi parametri di processo (intensità di corrente e tensione finale) al fine di modificare la morfologia risultante. Tutti i trattamenti sono stati effettuati in condizioni galvano-statiche. I campioni ottenuti mediante il trattamento ASD a base di silicio originale [8] (ASD trattamento con soluzione di SUM e seguenti etching chimico in NaOH) sono stati utilizzati come materiale di controllo (etichetta SUM Na). Dopo uno screening

preliminare, i trattamenti scelti per la caratterizzazione sono stati: SUM AgNPs, SUM NITAG CIST, SUM NITGAL CIST e SUM NITGAL OSS. Le etichette si riferiscono all'agente antimicrobico e all'agente chelante aggiunto in soluzione.

Metodi

Caratterizzazione chimico-fisica

SEM: tutti i campioni sono stati analizzati mediante ZEISS-50 EP EVO o Cambridge - Stereoscan 360 per valutare la morfologia della superficie.
EDS: l'analisi EDS e' stata effettuata a ingrandimento 500X e, in alcuni casi, a ingrandimento 5kX (Oxford, Inca energia 200) che corrispondono a porzioni superficiali micrometriche (170mm x 230mm e 17 mm x 23mm rispettivamente). Tale analisi ha permesso di valutare la composizione qualitativo-chimica fino a 2-3mm di spessore dello strato di ossido.
XRD: per valutare le fasi cristallografiche dell' ossido ottenuto sono state effettuate analisi con diffrattometro XRD (Philips PW 1710) a 40KV di tensione e ad un'intensità di corrente di 40 mA.
Profilometria: 3 misure per ogni campione con profilometro laser (UBM Microfocus,5600)
Angolo di contatto: per ogni superficie sono state effettuate 3 diverse deposizioni statiche di una goccia d'acqua a temperatura ambiente. Le misurazioni sono state effettuate da un dispositivo ottico (Dataphysics Mod Instruments OCA 15 più.) e dal relativo software (32-bit SCA20software).
GD-OES: tutti i campioni sono stati analizzati da Horiba Jobin-Yvon RF-GDOES fino a 20 μm di profondita'.
ICP-OES: al fine di valutare il rilascio di argento e silicio in PBS a 37 ° C dalle superfici dei campioni contenenti argento a dal materiale di controllo dopo un lasso di tempo di 6 ore, 24 ore, 5 giorni e 7 giorni.
Test di adesione dell'ossido: prove di flessione a 3-punti sono state effettuate su campioni di forma rettangolare precedentemente anodizzati. E' stata applicata una flessione di 30 °.

Caratterizzazione biologica

Sterilizzazione dei campioni: i campioni sono stati disinfettati tre volte su ogni lato con 1 ml di etanolo e successivamente sono stati sterilizzati con raggi UV.
Cellule: la biocompatibilità di tutti i campioni è stata valutata su fibroblasti murini 3T3 e osteoblasti Saos2 da osteosarcoma umano.
HPI Assay: la viabilita' e la proliferazione dei fibroblasti 3T3 sono state valutare con staining HPI dopo 24 e 48 ore di cultura diretta eseguita sui campioni. La risposta degli osteoblasti Saos2 è stata valutata dopo 48 e 72 ore di cultura diretta su tutti i diversi campioni.
SEM: ZEISS EVO-LS-15 è stato utilizzato per valutare la morfologia e l'adesione degli osteoblasti Saos2 dopo 48 e 72 ore di coltura cellulare su tutte le superfici.
Phalloidin Assay: lo staining con falloidina-rodamina è stato utilizzato per valutare lo spreading di osteoblasti Saos2 su tutte le superfici dopo 48 e 72 ore di cultura.

Risultati e discussione

Dall'analisi delle immagini al SEM, SUM Na ha mostrato una morfologia più uniforme sia in termini di distribuzione che di dimensione media dei pori rispetto a tutte le altre superfici. Al contrario, SUM AgNPs, SUM NITAG CIST e SUM NITGAL CIST hanno mostrato possedere zone con pori di diametro maggiore che crescono al di sopra di zone con pori piu' piccoli. Le analisi EDS mostrano che la specie antibatterica presente in soluzione elettrolitica e' stata inglobata in tutte le superfici tranne che nei campioni SUM NITAG CIST. Comunque, l'analisi GDOES conferma la presenza di argento e di gallio su tutte le superfici.

L'analisi XRD ha mostrato che su tutte le superfici è presente la forma cristallografica dell'anatasio e che nei campioni trattati con cisteina, i picchi di anatasio sono 2 volte più alti rispetto a quelli di titanio. Anche se i campioni con agenti antibatterici non sono post-trattati con etching chimico essi mostrano valori di rugosità vicini alla soglia minima percepibile dagli osteoblasti [91]. Tra i campioni dotati di rivestimento antibatterico, quelli trattati con cisteina hanno mostrato una rugosità piu' vicina al valore di SUM Na. Tutte le superfici sono idrofile in quanto l'angolo di contatto statico rilevato è inferiore ai 90 °. Le superfici idrofile migliorano le interazioni con i fluidi biologici, le cellule e i tessuti [95] e diminuiscono l'adesione dei batteri alla superficie stessa. [30]. Tutti i rivestimenti aderiscono perfettamente al substrato poiché, imponendo una flessione di 30°, non vi sono rilevabili delaminazioni dello strato di ossido, anche se gli strati in questione hanno uno spessore di pochi micrometri. In particolare, l'analisi GDOES dimostra che la cisteina presente nella soluzione elettrolitica provoca un aumento dello spessore di ossido in seguito ad ASD, mentre l'acido ossalico ha una forte azione inibente sulla sua crescita. Infatti sia i campioni SUM NITAG CIST che i campioni SUM NITGAL CIST presentano uno spessore di ossido maggiore rispetto agli altri campioni. Inoltre, l'analisi GDOES ha permesso di valutare la concentrazione di agenti antimicrobici in funzione della profondità degli strati di ossido in cui sono incorporati gallio e argento. Il gallio è incorporato nella matrice di ossido più interna e non solo nello strato superficiale dei campioni SUM NITGAL CIST e SUM NITGAL OSS, mentre la quantità di argento in SUM AgNPs e SUM NITAG CIST è concentrata nei primi 20 nm di spessore.

I campioni di SUM NITGAL OSS e SUM AgNPs mostrano una concentrazione di agenti antimicrobici più elevata nei rispettivi strati di ossido rispetto a SUM NITGAL CIST e SUM NITAG CIST.

Il rilascio di argento valutato mediante ICP conferma i risultati del GDOES: il rilascio, da entrambi i campioni contenenti argento, rimane a livelli similari a tutti i tempi punti sperimentali ma il rilascio dal campione CIST SUM NITAG è 5 volte inferiore di quello che si ha nel campione SUM AgNPs. Tuttavia, la quantità di argento presente su entrambe le superfici e quella che viene rilasciata sono comunque comprese nel

range ritenuto sufficiente a produrre un effetto antibatterico [54,99].
I test in vitro hanno dimostrato che nessuna delle superfici analizzate ha un effetto citotossico né sui fibroblasti 3T3 né sugli osteoblasti Saos2. La presenza di argento e di gallio sulle superfici e il loro rilascio sono quindi sotto il limite rilevazione citotossica.
Il tasso di vitalità degli osteoblasti su tutte le superfici è di circa il 90% sia dopo 48h che dopo 72h di coltura.
In particolar modo, dopo 72 ore di coltura con osteoblasti, il campione SUM Na ha mostrato un tasso di proliferazione delle cellule leggermente superiore al controllo (piastra per coltura cellulari), mentre tutti gli altri campioni hanno mostrato un marcato aumento della proliferazione cellulare sia in confronto al controllo cellulare sia in confronto a SUM Na. Nel caso di SUM AgNPS e dei campioni SUM NITAG CIST il tasso di incremento della proliferazione è circa il 50% -60% superiore a quello del materiale di controllo (SUM Na).
Generalmente in queste superfici la dimensione dei pori non è uniforme e le strutture che incorporano i pori più grandi sono più spesse. Quindi, il bordo dei pori più grandi emerge più marcatamente dallo
strato sottostante offrendo migliori siti ancoraggio agli osteoblasti.
Infatti, analizzando le micrografie SEM delle colture cellulari con osteoblasti su SUM AgNPs, SUM NITAG CIST e SUM NITGAL CIST, è chiaramente visibile che le cellule aderiscono con forza sulla superficie proiettando le loro membrane verso e attorno alle strutture a forma di ciambella che delimitano i pori. Lo staining con rodamina-falloidina ha mostrato chiaramente che i citoscheletri degli osteoblasti legano il bordo dei pori e, soprattutto dopo 72 ore di cultura sui campioni SUM AgNPS e SUM NITGAL CIST, sono stabilite interazioni cellula-materiale e cellula-cellula attraverso filopodia e focal points.

Conclusioni

SUM AgNPs, SUM NITAG CIST e SUM NITGAL OSS hanno mostrato un incremento nel potenziale osteointegrativo rispetto a SUM Na. Inoltre la caratterizzazione chimica ha dimostrato che sulle loro superfici sono effettivamente presenti gli agenti antimicrobici desiderati (Ag e Ga). Il trattamento ASD a base di silicio modificato con agenti antibatterici ha in conclusione consentito la produzione di rivestimenti su titanio caratterizzati da miglior capacita' osteointegrative .. e potenziali proprieta' antibatteriche. Tuttavia, test microbiologici da eseguire con le specie batteriche piu' rilevanti nella mobilitazione settica di impianti dentali e ortopedici.

1 Introduction

Scientific research on biomaterials has greatly contributed to the development of biomedical devices and implants that are fundamental in the most modern and effective healing techniques. In recent years, the number of applications of biomaterials has increased significantly the therapeutic efficacy has led to the restitution of compromised function, often essential for life, to a large number of patients.

Therefore biomaterials are one of the most important sectors of biomedical engineering in terms of health utility and economic interests. Biomaterials products had a market size of $25.5 billion in 2008; the biomaterial device market size was $115.4 billion in the same year and is expected to reach $252.7 billion in 2014. This massive revenue potential highlights the immense opportunity in the market. In the next years, the biomaterials market is expected to grow at a Compound Annual Growth Rate (CAGR) of 15% [1]. The U.S. and Europe hold a major share of the global biomaterials market. The U.S. is the dominant market for biomaterials, standing at $10.8 billion in 2008. The market is estimated to grow at a CAGR of 13.6% (2009-2014) to reach $22.8 billion in 2014. The European biomaterial products market is expected to grow to $17.67 billion in 2014 from $7.89 billion in 2008 at a CAGR of 14.6% from 2009 to 2014 [2].

Actually there are different types of biomaterials that can be used to produce medical devices: metals, polymers, ceramics and composites, natural or synthetic, biodegradable or not. A range of needs and requirements linked to an evaluation of advantages and disadvantages of the use of a specific material affects the choice of biomaterial related to the specific application (Table 1.1).

With the increase in life expectancy and with the aim of a better life quality for mature people, it is widely increased the prosthetic orthopaedic intervention use. The number of implants used for spinal, hip, knee and dental replacements are extremely high. Human joints suffer from degenerative diseases such as arthritis leading to pain or loss in function. The degenerative diseases lead to degradation of the mechanical properties of the bone due

to excessive loading or absence of normal biological self-healing process. In USA, it has been estimated that 90% of population over the age of 40 suffers from these kinds of degenerative diseases and the aged people population has increased tremendously in recent past and it is estimated there will be a seven times increase (from 4.9 million which was in 2002 to 39.7 million by 2010) [3]. Musculoskeletal disorders are most widespread human health problem, which is costing around 254 billion dollars to the society [4]. Artificial biomaterials are the solutions for these problems, as surgical implantation of these artificial biomaterials of appropriate shapes help in restoring the function of the otherwise functionally compromised structures. Actually there is a tremendous increase in the demand for the new long lasting implants, as the data collected on total joint replacements surgery it is estimated that by the end of 2030, the number of total hip replacements in the USA will rise by 174% (572,000 procedures) and total knee arthoplasties is projected to grow by 673% from the present rate (3.48 million procedures) [5]. The reason for joint replacements is attributed to diseases such as osteoporosis (weakening of the bones), osteoarthritis (inflammation in the bone joints) and trauma.

Materials	Advantages	Disadvantages	Examples
Polymers (nylon, silicone rubber, polyester, polytetrafuoroethylene, etc)	Resilient Easy to fabricate	Not strong Deforms with time May degrade	Sutures, blood vessels other soft tissues, sutures, hip socket, ear, nose
Metals (Ti and its alloys, Co–Cr alloys, Au, Ag stainless steels, etc.)	Strong, tough ductile	May corrode Dense Difficult to make	Joint replacements, dental root implants, pacer and suture wires, bone plates and screws
Ceramics (alumina zirconia, calcium phosphates including hydroxyapatite, carbon)	Very bio-compatible	Brittle Not resilient Weak in tension	Dental and orthopedic implants
Composites (carbon–carbon, wire- or fiber- reinforced bone cement)	Strong, tailor-made	Difficult to make	Bone cement, Dental resin

Table 1.1: Class of materials used in body [6].

The materials used for orthopaedic implants especially for load bearing applications should possess excellent biocompatibility, superior corrosion resistance in body environment, excellent combination of high strength and low modulus, high fatigue and wear resistance, high ductility and be without cytotoxicity [7]. While several materials are currently in use as biomaterials, the pure titanium and the titanium alloys are considered the first choice for

the majority of applications involving hard tissues especially due to the high mechanical properties, the weightlessness and the excellent corrosion resistance.

1.1 Introduction to biomaterials

A biomaterial is a substance that has been engineered to take a form which, alone or as part of a complex system, is used to direct, by control of interactions with components of living systems, the course of any therapeutic or diagnostic procedure, in human (or veterinary) medicine [8].

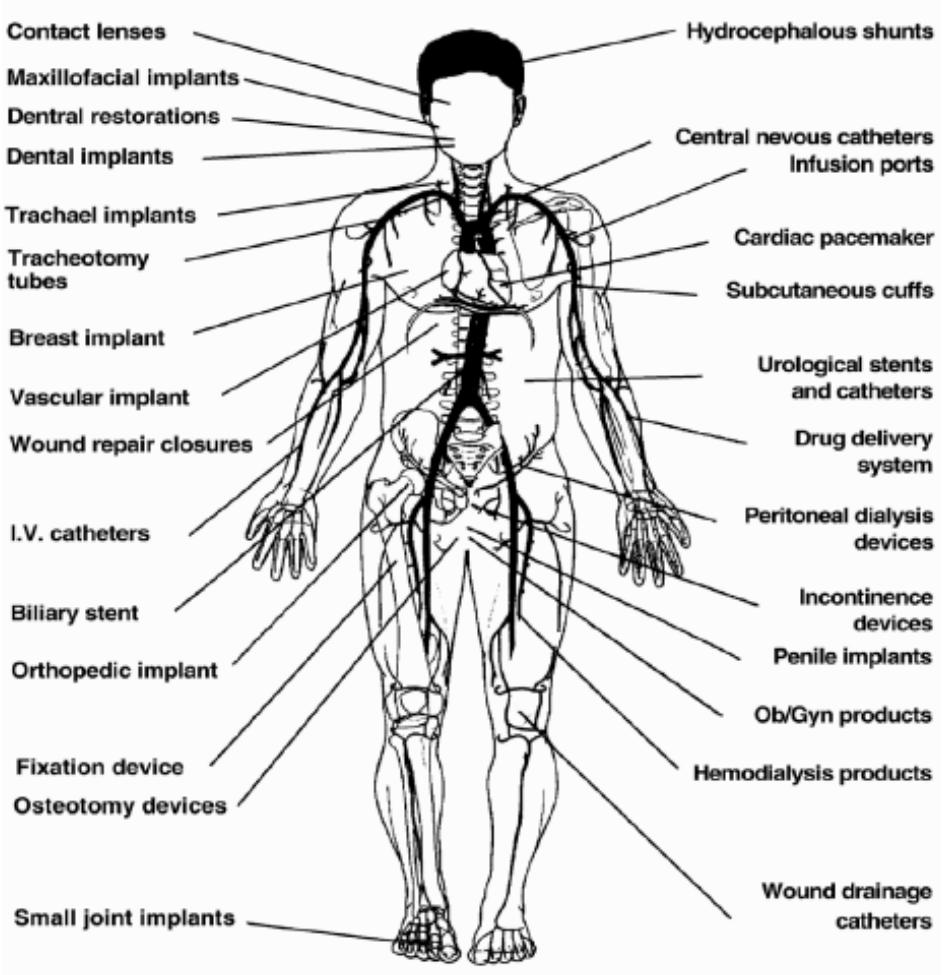

Fig. 1.1: Illustrations of various implants and devices used to replace or enhance the function of diseased or missing tissues and organs [6].

Generally biomaterials are used to develop system and biomedical device that allow the replacement of human organs or tissues affected by disease, injury and aging. Actually clinical practice relies on a large number of applications that use biomaterials and, in many cases, represent the most advantageous therapeutic response (Fig 1.1).
The most important factor that distinguishes a biomaterial from any other material is its ability to exist in contact with tissues of the human body without causing an unacceptable degree of harm to that body. Compatibility with the biological environment is a necessary condition for a proper use of implantable devices manufactured with biomaterials. Such compatibility is expressed mainly in three issues:

1. **Morphological compatibility**: dimensional interface, shape, mass.
2. **Functional compatibility**: function performed by the implant compared to the required role.
3. **Biological compatibility or biocompatibility**: chemical and biological aspects that can cause harmful modifications to the natural tissue and to the materials of which the implant consists [9].

The compatibility depends on a set of properties related to the interaction between device and body; interaction always exists because the device must perform its function within a living organism.
Unfortunately, the compatibility issues are often unknown quantitatively, because of the interaction between the device and living organism is a dynamic phenomena since the body, a biological structure, evolves and changes with time. It is possible only to know the initial conditions of the interactive dynamic phenomena, such that the conditions that occur at the time of implantation. It is extremely hard to predict the evolution of interface conditions if is not available an adequate clinical experience that allows the implementation of probabilistic model.

1.1.1 Biological reactions to biomaterials implants

The biocompatibility, that all biomaterials should have, is essential to direct positively the reaction process of the human body to the implant. Such reaction is always present when a biomaterial is implanted in a living tissue and appears as a series of responses that are initiated by the implantation procedure, as well as by the presence of the same biomaterial. The effects of host material implantation can be mainly distinguished in:

1. **Effects on tissue caused by implant**:
    a. Local events: blood interactions (coagulation, hemolysis, leucocytes adhesion and activation), cytotoxicity, inflammation, infection;
    b. Systemic events: embolism, accumulation of released materials in far target organs, systemic toxicity, immune reactions and allergic sensitization.
2. **Effects on implant caused by tissue:**
    a. Physics and mechanics: wear, fatigue, corrosion, surface cracking, degradation, dissolution;
    b. Biological: adsorption of substances by tissue, enzymatic degradation, calcification;
    c. Mixed: environmental stress cracking [10].

After implantation, a series of events occurs near the implant site. The same process of implantation of a biomaterial results in injury to tissue or organs and to the subsequent perturbation of homeostatic mechanisms that lead to the cellular cascades of wound healing. The response to injury depends on multiple factors including the extent of injury, the loss of basement membrane structures, blood-material interactions, provisional matrix formation, the extent or degree of cellular necrosis and the extent of the inflammatory response that involves the activation of several types of humoral components and cells. This first acute inflammation lasts until few days and consists in exudation of fluids and plasmatic proteins (oedema), poly-morphonuclear leucocytes migration toward the injury site, activation of mast cells. Their activity is accompanied by the production of chemiotactic agents stimulating tissue cells such as the fibroblasts, which modulate the growth of the new tissue. The resorption and remodelling of the clot into a new matrix

follow the first healing response and also trigger the angiogenesis, which is stimulated by many factors such as enzymes and chemio-attractans. This multi-step process that normally leads to a correct healing may be disrupted by the foreign body reaction involving factors such as necrosis, chronic inflammation, tissue perfusion, infection, mechanical stress, and oedema. Chronic inflammation remains circumscribed to the implant site and it causes migration of monocytes, macrophages and lymphocytes. Foreign body reaction is the key problem occurring during the wound healing process, which follows the device implantation, and a normal wound healing process cannot always resolve it. Foreign body reaction implies proliferation of fibroblasts and endothelial cells and, in a second time, the giant cells formation (Fig 1.2). His continuous presence in conjunction with the friction between the implant and the healing tissue can interfere with the physiological repairing process leading to the formation of a fibrotic capsule surrounding the implant. A fibrotic capsule surrounding the implant has to be minimised especially around bone implants because it interferes with the perfect integration between implant and live tissue: the next structural discontinuity could impair the mechanical performances of the implant.

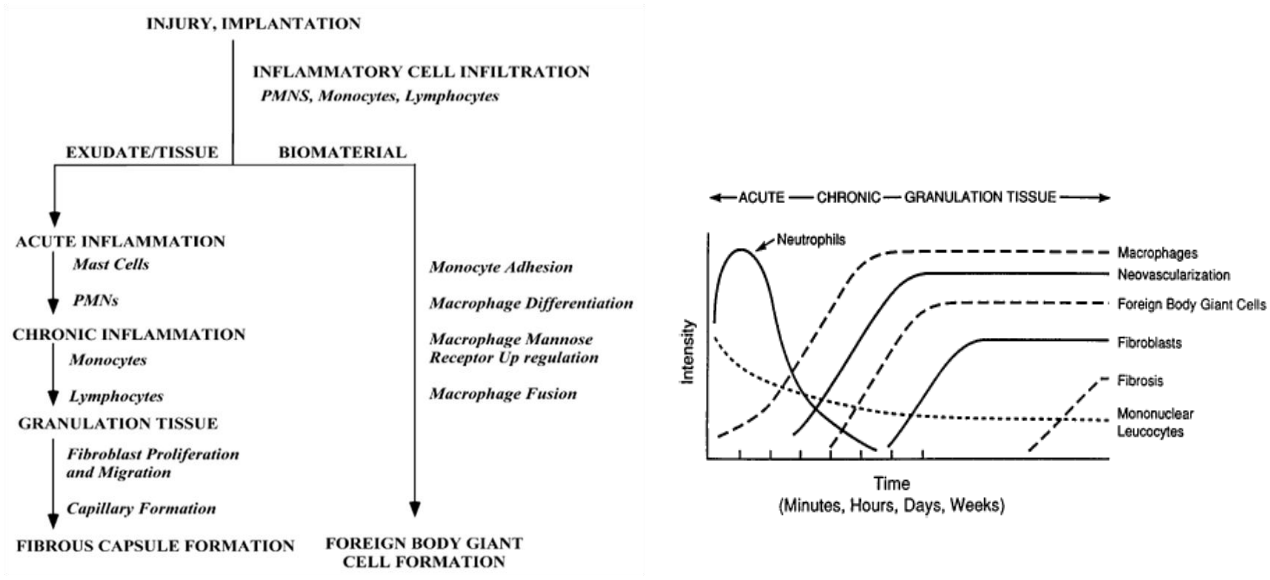

Fig. 1.2: Sequence of events involved in inflammatory and wound healing responses leading to foreign body giant cell formation and temporal variation in the acute inflammatory response, granulation tissue development and foreign body reaction to implanted biomaterials [11].

In situations where injury has occurred and exudative inflammation is present, but no cellular necrosis or loss of basement membrane structures has occurred, the process of resolution occurs and cells of the same type substitute the damaged tissue. In presence of necrosis, instead, granulation tissue growths into the inflammatory exudates and the process of organization with development of fibrous tissue occurs [11]. The perfect healing implies hence a reconstruction of the normal tissue and the total absorption of the fibrotic capsule. At the biomaterial surface level, the principal processes due to implantation and to contact with living tissue are [10][12]:

1. **Surface absorption of proteins**: the composition of the protein layer depends on the properties and topography of the biomaterial surface and on the proteins typology that the surrounding fluid contains. These proteins first come from blood and tissue fluids at the wound site and later from cellular activity in the periprosthetic region. Once on the surface, proteins can desorb (native or denatured, intact or fragmented) or remain to mediate tissue-implant interactions.
2. **Material's surface modifications**: biological fluids may totally change the chemical composition of the polymeric implants surface. Metallic surfaces can undergo to electrochemical modifications like oxidation or to release of metal ions into tissues.
3. **Cells adhesion**: function of the type, conformation and following rearrangement of the proteins film absorbed. It can be non-specific and non-mediated by receptors, weak due to non-adhesive surface, specific with receptors mediation.
4. **Cells activation**: function of the type, conformation and following rearrangement of the proteins film absorbed. It also depends on the presence of activation factor in the surrounding environment (i.e. growth factors release, surface silicon for the osteoblasts activation).

The biological response is always related to material recognition and never to function; it always depends on a local reaction and never on a global or necessary improvement [9].

1.1.2 Failure of implants and infections caused by biomaterials

The clinical practice based on biomaterials has undeniable advantages. Nevertheless, still remain some problems due to their use whose resolution is necessary to reduce the failure rate and to reduce the social and health costs ensuing.

Among the different causes of implants failure, the event of infections still represents the most serious and devastating complications that may involve biomaterial devices.

The incidence of infections due to biomaterials varies from 100% for urinary tract catheters after 3 weeks use to 4% for hip prostheses [13] (Table 1.2).

Topical devices (e.g., contact lenses) are colonized as soon as they are placed on tissue surfaces, percutaneous devices (e.g., central venous catheters) are progressively colonized by skin organisms, implanted devices may be colonized by bacteria at the time of surgery or by organisms that reach their surface from a distant source through a hematogenous or lymphatic route.

Body site	Implant or device	Incidence (%)
Urinary tract	UT catheters	10–20
Percutaneous	CV catheters	4–12
	Temporary pacemaker	4
	Short indwelling catheters	0.5–3
	Peritoneal dialysis catheters	3–5
Subcutaneous	Cardiac pacemaker	1
Soft tissue	Mammary prosthesis	1–7
	Intraocular lenses	0.13
Circulatory system	Prosthetic heart valve	1.88
	Multiple heart valve	3.6
	Vascular graft	1.5
	Artificial heart*	40
Bones	Prosthetic hip	2.6–4.0
	Total knee	3.5–4

*From experiments in calves and sheep.

Table 1.2: Incidence of infection of different biomedical implants and devices according to body site [13].

Generally, large and complex medical devices that require long and complicated surgery for their placements are at high risk of bacterial infection and transcutaneous devices in this category (e.g., the Jarvick artificial hearth) automatically become infected [14].

Focusing on the bone implants area, considering the enormous patients population with orthopaedic implants, even a currently low risk of infection, estimated to be in the range of 0.5–5% for total joint replacements, has to be considered very relevant for its serious consequences [15]. For example, during the first 2 years following the interventions of total knee arthroplasty, infections have variously been reported as the first or second main cause of revision just after instability. Simple debridement procedures with the retention of prosthesis and chemotherapy with antimicrobial agents are treatments that are not often effective on infections that are already established. Sometimes the prosthesis removal and replacement represent the unique option to definitively eradicate severe infections. These

drastic interventions cause obvious implications in terms of attendant patient trauma, prolonged hospitalization and in terms of health and social costs (for example, it has been estimated that the treatment of each single episode of infected arthroplasty costs $50,000 [16]). Furthermore, following revision surgery there is also a significantly high risk (up to 10%) of a recidive and implants replacement [15].

In light of these considerations, scientific research on biomaterials nowadays is focused on the prevention of bacterial adhesion and/or the inhibition of proliferation on the implantable devices surfaces. This results in the development of innovative materials or surface modifications of materials.

1.2 Bacterial adhesion

Bacterial adhesion to biomaterials surface is the most critical aspect in the pathogenesis of infections and the initial step in microbial colonization. As first noted by Zobell in 1943 [17] bacteria prefer to grow on available surfaces rather than in the surrounding aqueous phase. Stable adhesion of a bacterium on a surface requires the following events: transport to the vicinity of the biomaterial surface, attachment to the surface, then by molecular interactions the resistance of detachment in the presence of any dislodging force.

Both specific and non-specific interactions may play an important role in the bacterial ability to attach to (or to resist detachment from) the biomaterial surface. The relative contribution of specific and non-specific mechanisms is strongly dependent from the surface properties of the implanted material. Bacterial adhesion can be mediated by surface protein adsorbed at the time of implant from body fluids (blood, saliva, interstitial fluid, etc.) or can directly take place on the surface mediated by physic-chemical force [18].

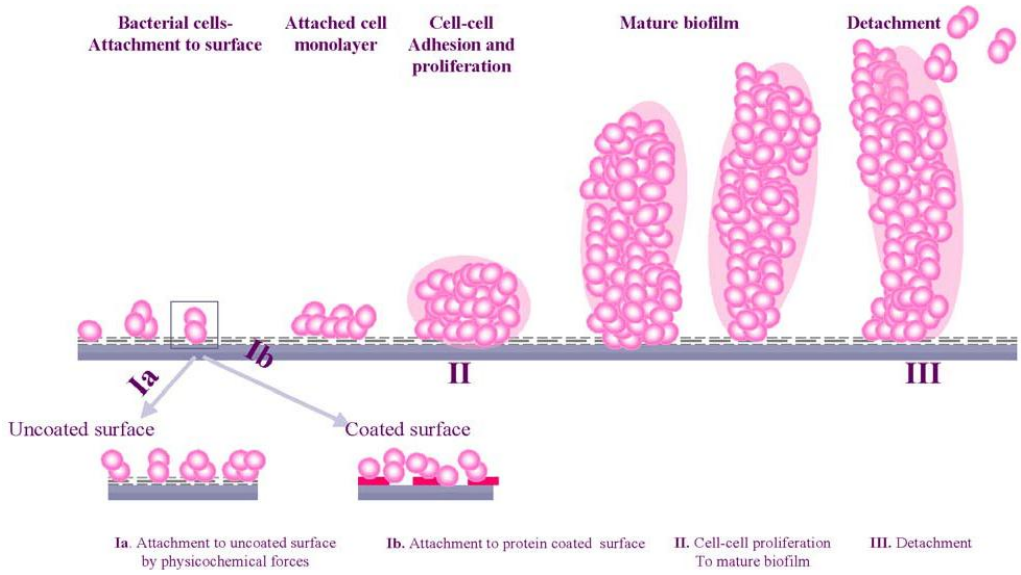

Fig. 1.3: Phases of biofilm formation on biomaterial surface [18].

Since the bacteria adhere to material surface, they start to proliferate forming multilayered cell clusters on the implant surface, which are embedded in extracellular material.

An accumulated biomass of bacteria and their extracellular material (*slime)* on a solid surface is called *biofilm* (Fig 1.3). The main components of *slime* are exopolysaccharides, glycoproteins and glycolipids. Production of *slime* is especially important for events after the initial phase of adhesion, which include improve of surface colonization, protection against phagocytosis, interference with the cellular immune response and reduction of antibiotic effects [18].

After biofilm establishment, non-adherent and some adherent daughter cells escape from the slime layer, either by switching off slime production through a mechanism of phenotypic modulation, or by exhaustion conditions that support slime production, and are then free to drift to new colonization sites to repeat the colonization process.

1.2.1 Phases of Bacterial Adhesion

Adhesion of bacteria to solid surface has been described as a two-phase process: an initial, instantaneous and reversible physical phase (phase 1) and an irreversible molecular and cellular phase (phase 2) (Fig. 1.4) [19].

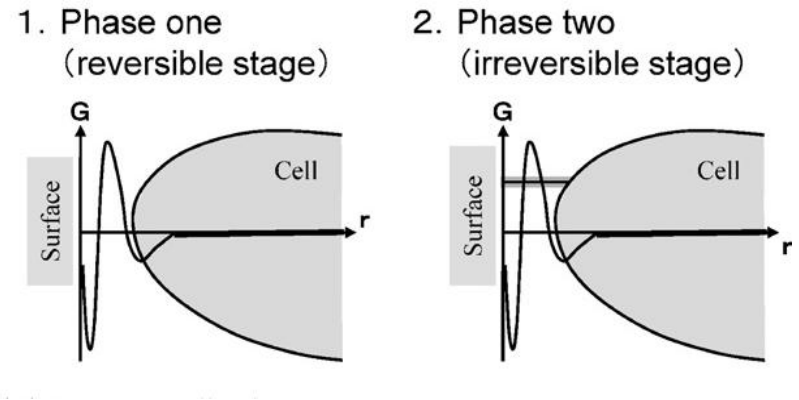

Fig. 1.4: Schematic of two-step adhesion process [20].

Phase 1 – Physicochemical interactions

Among microorganisms, bacteria are about 0.5–2 μm in size, that is, nearly in the range of colloidal particles. Therefore, bacterial adhesion can be described by the DLVO theory [21,22] which originally described the interaction of a colloidal particle with a surface. According to this theory, the total interaction between a surface and a particle is the combination of their van der Waals and electrical double-layer (or Coulomb) interactions.

Van der Waals forces are generally attractive and result from induced dipole interactions between molecules in the colloidal particle and molecules in the substrate. Electrical double-layer forces result from the overlap of counter ion clouds near charged surfaces and the change in free energy as the surfaces are moved closer or farther apart. The result is an attractive force for like-charged surfaces and a repulsive force for oppositely charged surfaces [19]. Since the Van der Waals attractive force is dominant in proximity of a surface, particles cannot separate from the surface by Brownian motion, and therefore adhere irreversibly. In contrast, the Coulomb interaction becomes dominant at a distance away from the surface because the van der Waals force decreases sharply with distance. In the presence of a charged particle in an aqueous solution, hence, counter ions against the surface charge are attracted by the particle, forming an electric double layer. As bacteria and natural surfaces in aqueous solution are usually negatively charged, repulsive electrostatic energy is caused by overlap of the electrical double layers of bacterial cells and the substratum. This repulsive energy increases as the ionic strength of an aqueous solution decreases because shielding of the surface charges by the ions in the electrical double layers lessens. At low ionic strengths, when a bacterial cell approaches a surface, there is an energy barrier which bacterial cells cannot exceed by voluntary or Brownian motion (Fig. 1.5).

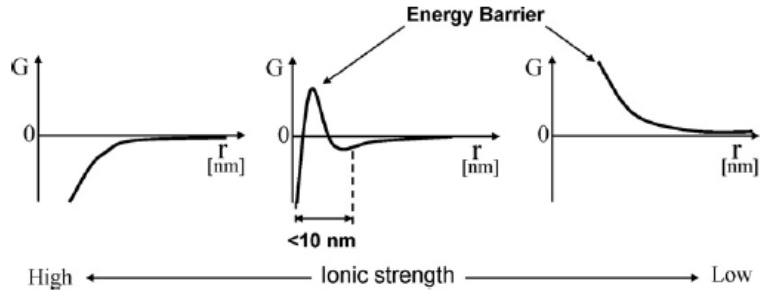

Fig. 1.5: Total interaction energy between a bacterial cell and a surface depending on ionic strength.

In these conditions, there is a secondary energy minimum outside of the energy barrier. The distance from the surface to the secondary energy minimum is usually within several nanometres, depending on the ionic strength. In the first step of cell adhesion, a bacterial cell comes to this position by its motility or Brownian motion, and adheres to the surface reversibly [20].

Phase 2 – Molecular and cellular interactions

If the local environment is suitable to bacteria, such as adnormal tissue integration and a weak host defence, they will remain on the material surface and complete the second phase of adhesion where molecular reactions between bacterial surface structures and substratum become predominant.

The bacterial cell uses nanofibers, such as capsules, pili and flagella, or produces exopolymeric substances (*slime*), which can pierce the energy barrier due to their small radii, for bridging between the cell and surface. When the energy barrier becomes higher and farther from the substratum at lower ionic strengths, however, it becomes difficult for the nanofibers and the exopolymeric substances to reach the substratum, and bacterial cells become unable to adhere. On the contrary, at high ionic strengths (Fig. 1.5), the energy barrier disappears and bacterial cells easily and rapidly attain irreversible adhesion [20].

Current opinion is that the *slime* production is very important in the second phase of bacterial adhesion because not only helps the bacterial cell to overcome the energy barrier between her and the surface but also provides a defence environment against immune system or antibiotic therapy. Consequently, the bacterial strains that don't produce *slime* are fewer adherent and less pathogenic [18].

1.2.2 Factors influencing bacterial adhesion

Bacterial adhesion is affected by many factors including the environmental factors, such as associated flow conditions, some characteristics of the bacteria, the presence of serum proteins or bactericidal substances, and the chemical and physical nature of the target material surface.

1.2.2.1 Environment

Some factors in the general environment, such as temperature, time of exposure, bacterial concentration, the presence of antibiotics and the flow conditions affect bacterial adhesion.

Flow condition

Flow conditions are considered dominant factors that strongly influence the number of attached bacteria as well as the biofilm structure and performance. It is generally

considered that higher shear rates result in higher detachment forces that result in decreasing the number of attached bacteria, whereas they make the biofilm denser and thinner. There is an optimum flow rate for bacterial attachment reflecting the balance between rate of delivery and the force acting on attached bacterium. Once in contact with a material, the bacteria are able to engage in interactions dependent on the surface characteristics of both the bacterium and the material surface. At lower flow rates, where shear stress and bond number required to maintain attachment are low, an increase in both receptor and ligand concentration have a negligible effect on attached bacteria. At higher flow rates, where shear effects lead to higher forces on attached bacteria, the potential to form higher numbers of bonds is of much greater significance [23]. Higher dehydrogenase activity (indicator of bacteria death) and lower growth yield are obtained when the shear rate is raised. Therefore, a biological phenomenon, besides a simple physical effect, may underline the observed relation between the shear rate and the resulting biofilm structure. Quantitative assessment of the shear stress values favourable to attachment and those required to detach pre-adsorbed bacteria shows that there is an order of magnitude difference. Ming et al. showed that the shear stress generating detachment increases with incubation time up to a maximum value, suggesting that additional interactions are progressively formed after the initial bacterial attachment [24].

Concentrations of electrolytes and PH

Concentration of KCl, NaCl and pH value in the culture environment also influences bacterial adhesion. Bunt et al. showed that the pH and the ionic strength of the suspending buffer influence the cell surface hydrophobicity (CSH). CSH was found to be significantly lower at higher pH 7.4 and low ionic strength 0.5M, while CSH was greater at pH 2.2 and ionic strength 1 M. Greatest adhesion to hydrophobic surfaces was found at pH between 2.2 and 4, in the range of the isoelectric point when bacteria are uncharged, and ionic strength 1 M [25]. The effect of increased ionic strength is probably due to the suppression of the solvation barrier and the neglectable electrostatic interactions (repulsive). Therefore, ionic strength and pH influence bacterial adhesion by changing surface characteristics of both the bacteria and the materials (hydrophobicity-charge) and therefore changing interactions in phase 1.

Antibiotic Presence

The presence of antibiotics decreases bacterial adhesion depending on bacterial susceptibility and antibiotic concentration. Leon et al. showed that *Staphylococcus epidermidis* adhesion on catheters was reduced when impregnated with minocycline and rifampin thanks to the slowly release from catheter surface [26]. Arciola et al. showed that sessile *Staphylococcus epidermidis* was less susceptible to antibiotic treatment than planktonic cells [27]. This may be explained by bacterial altered metabolism, slime production and a system of bacterial resistance to unfavourable conditions (lower growth rate) after adhesion; under the selective pressure of a drug or the adhesion to specific surfaces, some antibiotics-resistant bacteria could even find favourable conditions and increase the proliferation.

1.2.2.2 Bacterial properties

For a given material surface, different bacterial species and strains adhere differently since different species and strains have different physicochemical characteristics.

Bacterial hydrophobicity

Surface hydrophobicity of bacteria is an important physical factor for adhesion, especially when the substrate surfaces are either hydrophilic or hydrophobic. The hydrophobicity of bacteria varies according to bacterial species and is influenced by surrounding medium environment, bacterial age and bacterial surface structure such as fimbriae, polypeptides and proteins (for example prodigiosin for *Streptococcus sanguis* and amphypathic aminolipids for *Serratia marcescens*). Generally, bacteria with hydrophobic properties prefer hydrophobic material surfaces; the ones with hydrophilic characteristics prefer hydrophilic surfaces and hydrophobic bacteria adhere to a greater extent than hydrophilic bacteria [28]. Satou et al. found *Streptococcus sanguis* strains with hydrophobic surfaces adhered more to hydrophobic glass slides than others with a less hydrophobic character [29].

Bacterial surface charge

The surface charge of bacteria is another important physical factor for bacterial adhesion. Indeed, it is involved in the initial step of bacterial colonization, also governed by long-range Van der Waals forces. The surface charge varies according to bacterial species and is influenced by the growth medium, the pH and the ionic strength of the suspending buffer, bacterial age, and bacterial surface structure [18]. Most particles acquire a surface electric charge in aqueous suspension due to the ionization of their surface groups. The surface charge attracts ions of opposite charge in the surrounding environment and results in the formation of an electric double layer. Bacteria in aqueous suspension are almost always negatively charged; a hydrophilic character of the bacteria implies a high surface charge, but a hydrophobic bacterium may still have a rather high surface charge [30].

1.2.2.3 Material surfaces properties

Bacterial adhesion on biomaterials is strongly related to material surfaces properties and particularly to surface chemical composition of the material, to the surface charge, to the hydrophobicity, to the surface roughness or physical configuration. The absorption or binding of serum proteins or the formation of biofilm can quickly modify the surface energy, the number of empty binding sites, and the hydrophobic and hydrophilic characteristic.

Surface chemical composition

Surface chemistry influences bacterial adhesion and proliferation. Different functional groups on the surface cause different surface charge and hydrophobicity; these properties can affect the bacterial adhesion [18]. Chu and Williams examined the effects of physical configurations of suture materials on bacterial adhesion. Polydioxanone absorbable sutures exhibited the smallest affinity with *Escherichia Coli* and *Staphylococcus aureus*, Dexon sutures had the highest affinity toward these two bacterial strains [31]. According to Gristina et al., *Staphylococcus epidermidis* preferentially adheres to polymers and *Staphylococcus aureus* to metals [32]. This result may explain because *Staphylococcus epidermidis* often causes polymer implant infection while *Staphylococcus aureus* is often the major pathogen in metal implant infections. Tegoulia and Cooper showed that

Staphylococcus aureus adhesion on self-assembled monolayers (SAMs) terminated with methyl, hydrohylic, carboxylic acid and tri-ethylene oxide was lowest on ethylene oxide-bearing surfaces followed by the hydroxyl surfaces and higher on carboxylic- and methyl-terminated SAMs [33]. Kiremitci-Gumustedereliogl ou and Pesmen showed that bacterial adhesion was reduced on the negatively charged PMMA/AA (polymethilmetacrylate /acrylic acid), while it was increased on the positively charged PMMA/DMAEMA (polymethilmetacrylate/dimethylamino ethyl methacrylate) in a manner depending on the comonomer content [34]. As the surface composition is strongly related to the bacterial capacity to adhere on surfaces, its modification may be an effective tool to avoid or reduce the bacterial adhesion. The modification of the implant surfaces using plasma coating, antimicrobial peptide, non-steroidal anti-inflammatory drugs, antibacterial species graft or anodization can discourage the bacterial adhesion on these surfaces [18,28] as well as coating with Pluronic surfactant or polyvinylpyrrolidone, cationic absorbed solid surface or amine-containing organosilicon [30].

Surface Roughness

Roughness is a 2-D parameter that represents the average distance between the peaks and valleys on a material surface and doesn't summarize his morphological configuration.

It has been found that the irregularities of surfaces promote bacterial adhesion and biofilm deposition whereas the smooth surface doesn't favour these. A rough surface has a greater surface area and the depressions in the rough surfaces may provide more favourable sites for attach and colonization and a protection against shear forces thanks to irregularities of surface [18].

Focusing on titanium characterization, a recent study of Puckett et al. compares the response to bacterial adhesion of four different titanium surfaces (Conventional, Nanorough, Nanotubular, Nanotextured) with different roughness level. It is demonstrated that different roughness correspond to different surface energy and, particularly, an increased surface roughness correspond to higher surface energy (Fig 1.6a). The two rougher surfaces (Nanotubular and Nanotextured) promote adhesion and proliferation of three different bacterial species, *Staphylococcus aureus*, *Staphylococcus epidermidis* and *Pseumodonas Aeruginosa* (Fig. 1.6b) [35].

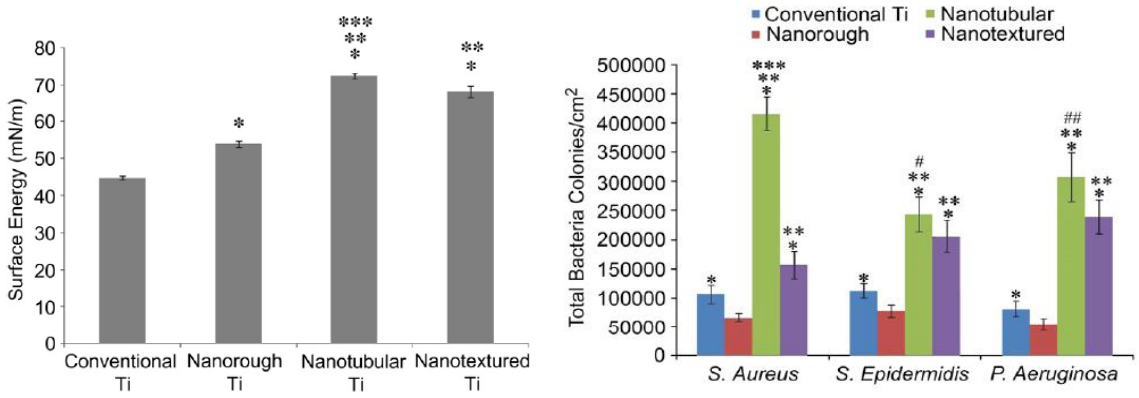

a. **b.**

Fig. 1.6: **a**. Total surface energy proportional directly to surface roughness; **b.** *S. Aureus*, *S. Epidermidis*, and *P. Aerugionsa* colonies/cm^2 after 1 hour of culture on the different Ti surfaces [35] .

Tang et al. studied the *Staphylococcus epidermidis* adhesion on fluoroalkylsilane (FAS)-coated silicone whose hydrophobicity and roughness were varied, respectively, by mechanically assembled monolayer (MAM) preparation methods and by casting the silicone to templates prepared with different abrasive. The influence of roughness on bacterial adhesion was promoted only above a threshold of 200 nm of average roughness (Ra) [36]. Taylor et al. found a similar trend on correlation between bacterial adhesion and roughness some years before. A small increase in surface roughness of PMMA treated with silicone carbide paper grade P1200 had a significant increase in bacterial adhesion, while, larger roughness increases produced by silicone carbide paper grades P400 and P120, had no significant effect in bacterial adhesion compared to the smooth surface [37]. Probably a big difference between the bacterial dimensions and the roughness value causes the bacteria incapacity to recognize the roughness. However, this non-linear dependence of bacterial adhesion on surface roughness is a purpose for further studies.

Surface morphology or configuration

An irregular surface morphology promotes bacterial adhesion, biofilm deposition and accumulation of biliary sludge more than a smooth and regular surface [30] . The rate of infection on porous materials is much higher than the infection rate on dense material. This implies bacteria adhere and colonize the porous surface preferentially. Moreover bacteria adhere more on grooved and braided materials compared to flat ones as the available surface area increase. However, bacteria preferentially adhere to irregularities that conform

to their size since this maximizes bacteria-surface area. Grooves or scratches on order of bacterial size increase the contact area and hence the binding potential, whereas grooves that are much larger-wider than the bacterial size maintain approximately the binding potential of a flat surface. Grooves or scratches too small reduce the contact area between bacterium and surface that, consequently, show a less binding potential [18].

Surface hydrophobicity

The hydrophobicity of a material surface is determined mainly by contact angle measurement. A water contact angle is defined as the measurement of the contact angle between a water drop and a surface. If it is greater than 90° the surface is *hydrophobic*, if it is less than 90° the surface is hydrophilic.

Generally speaking the metal surfaces are hydrophilic, have a high surface energy and are negatively charged while polymers (i.e. UHMWPE or Teflon) are hydrophobic, have a low surface energy, are less electrostatically charged [30] . Depending on the hydrophobicity of both bacteria and material surface, bacteria adhere to materials with different hydrophobicity. Hydrophilic materials are more resistant to bacterial adhesion than hydrophobic materials [28]. Satou et al. studied the adhesion of *Streptococcus Sanguis* and *Streptococcus Mutans*, two of the main oral cavity bacteria, to four surface-modified glass slides with different hydrophobicity. *Streptococcus Sanguis* strains, which is more hydrophobic than *Streptococcus Mutans* adhered more to hydrophobic glass slides than others whereas Streptococcus Mutans adhered preferably on the hydrophilic glasses [29]. Tang et al. studied the *Staphylococcus epidermidis* adhesion on fluoroalkylsilane (FAS)-coated silicone whose hydrophobicity was varied by mechanically assembled monolayer (MAM). They show that FAS coated on silicone results in significantly reduced bacterial adhesion with a degree of reduction inversely related to surface hydrophobicity [36].

1.2.2.4 Serum or Tissue Proteins

The serum or tissue proteins promote or inhibit bacterial adhesion by altering binding to substrata surfaces, binding to bacterial surfaces or by their presence in surrounding medium during the adhesion process. Most of the protein inhibited bacteria adhesion by their association with the bacterial cell surface, the material surface or both. Most of the binding between bacteria and proteins is specific ligand-receptor-like interactions. Protein

may also change the adherent behaviour of bacteria by changing bacterial surface physicochemical characteristic [30].

For instance fibronectin (Fn) is one of the major protein components of blood plasma while the insoluble cellular Fn is one of the major components of extracellular matrix. Fn, which has a pronounced ability to mediate surface adhesion of eukaryotic cells, has also been shown to bind *Staphylococcus aureus* and promote his adhesion to substratum surfaces [30]. Another important serum protein is albumin which is adsorbed on material surface has shown inhibitory effects on bacterial adhesion to polymer, ceramic, and metal surfaces. An et al. found human serum albumin (HSB) inhibit *Staphylococcus epidermidis* adhesion to commercially pure Ti surfaces after treatment with 200 mg/mL of HSA at 37℃ for 2 hours [30].

Fibrinogen is a serum protein that mediates bacterial adhesion to biomaterials. Most studies show that adsorbed fibrinogen promotes adherence of bacteria, especially staphylococci, to biomaterials. Dickinson et al. found that pre-treatment of bacteria or both bacteria and surface of three different polyurethane ionomers with fibrinogen enhances bacterial adhesion without correlation with shear stress rate up to $200s^{-1}$ [38]. This suggests the presence of ligands for fibrinogen on staphylococcal cell surface.

The Laminin is the major components of basement membrane. It was shown that laminin is able to bind some strains of Streptococcus Pyogenes [28]..

Laminin has a promoting effect on *Staphylococcus aureus* adhesion to PMMA coverslips, but to a lesser extent compared to the effects of fibronectin and fibrinogen [30].

Thrombin (known as coagulation factor II), increases significantly *Staphylococcus aureus* adhesion on Polyurethane surface since it polymerises fibrinogen in platelet poor plasma to fibrin. Fibrin strands surround and link the platelet aggregate to stabilize the thrombus, which also promotes bacterial adhesion [39].

1.3 Prevention of bacterial adhesion

In order to limit the serious clinic consequence due to implant infections, remarkable improvements have currently been reached in medical treatments. However to prevent the bacterial adhesion or to limit the bacteria proliferation represent one of the main goal of biomaterial research. In the past decades, control of environmental and medical personnel contamination has been a principal target to cut down the rate of nosocomial and post-surgical infections. Parallel there has also been the establishment of effective protocols of peri-operative antibiotic prophylaxis. Although the introduction of strictly hygienic rules, the antibiotic prophylaxis, and the improvement of surgical techniques have been reduced the infection rate, still remains a risk of infection with critical consequences.

As explained, bacterial adhesion and anchorage on implant surfaces represent an initial crucial step in the pathogenesis of infections. Consequently, the most convenient way to contrast the bacterial infection is inhibit or avoid the bacterial adhesion by means of:

1. Surface physical-chemical modification of surfaces;
2. Incorporation of antimicrobial agents.

The table 1.3 shows the main surface treatments nowadays in use and the kind of material substrates on which they can be apply.

Disinfectants, bacteriostatic drugs or antibiotics, inorganic ions or particles with toxic effect on bacteria directly integrated in the biomaterial surface have a direct action on the bacterial survival. Their presence on surface allows reaching high concentrations of antimicrobial substances by release directly at the interface between implant and biological tissue and may also prevent contaminations during the surgical procedure. Vice versa peri-operative systemic antibiotics reach the tissues to the interface with the implant through vascular blood system. Consequently, the action on the biomaterial surface is indirect and less effective especially in the case of just adhered bacteria.

	Polymer	Metal	Ceramic	Glass
Noncovalent coatings				
Solvent coating	✓	✓	✓	✓
Langmuir–Blodgett film deposition	✓	✓	✓	✓
Surface-active additives	✓	✓	✓	✓
Vapor deposition of carbons and metals[a]	✓	✓	✓	✓
Vapor deposition of parylene (*p*-xylylene)	✓	✓	✓	✓
Covalently attached coatings				
Radiation grafting (electron accelerator and gamma)	✓	—	—	—
Photografting (UV and visible sources)	✓	—	—	✓
Plasma (gas discharge) (RF, microwave, acoustic)	✓	✓	✓	✓
Gas-phase deposition				
• Ion beam sputtering	✓	✓	✓	✓
• Chemical vapor deposition (CVD)	—	✓	✓	✓
• Flame spray deposition	—	✓	✓	✓
Chemical grafting (e.g., ozonation + grafting)	✓	✓	✓	✓
Silanization	✓	✓	✓	✓
Biological modification (biomolecule immobilization)	✓	✓	✓	✓
Modifications of the original surface				
Ion beam etching (e.g., argon, xenon)	✓	✓	✓	✓
Ion beam implantation (e.g., nitrogen)	—	✓	✓	✓
Plasma etching (e.g., nitrogen, argon, oxygen, water vapor)	✓	✓	✓	✓
Corona discharge (in air)	✓	✓	✓	✓
Ion exchange	✓[b]	✓	✓	✓
UV irradiation	✓	✓	✓	✓
Chemical reaction				
• Nonspecific oxidation (e.g., ozone)	✓	✓	✓	✓
• Functional group modifications (oxidation, reduction)	✓	—	—	—
• Addition reactions (e.g., acetylation, chlorination)	✓	—	—	—
Conversion coatings (phosphating, anodization)	—	✓	—	—
Mechanical roughening and polishing	✓	✓	✓	✓

[a] Some covalent reaction may occur.
[b] For polymers with ionic groups.

Table 1.3: Physical and chemical surface modification treatments to prevent the bacterial adhesion [40].

1.3.1 Physical-chemical approach

Scientific research on biomaterials has always searched solutions among the organic and inorganic chemical and materials science in order to develop surfaces with antibacterial properties. In the last decades many efforts were concentrated to develop specific antibacterial materials and coatings. Examples of this approach are coating represented by device surfaces using surfactants, proteins such as albumin, hydrophilic negatively charged polysaccharides such as hyaluronan and heparin, which, in light of the known factors involved in microbial adhesion, can reach the scope to generate adhesion-resistant or even bacteria repellent surfaces [15].

A promising bioactive material is chitosan, a polysaccharide with intrinsic large spectrum anti-microbial properties. Recent studies investigated the use of chitosan in orthopaedic area as scaffold of tissue engineering of bone tissue or as bioactive coating for orthopaedic and craniofacial devices [41,42]. The nanoparticles of chitosan have shown bactericidal properties due to their high surface charge density which are able to interact and disrupt the

bacterial cell membranes. A recent study of Shi et al. show this phenomenon studying the antibacterial properties of PMMA bone cement impregnated with chitosan nanoparticles (CS NP) and quaternary ammonium chitosan derivative nanoparticles (QCS NP) against *Staphylococcus aureus and Staphylococcus epidermidis* [43]. They found a sensible decrease of bacterial adhesion due to presence of chitosan nanoparticle (Fig. 1.7).

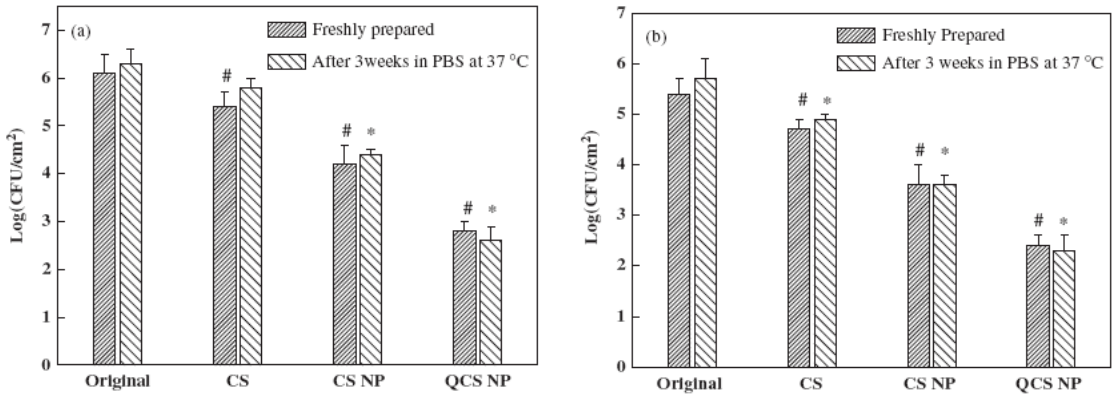

Fig. 1.7: Number of viable adherent *S. Aureus* (a) and *S. Epidermidis* (b) cells on PMMA cement with chitosan (CS), chitosan nanoparticles (CS NP) and quaternary ammonium chitosan derivative nanoparticles (QCS NP) [43].

The use of quaternary ammonium compounds to generate ‘‘self-sterilising’’ surfaces represents a new promising approach. In this case the functional groups able to produce damage to cell membranes are covalently bounded to a carrying polymer anchored to the implant surface enhancing its bacteriostatic potential.

The study of Milovic et al. on antibacterial activity of an amino-glass slide covalently derivatized with N-hexyl, methyl-polyethylenimine (PEI) against *Escherichia Coli* and *Staphylococcus Aureus* show a remarkable bactericidal action up to 10-fold reduction in live bacteria and a lack of citotoxicity to mammalian cells [44].

Another interesting method reducing bacterial adhesion and thus implant infections is the both use of (PLL-g-PEG) coating and RGD-conditioning (Arginine-Glycine-Aspartic acid) of titanium oxide proposed by Harris et al. A poly(L-lysine)-grafted-poly(ethyleneglycol) (PLL-g-PEG) coating has been used to render titanium surfaces resistant against protein adsorption from biological media, while the short peptide sequence RGD attached to a fraction of the PEG chains have been proved to interact with integrin receptors of eukaryotic cells favouring recognition and thus adhesion on surfaces. This coated and

functionalized titanium surface shown to reduce the adhesion of *Staphylococcus Aureus in* comparison to uncoated titanium surface [45].

Titanium surface antibacterial property studied by Del Curto et al. in which were shown the antimicrobial properties of surface-treated titanium with an external layer of crystalline anatase titanium dioxide (TiO_2) [46].

1.3.2 Pharmacologic approach

As well as the chemical and physical science, a lot of solutions can be found in the pharmacologic science. The well known improvements of the last century in the antibiotics and antiseptics research and their consolidated use against systemic and topical bacterial infections have encouraged researchers to essay their efficacy in the biomaterials field.

Have been hence developed coatings able to release antibiotics as vancomycin, gentamicine, minocycline-rifampin, teicoplanin, cefazolin or antiseptics silver-sulfadiazine, chlorhexidine and benzalconium chloride. Instead of incorporated in a coating, antibiotics or antiseptics can be incorporated into bulk materials and cavity filling materials, either by impregnation or covalent bonding. Among these drugs delivering, coatings incorporating chlorhexidine–silver sulfadiazine and minocycline-rifampin have already demonstrated to prevent infections *in vivo* and are currently clinically used on catheters [15].

Rupp et al. examined the antibacterial efficacy *in vivo* of a second-generation antiseptic venous catheter, coated with chlorhexidine and silver sulfadiazine on the internal and external surfaces. The rate of definitive catheter-related bloodstream infection was 1.24 per 1000 catheter-days for the control group versus 0.42 per 1000 catheter-days for the antiseptic catheter group [47]. Leon et al. studied the benefits of antibiotic central venous catheter, impregnated with minocycline and rifampin. The episodes per 1000 catheter days of clinical infectious complications decreased from 8.6 (untreated catheters) to 5.7 (impregnated catheters) [26].

The undeniable advantage of incorporated antibiotics and antiseptics in biomaterials coating is their rapidly release in significant quantity in the tissues surrounding implants. This results in a marked antimicrobial activity during the first time after implantation. However, this release characteristic may be problematic in implants requiring more time to

conclude the integration process (i.e. bone implants) or in patients with characteristics affecting a fast integration (i.e. age, chronicle disease, etc.).

Furthermore, many clinical evidences show an alarming growing level of antibiotic resistance in many important and virulent pathogens like *Staphylococcus aureus* and *Staphylococcus epidermidis* [15]. This emerging problems direct researcher's efforts towards new antimicrobial strategies including the use of metal antimicrobial agents like Silver and Gallium.

1.3.3 Silver as antimicrobial agent

The formulation of antimicrobial silver has changes during history, from bulk silver in vessels and coins during Antiquity, to ionic silver supplemented as silver salts like $AgNO_3$ or adsorbed on carrier materials like in the case of zeolite and, nowadays, to silver nanoparticles. In all these chemical forms silver has shown several advantages for antibacterial purpose, such as [48]:

1. A broad antibacterial spectrum to gram-positive, gram-negative and drug-resistance bacteria at very low concentration as well;
2. Inhibition of bacterial adhesion on biomaterials surface;
3. Low proneness to resistance development;
4. Relative stability that allows easy use in the main methods of surface modifications (for example ion implantation, chemical vapour deposition, magnetron sputtering)
5. Possible employ on all the main biomaterials including metals, polymers, bioactive glass and ceramics, and so forth.

In the next page will delve into the main characteristic and the suggested mechanisms of action of the more in use silver forms, silver ions from silver salts and silver nanoparticles.

1.3.3.1 Effect of silver on bacteria

Silver in the metallic form is considered an inert and exhibits no biocidal action. Silver metal and the majority of silver compounds (for example $AgNO_3$, AgCl, Ag_3PO_4, etc.) ionize to release Ag^+ in the presence of water, body fluids and tissue exudates. Silver cations are highly reactive and binds strongly to electron donor groups of biological

molecules contain sulphur (-SH), oxygen and nitrogen that are normally present as thiols or phosphates on amino acids and nucleic acids.

The mechanisms of antibacterial action comprehend:

1. **Binding of silver ions to cell membrane and intracellular absorption**: silver binds to electron donor receptors, particularly disulphide, amino, imidazole, carbonyl and phosphate residues on membranes leading to intracellular absorption by endocytic vacuoles and phagocytosis. Membrane-related enzymes like phosphomannose isomerise are inactivated and the bacterial membrane undergoes denaturation (Fig. 1.8a) with loose of its functional capacity to regulate the inward diffusion of nutrients. At the same time, the effusion of essential electrolytes and metabolites is limited.
2. **Impairment of intracellular compounds**: silver ions denature the 30s ribosome unit, suppress the expression of enzymes and proteins essential to ATP production, inhibit respiratory enzyme such as NADH dehydrogenase in the respiratory system.
3. **Interaction with nucleic acids**: silver ions interact with hydrogen bonds of DNA and RNA, resulting in marked enhancement of pyrimidine dimerization by photodynamic interaction and inhibition of DNA or RNA replication. The free state of DNA changes to a condensed form (Fig. 1.8b) incompatible with replication and duplication [49-52].

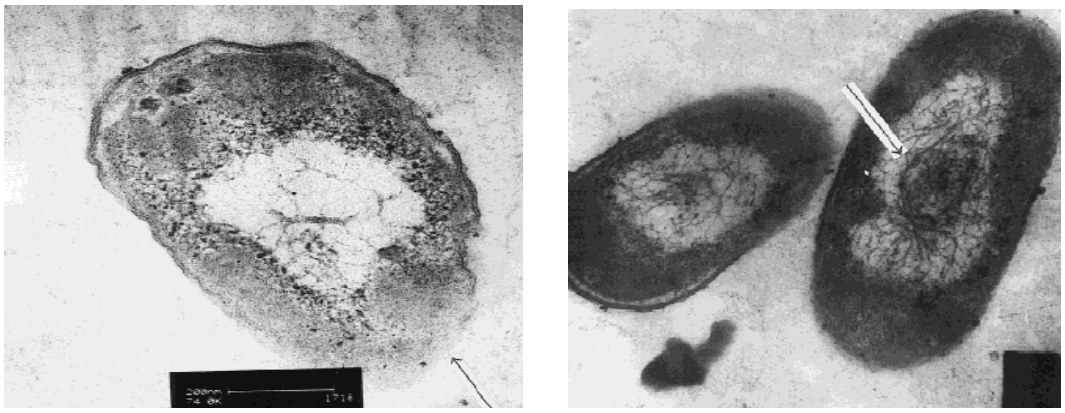

a. **b.**

Fig. 1.8: Effect of Ag^{+} on *Escherichia Coli*. **a.** Cell membrane denaturated. **b.** Condensed DNA [52].

Therefore, the ionizing capacity of the silver metal or silver compound is critical in comparing their antimicrobial activities, as the ions are the main performers of the bacterial inactivation. Silver nitrate ($AgNO_3$) has a very high ionizing capacity justifying his massive use in silver containing antibacterial devices. Silver phosphate (Ag_3PO_4) and

silver chloride (AgCl) have ionizing capacity moderate and low respectively. In light of these considerations the use of silver nitrate is more effective. Balazs et al investigated the antimicrobial properties of silver nitrate. They studied the adhesion of *Pseudomonas aeruginosa* on poly(vinyl chloride) (PVC) endotracheal tube chemically modified with sodium hydroxide and silver nitrate. They shown a 100% reduction in initial bacterial adhesion compared to the same material without silver incorporation [53].

Song et al. compared the antimicrobial properties of titanium oxide developed with micro-arc oxidation and enriched with high and low concentrations of silver nitrate or platinum chloride. The antibacterial efficacy against *Staphylococcus Aureus* and *Escherichia Coli* was almost 100% for both coatings containing high and low concentration of silver. The efficacy of platinum containing coatings was around 20% [54].

1.3.3.2 Silver nanoparticles

Silver nanoparticles are insoluble silver particles that are smaller than 100 nm in size. They can be synthesised by chemical vapour deposition or wet chemical methods. The wet chemical methods typically involve the reduction of a silver salt (i.e. silver nitrate) with a reducing agent (i.e. sodium borohydride) in the presence of colloidal stabilizer (i.e. polyvinyl alcohol).

The silver nanoparticles show efficient antimicrobial property compared to other salts due to their extremely large surface area, which provides better contact with microorganisms. The antibacterial activities are related to the size of the nanoparticles, with the smaller particles having higher activities on the basis of equivalent mass content. It has been shown that the nanoparticles get attached to the cell membrane and also penetrate inside the bacteria. They are indeed able to bind sulphur-containing proteins of bacterial membranes and of DNA but preferably attach the respiratory chain inhibiting NADH dehydrogenase. Such a biological mode of action is similar to that found for $AgNO_3$ solution, suggesting that silver nanoparticles represent a special physicochemical system which confers their antimicrobial activities via Ag^+ [55]. The enhanced antimicrobial activity of nanoparticles may in addition be explained by their capacity to release Ag ions even in the inner of bacterial cells with following increase of Ag^+ concentrations and time of action [50]. In a recent study Juan et al. show the antibacterial effect of silver nanoparticles deposed on titanium substrata using a silanization method. They found that

even a surface atomic concentration of only 4.26% of silver has a remarkable antibacterial and anti-adhesive efficacy. Indeed the bactericidal ratio was 94.56% on Staphylococcus Aureus and 95.42% on Escherichia Coli [56]. Lara et al. showed that silver nanoparticles are effective bactericidal agents regardless of the drug-resistance mechanisms that exist in multidrug-resistant *Pseudomonas aeruginosa*, ampicillin-resistant *Escherichia coli* and erythromycin-resistant *Streptococcus pyogenes*. In addition, silver nanoparticles showed bactericidal rather than bacteriostatic effect on the tested bacteria [57]. Therefore, silver nanoparticles can be used as an effective broad-spectrum bactericidal agent.

Actually, parallel to find methods to optimize the integration of silver into biomaterials, Scientific Community is questioning the hypothetical toxic effects of silver. A recent review of Alan B. G. Lansdown on pharmaceutical and toxilogical profile of silver in the biomaterials field shows that health risks associated with systemic absorption of silver as Ag^+ are low. The long-term exposure to ingestion or inhalation of metallic silver or ionisable silver compounds may cause argyria or argyrosis, effects associated with heavy deposition of insoluble silver precipitates in the dermis and cornea/conjunctiva. There is no evidence of tissues damaging if the release of silver in body environment is under the threshold attributed to the development of argyria [58]. However, there are still controversial opinions.

1.3.4 Gallium as antimicrobial agent

The discovery of antimicrobial properties of gallium, a group IIIA metal, is very recent. An article published by Olakanmi et al. in 2000 showed that gallium is able to interfere with mycobacteria residing within human macprophages and, particularly, to disrupt acquisition and utilization of iron by mycobacteria [59]. They hypothesized this capacity from the just known ability of gallium (particularly in the form of gallium nitrate [$Ga(NO_3)_3$]) to concentrate within mononuclear phagocytes and the evidence that gallium disrupts iron-dependent metabolic pathways. In 2007 Kaneko, Olakanmi et al. showed that gallium inhibits *Pseudomonas aeruginosa* growth and biofilm formation, kills planktonic and biofilm bacteria in vitro [60]. They found that gallium is able to disrupt the bacteria iron metabolism. Iron, in almost all bacteria, is essential for growth and the functioning of key

enzymes, such as those involved in DNA synthesis, electron transport, and oxidative stress defence. Free iron levels are extremely low *in vivo* due to multiple host defences that sequester iron, and this represents a potent deterrent to both acute and chronic infection. In light of these considerations, bacteria are susceptible to iron metabolis affections that can be damage seriously several biological mechanisms.

The transition metal gallium can be act as a 'Trojan Horse' to disrupt bacterial iron metabolism. The suggested reasons are:

1. Gallium has an ionic radius nearly identical to that of Fe, and many biologic systems are unable to distinguish Ga^{3+} from Fe^{3+}.
2. Gallium disrupts iron-dependent processes because, unlike Fe^{3+}, Ga^{3+} cannot be reduced, and sequential oxidation and reduction are critical for many of iron's biological functions[60,61].

The use of gallium could be a response to the growing needs of new antimicrobial agents against the antibiotic-resistant species. Furthermore, gallium is already approved by Food and Drug Administration to treat hypercalcemia of malignancy.

1.4 Titanium and titanium alloys as biomaterials

Currently metals are widely used for several clinical applications. The attributes of strength, stiffness, toughness and impact resistance are particularly suitable for load-bearings applications such as orthopaedic devices and dental implants.

Nowadays titanium and its alloy are the most used metal in biomedical field by virtue of their makeable attributes of high generalized and localized corrosion resistance, high mechanical resistance, lightness, good workability and excellent biocompatibility. They are used in dentistry, maxillofacial surgery, hip-joint replacement, heart valves, coating for bio-immersed devices like pacemakers, cardiovascular stents [64, 65]. Actually, titanium represents the first choice in applications involving hard tissues. Indeed it is widely used as implantable material in dental and orthopaedic field in order to restore impaired bone functions and simultaneously to promote the osteointegration.

Osteointegration consists of a direct bone-to-biomaterial interface without interposition of non-bone tissue. An implant is considered as osteointegrated when there is no progressive relative movement between the implant and the bone with which it has direct contact [63]. The direct anchorage of bone on the implant surface leads indeed to an appropriate distribution of loads at the interface and to their transferring to the surrounding bone tissue. The host response of bone implanted materials involves several events at cellular and matrix level as mentioned in par 1.1.2. This response should ideally culminate with apposition of new bone directly in contact with the implant surface. The lack of osteointegration is strongly related to loosening and failure of the implant. The rigid fixation between the implant and the host bone, especially in the first time after implantation, confers mechanical stability that prevents micro-motion of the implants or minimal distortional strain. Excessive implant motion or poor implant stability results in tensile and shear motions, stimulating a fibrous membrane formation around the implant and causing displacement at the bone-implant interface, thus inhibiting osseointegration and leading to bacterial adhesion and failure of the implant [63]. To achieve a fast and effective osteointegration of titanium implants, in recent years were developed several surface modifications techniques in order to direct the biological response conferring specific characteristics to the surface oxide layer.

1.4.1 Main Properties

Titanium is the ninth most abundant element and the forth most abundant metallic element in the earth's crust. In Nature it occurs as titanium oxide, mainly rutile (TiO_2) and ilmenite ($FeTiO_3$) [64]. Titanium is obtained using the Kroll method that involves the reaction of chlorine and carbon upon ilmenite or rutile. The resultant titanium tetrachloride ($TiCl_4$) is separated from the iron tri-chloride ($FeCl_3$) by fractional distillation. Finally titanium tetrachloride is reduced to metallic titanium by reduction with magnesium. A further purification of metallic titanium is reachable through vacuum ovens, recasting or additional steps of purifications [65]. The purity grade of titanium is related to the maximum contents of oxygen, carbon, nitrogen and iron as indicated by the ASTM (American Society for Testing and Materials) standards. The rate of elements contained affects the mechanical properties (Table 1.4).

Purity Grade	N [%]	C [%]	H [%]	O [%]	Fe [%]	Young Module [GPa]	Maximum Tensile Stress [MPa]	Maximum Tensile Strain [%]
Ti grade 1	0.03	0.10	0.01	0.18	0.20	103	240	24
Ti grade 2	0.03	0.10	0.01	0.25	0.30	103	340	20
Ti grade 3	0.05	0.10	0.01	0.35	0.30	107	450	18
Ti grade 4	0.05	0.10	0.01	0.40	0.50	107	550	15

Table 1.4: Chemical composition and mechanical properties of the different purity grade titanium [ASTM F67, F136] [66].

1.4.2 Corrosion resistance and oxide characteristics

Corrosion consists of a set of chemical reactions, often spontaneous, that alter the metallic surfaces in contact with the external environment. Corrosion occurs when the metal atoms become ionized and are solubilised as well as they combine with oxygen or other species to form a compound that flakes off or dissolves.

Chemical corrosion on metals is caused by the action of a reagent (acid, base, salt), an atmospheric agent (oxygen, carbon dioxide, water vapour, humidity) or an agent dissolved in water. The degradation process is mediated by two simultaneous reaction that transfer electrons, the oxidation and the reduction. The metal oxidation causes a release of electrons which are accepted by the reducing agent:

Oxidation reaction:
Reduction reaction:

The corrosion rate can be defined by:

- Current density [A/m^2]
- Penetration velocity [mm/year]
- Weight loss [g/m^2*day]

Environment characteristics as temperature, pressure, type of reduction agent present, and the state of metal surface strongly affect the corrosion rate and velocity. Corrosion can mainly be:

- uniform, if stretches along the entire metal surface;
- bi-metallic, if between two metals the nobler one is not affected by corrosion and therefore aids to increase the other's corrosion rate;
- in crevice;
- by pitting, cavitations or inergranular.

Titanium shows an excellent resistance to corrosion due to the fast growing of a thin oxide layer on his surface when is exposed to air. This phenomenon can be defined as 'auto-passivation'. The surface oxide layer (thickness from 2nm to 800nm) is able to slow down the oxidation of the underlying metal until a rate less than 0.03 µg/dm^2*day [67].

This characteristic of titanium can be explained by the different oxidative behaviour between 'active' and 'passive' metals (Fig 1.9). Environments with strong oxidative power have a high thermodynamic work available. An active metal dissipates kinetically a few amount of the work available and the consequence is a high corrosion rate. The passive metal, like titanium, dissipates kinetically a big amount of the work available with a consequent slow corrosion rate.

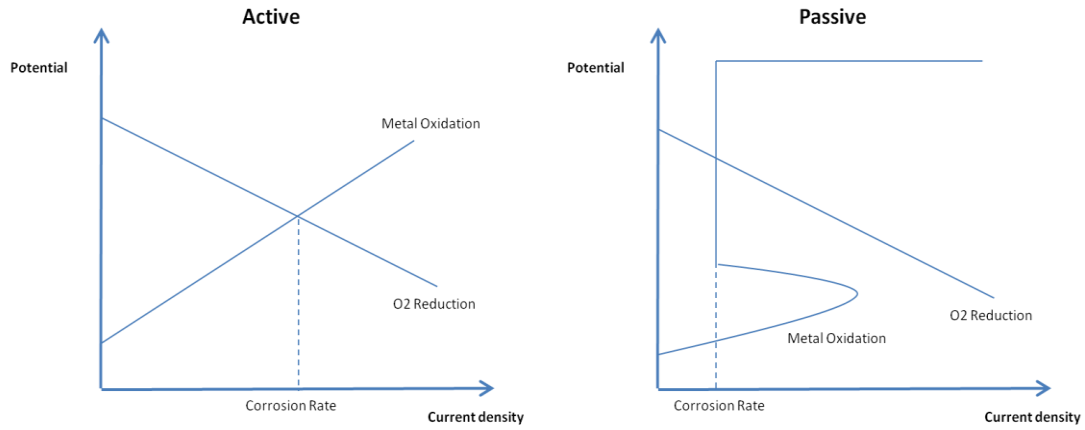

Fig. 1.9: Potential/Current density of active and passive metals [67]

In nature there are several types of titanium oxide thermodynamically stable: TiO, TiO_2, Ti_2O_3, Ti_3O_5, Ti_3O_2, Ti_3O and Ti_2O. However, the titanium oxide more stable is TiO_2 (oxidation number +4) which exists in three crystallographic forms: rutile, anatase and brookite (Fig. 1.10).

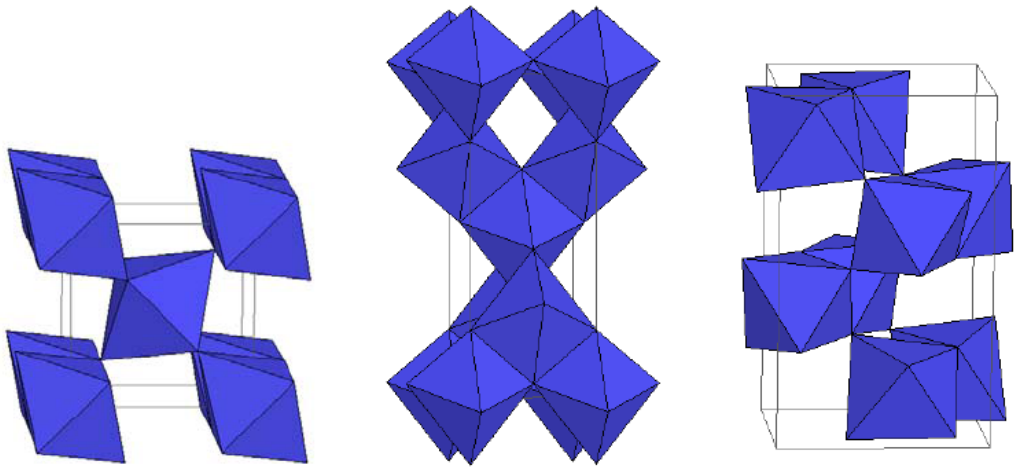

a. **b.** **c.**

Fig. 1.10: Structure of: **a.** Rutile; **b.** Anatase; **c.** Brookite.

1.4.2.1 Corrosion of titanium in biological environment

As said before, the corrosion of a material is strongly related to the characteristic of the surrounding environment. Particularly, the biological environment is very aggressive due to the high proteins concentration. Although in a protein-free solution the corrosion

resistance of titanium is similar to stainless steel 316, the stainless steel shows a makeable reactivity when incubated with protein solution *in vitro* and when implanted *in vivo* [68].A protein solution enhances the corrosion rate of stainless steel, compared to a saline solution [69]. On the contrary the corrosion rate of titanium is not increased by the presence of proteins in the surrounding environment. However the mechanical stress and the wear are involved in the corrosion velocity of titanium.

Steinemann found that in the bone tissue the pure titanium shows a less corrosion rate than titanium alloys (TiAlV). Hence, titanium alloys show a lower capacity of osteointegration than pure titanium due to their higher corrosion rates [68].

1.4.3 Titanium surfaces modifications

In the last thirty years many attempts have been made up to improve the ability of titanium implants to osteo-integrate. Particularly, several types of treatments have been developed to give particular properties to the titanium surfaces in light of the factors involved in the osteointegration process. The main treatments can be categorized as:

- **Physical-Chemical** treatments direct to improve the surface macro-roughness which enhances the adhesion and proliferation of the bone synthesizing cells.
- **Chemical-electrochemical** treatments direct to improve the surface micro-roughness and to modify the chemical composition in order to stimulate the adhesion and the ostheogenic activity of the bone cells.
- **Chemical-biological** treatments direct to produce functional groups (i.e. protein coating or bioactive compounds) in order to favour the surface reconnaissance by the cells and stimulate the regeneration process.

In recent times, research is concentrating its efforts on development of 'biomimetics' surfaces on titanium using biological or chemical and electrochemical treatments. The purpose of this approach is the production of surfaces that 'mime' the biological characteristics of bone tissue in order to promote the recognition and to stimulate an effective regeneration process *in vivo*. The use of chemical and electrochemical treatments in comparison to biological treatments resulted in the obtainment of biomimetic surface of better quality and reproducible conditions. Furthermore, they favour a simpler industrial

processing since have the advantage, unlike the biological treatments, of being free of potential biological biohazard or storage problems [67].

Treatments with biomimetic aim such as sand-blasting, plasma nitriding, acid etching, titanium vacuum plasma, titanium micro-filaments, and titanium micro-beads were applied on the surface of prostheses to improve the ability of implant to bind the bone [70,71]. However, a large portion of the titanium prosthetes market is nowadays represented by hydroxylapatite (HA)-coated implants. The most commonly techniques applied to perform HA deposition is the plasma spraying that permits to coat titanium surfaces with either HA or calcium-phosphate layer (50μm of thickness). The main reason for covering the surface of implants with a ceramic material is the rapid formation of new bone on their surfaces from the early stage of implantation. These coatings were shown to be very effective in improving the implant/bone bonding reducing the formation of fibrous tissue at the interface as the HA layer 'mimes' the bone environment and favour the bone cells reconnaissance [72]. The plasma spray process uses an electrical arc to melt and spray materials onto a surface. A DC electric arc is struck between two electrodes, while a stream of (mixed) gases passes through this arc. This results in an ionized gas of high temperature up to 30000°C, with a highs-peed (near to sound speed) due to the large expansion resulting from this temperature increase. Hydroxylapatite powder is suspended in a carrier gas stream which is fed into the plasma flame. The plasma has two effects: first, melt the HA a particle due to its high temperature; second, its high-speed causes a strong acceleration on the melted particles that are deposed on the substratum surface where solidify quickly [73] (Fig. 1.11).

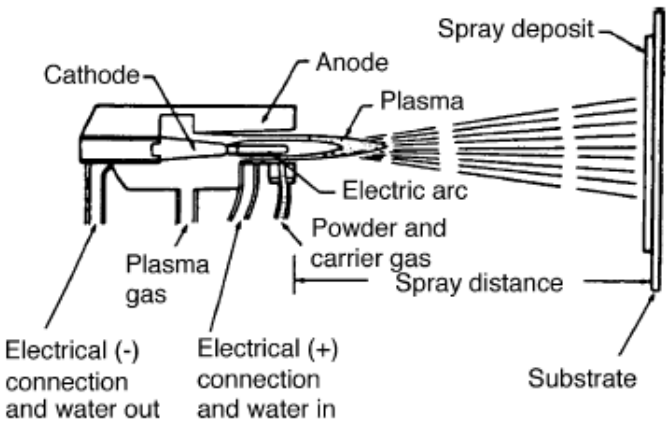

Fig. 1.11: Scheme of Plasma spray technique [71].

Unfortunately, such coatings have shown long-term failures related to the weak adhesion of the HA coating to the metal substrate and to the dissolution rate of the coatings, which depends on the degree of cristallinity of the layer. The HA layer delamination causes a discontinuity between implant and surrounding bone resulting in decreasing of mechanical properties; the dissolution causes a debris release resulting in inflammatory response. These results induced researchers to look for alternative deposition methods of ceramic coatings such as electro-deposition, magnetron sputtering and ion beam sputtering [74].
Among the chemical and electrochemical biomimetic techniques, the most innovative are the Redepenning method [75], the Kokubo method [76] and the anodic spark deposition (ASD). The ASD technique allows the modification of titanium oxide composition in order to optimizing the bone regeneration process and the osteointegration by favour at the same time a selective protein adhesion and the osteoblasts proliferation.

1.4.4 Anodic Spark Deposition (ASD)

Anodic Spark Deposition (ASD) is an electro-chemical technique that can be used to achieve micro-porous morphology on titanium and titanium alloys surfaces whilst modifying their surface oxide film [77]. The titanium sample involved in the ASD treatment represents the anode (positive electrode) of an electro-chemical circuit constituted by two electrodes and an electrolytic solution. When the circuit is alimented, a current flow traverses the sample due to oxidation and reduction reactions on the electrodes and due to the presence of the conductive ionic solution. In particular, the occurring reactions are:

- **Ti/TiO_2 interface:**

- **TiO_2/electrolytic solution:**
    - Oxygen ions react with titanium generating TiO_2.
    - Gaseous oxygen is released and remains in correspondence of electrode.

- **At both the interfaces:**

The red-ox reactions cause a release of oxygen and titanium ions that, driven by the electric field, lead to oxide film formation on the anode surface. The oxide will carry on growing as long as the electric field is strong enough to drive the ions through the film. The oxide film will increase its thickness and its growth will be almost linearly dependent to the applied voltage until the breakdown of the film occurs. When the voltage applied between the anode and the cathode exceeds the dielectric strength of the anodic coating, a dielectric breakdown of the layer occurs. In the so-called "build-up step", the dielectric breakdown is characterized by a large number of small sparks, which appear to move across the surface of the anodized titanium [74]. The number of sparks and the current flowing through the sample decrease exponentially when the ASD coating has completely covered the surface. The sparks cause punctual micro-melting of the oxide layer resulting in a remixing of titanium substrate, titanium oxide and chemical species present in the electrolytic solution. Consequently, the final oxide layer is characterized by a micro-porous morphology and is enriched with chemical species of the electrolytic solution. The sparking may be associated with a discharge effect generated by gas bubbles at the surface of the anode [78]. Moreover, the presence of oxygen and hydrogen atoms at the anode strongly influences the formation of the anodic film. Usually, to avoid or minimize the formation of bubbles, the solution is maintained stirred during the process.

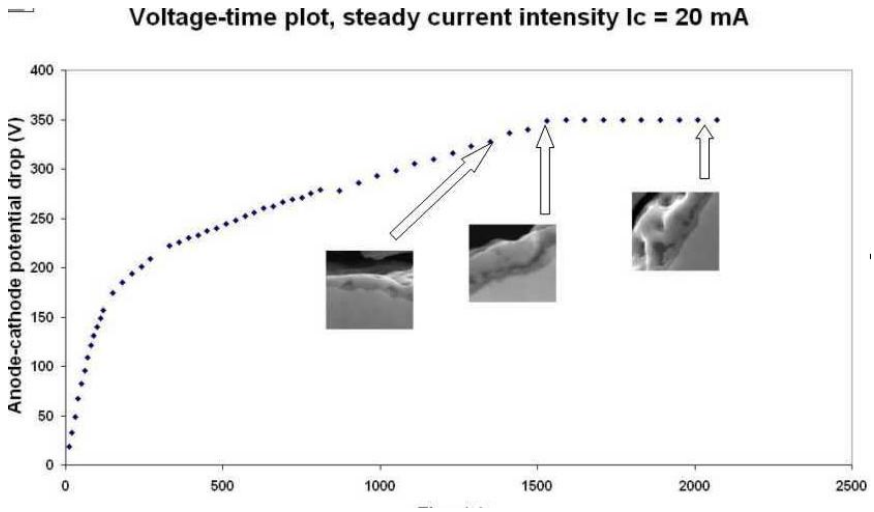

Fig. 1.12: SEM picture of a section of a c.p. grade 2 titanium during ASD treatment [74].

The morphological and chemical properties are principally related to:

- **Electrical variables**: in galvano-static condition, film thickness is a function of the total current passed per area unit (Fig 1.12); in tension-static condition, higher voltage means thicker oxide [74,77]. Furthermore, current density has effects on porosity and roughness of the oxide layer. Usually, the diameter of the pores and the roughness of the film increase with increasing current density (Fig. 1.13) [74,79].

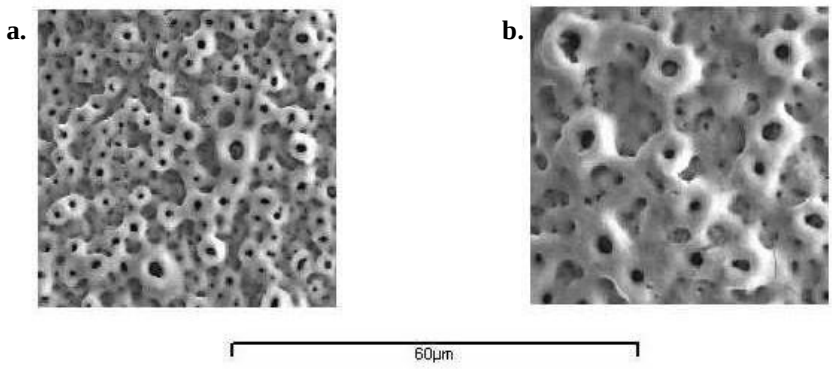

Fig. 1.13: SEM picture of the same ASD treatment at: **a.** 20mA; **b.** 60mA [74].

- **Electrolytic solution:** the chemical composition of oxide surface is directly influenced by the electrolytic solution composition. Furthermore, as the solution contains ionic species, the precipitation must be avoided in order to improve the reproducibility of the process. To reduce or stabilize the precipitation of chemical species, the electrolytic solutions can be enriched with stabilizing compound (i.e. coordination compound or chelating agents) [80].

Since ASD technique directly acts a modification of the pre-existing oxide layer and don't carry out a film deposition, it permits a better interaction between oxide and underlying substratum resulting in an increased mechanical stability of coating [81,82].

A biomimetic treatment based on the ASD technique was recently patented by Politecnico di Milano [83]. The proceeding is based on two different phases: an ASD treatment followed by alkali etching. The resulting coating is an oxide layer characterized by micro-roughness, micro-porosity and anatase cristallinity form. Furthermore, the patented electrolytic solution allows enriching of coating with chemical species known to enhance the osteointegration of the implants (i.e. Ca, P, Na, Si). Consequently, titanium coatings

realized by this new treatment have excellent characteristics of bioactivity and osteointegration.

1.5 Aim of the work

The aim of this work is to develop new biomimetic treatments on titanium characterized by antibacterial properties and a high osteointegrative potential.
Particularly, the purpose is to obtain antibacterial coatings using different antimicrobial agents such as silver and gallium which are widely known for their bactericidal properties. The technique chosen to reach this goal is the Anodic Spark Deposition (ASD) which allows to obtain homogeneous coatings characterized by a good stability.
The starting-point of this work is the ASD silicon-based osteointegrative treatment recently developed and patented by Politecnico di Milano [83,84], which is nowadays used in clinical practice (dental field) with excellent results. Changing the electrolytic solution used for this osteointegrative treatments with appropriate bactericidal agents, we try to combine the excellent osteointegrative potential of the biomimetic treatment and the antimicrobial effect induced by the bactericidal agents. Finally we perform the chemical-physical and biological characterization of the obtained treatments.

2. Materials and Methods

In this chapter will be described all the procedures applied to modify the titanium surface in order to confer osteointegrative and antibacterial properties. Following the preparation procedures, the techniques used for the chemical, physical and biological characterization will be deepened.

2.1 Materials

The procedures applied for the preparation of a ceramic coating on titanium with osteointegrative and antibacterial properties is based on a recent patent of Politecnico di Milano [83] that was used during the present study as a starting point for the methodology and comparison of the biocompatibility performances.

2.1.1 Titanium samples

All the samples used for the chemical, physical and biological characterization were obtained from a plate of pure titanium grade 2 for biomedical use provided by Torresin Titanio Metalli s.r.l, Limena (PD) and had circular shape with diameter 12mm. Only for the oxide adhering tests were used samples of rectangular shape (20mm x 50mm), obtained from the same plate. Before undergoing any treatments, all the samples were cleaned by ultrasonic rinsing (Elma Elmasonic S 60/H, Deutschland) in acetone (Carlo Erba Reagenti. 401002) for 10 minutes and afterwards in water *Millipore* for further 10 minutes. Finally the samples were dried in a thermostat oven at 37°C for 2 hours.

2.1.2 Anodic Spark Deposition treatment

In order to confer antibacterial and osteointegrative properties to titanium coatings, were carried out different anodization treatments modifying electrolytic solutions, and the

electrical setting such as the final voltage and the current intensity; these settings represent the process variables and are directly related to the chemical composition, the physical and morphological properties of the resulting coatings. The experimental setup is represented by the electrolytic cell shown in figure 2.1.

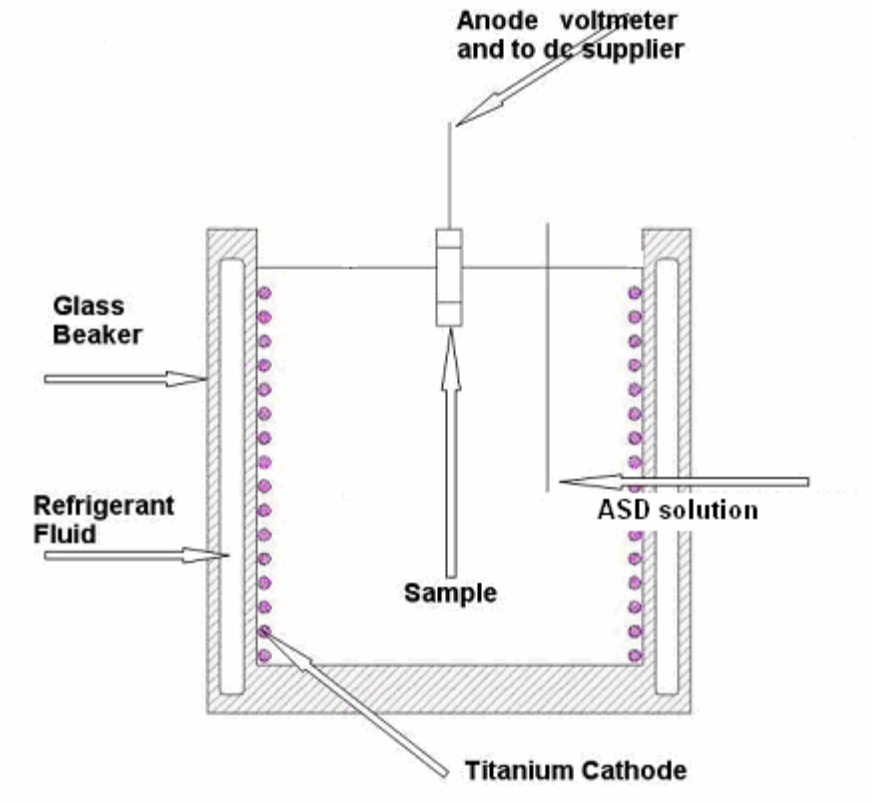

Fig. 2.1: Scheme of the electrolytic cell.

The electrolytic solution is poured in a jacket baker where a refrigerating fluid runs. The temperature of refrigerant fluid is automatically controlled and set to 0 °C. A cylindrical titanium grade 2 (same grade of the samples) net is used as cathode and is placed in the inner of the beker, adhered to the wall, and connected with the positive pole. The titanium samples represent the anode of the cell, are connected to the negative pole and are immersed in the electrolytic solution by means of a multi-support designed *ad hoc* to permit the contemporaneous treatment of several samples.

2.1.2.1 Electrolytic solutions

To prepare the electrolytic solutions were used the reagents shown in table 2.1, the antibacterial species shown in table 2.2 and the chelating compounds shown in table 2.3. The chelating agents were used to avoid the massive precipitation of silver and gallium salts in the electrolytic solution. Indeed, the event of precipitation may reduce the silver and gallium embedding into the growing oxide layer during the anodization treatment.

Reagents	Chemical Formula	Molecular Weight [g/mol]
Sodium Silicate (Carlo Erba Reagenti, 373908)	$Na_2SiO_3*2H_2O$	182.13
Beta-glycerhophosphate (β-GP) Disodium Salt Pentahydrate (Fluka, 50020)	$C_3H_7Na_2O_6P*5H_20$	306.12
Calcium Acetate (Fluka, 21052)	$C_4H_6CaO_4*H_2O$	158.7
Sodium Hydroxide (Fluka, 71690)	NaOH	40

Tab. 2.1: Reagents used.

Antibacterial Agents	Chemical Formula	Molecular Weight [g/mol]
Silver Nanoparticles (Sigma-Aldrich, 576832)	Ag	107.87
Silver Nitrate (Sigma-Aldrich, 204390)	$AgNO_3$	169.87
Silver Acetate (Sigma-Aldrich, 204374)	CH_3COOAg	166.91
Gallium Nitrate (Sigma-Aldrich, 289892)	$Ga(NO_3)_3*H2O$	225.74

Tab. 2.2: Antibacterial agents.

Chelating Compounds	Chemical Formula	Molecular Weight [g/mol]
L-cysteine (Sigma-Aldrich, W326305)	$HSCH_2CH(NH_2)CO_2H$	121.16
Oxalic Acid Dihydrate (Sigma-Aldrich, 75699)	$HO_2CCO_2H*2H_2O$	126.07
Ethylenediaminetetraacetic acid disodium salt dihydrate (Sigma-Aldrich, E5134)	$C_{10}H_{14}N_2Na_2O_8 \cdot 2H_2O$	372.24

Tab. 2.3: Chelating Compounds.

Starting from the SUM solution were prepared all of the different electrolytic solutions (Tab. 2.4). The SUM solution was according to the following steps:

$Na_2SiO_3*2H_2O$ 0.03M, β-GP 0.1M, $C_4H_6CaO_4*H_2O$ 0.3M, NaOH 0.036M in distilled water; were used 2 intermediate solutions to prepare 1L of SUM solution:

- 5.464g of $Na_2SiO_3*2H_2O$ and 1.457g of NaOH in 600 ml of distilled water; the solution was stirred for 30 minutes and let stand for the following 10 min.
- 47.45g of $C_4H_6CaO_4*H_2O$ and 30.612g of β-GP in 400 ml of distilled water constantly stirred.

The first solution was gradually mixed in the second solution and then constantly stirred for 1 hour. The result was a milky-looking solution. Before its use in the ASD treatment, was let stand for 24h to permit a total salts solubilisation [84].

The addition of antimicrobial and chelating agents occurred in a complete solubilised SUM solution therefore after the 24h of standing. The table 2.4 shows the scheme of all the electrolytic solutions prepared.

Solution Label	Antimicrobial Agent	Chelating Agent	Stirring Time [h]
SUM AgNPs	Silver Nanoparticles - 3.0g/L	-	1
SUM ACAG 1	CH3COOAg - 0.00003M	-	2
SUM ACAG 2	CH3COOAg - 0.0005M	-	2
SUM ACAG 3	CH3COOAg - 0.004M	-	2
SUM NITAG 1	AgNO3 - 0.00003M	-	2
SUM NITAG 2	AgNO3 - 0.0005M	-	2
SUM NITAG 3	AgNO3 - 0.004M	-	2
SUM NITAG EDTA	AgNO3 - 0.004M	EDTA - 0.6M	12
SUM NITAG CIST	AgNO3 - 0.004M	L-cysteine - 0.002M	12
SUM NITGAL	Ga(NO3)3 - 0.004M	-	2
SUM NITGAL EDTA	Ga(NO3)3 - 0.004M	EDTA - 0.153M	12
SUM NITGAL CIST	Ga(NO3)3 - 0.004M	l-cysteine - 0.006M	12
SUM NITGAL OSS	Ga(NO3)3 - 0.004M	Oxalic Acid - 0.306M	12

Tab. 2.4: Electrolytic solutions prepared.

2.1.2.2 Parameters of ASD treatments

Programmable DC power supply (Eutron BVR 1200-500-1.5 Rivoli, Italia; voltage resolution 0.03%, current intensity resolution 0.05%) was used to obtain the coating. Using the electrical setting it was possible to modify the current intensity applied to the electrolytic solution and the final voltage necessary to reach during the anodizing process.

Current intensity and final voltage are directly related to the properties of the resulting oxide layers in terms of titanium oxide layer thickness, surface chemical elements and morphological aspect. All the different anodization treatments were carried out in galvanostatic conditions until the achievement of the set final voltage and subsequently in tensiostatic conditions during current intensity fall until 20% of the set value.

2.1.3 Chemical Etching

The titanium samples treated with ASD often shown an oxide layer characterized by micro-porous morphology and enriched with the chemical species present in the electrolytic solution. The chemical and morphological properties of the oxide layers can be modified by chemical etching, a treatment that allows to obtain the variation of their concentration in the superficial oxide layers. Furthermore, this treatment favours the surface hydroxylation and the surface exposition of charged chemical groups which can act as nucleation sites for several reactions [85]. Hot chemical etching was carried out in NaOH 5M (Fluka, 71690) at temperature of 60±1 °C for 2 hours. After the treatment, the samples were washed in water Millipore and then dried in oven at 37 °C.

2.1.4 Experimental matrix

The table 2.5 shows all the treatments carried out during this work. For each treatment are indicated the current intensity and the final voltage set during the anodization process. The label Na after the treatment label means that was carried out the post-chemical etching according to par 2.1.3.

Treatment Label	Current Intensity [mA/cm2]	Final Voltage [V]	Chemical Etching
SUM	10	295	
SUM Na	10	295	•
SUM AgNPs	10	295	
SUM AgNPs Na	10	295	•
SUM AgNPs 1	10	350	
SUM AgNPs 2	8	295	

SUM ACAG 1A	10	295	
SUM ACAG 1A Na	10	295	•
SUM ACAG 1B	10	350	
SUM ACAG 1C	20	350	
SUM ACAG 1D	20	400	
SUM ACAG 2A	10	295	
SUM ACAG 2A Na	10	295	•
SUM ACAG 2B	20	350	
SUM ACAG 2C	30	400	
SUM ACAG 3A	30	295	
SUM ACAG 3A Na	30	295	•
SUM ACAG 3B	30	350	
SUM ACAG 3C	30	400	
SUM NITAG 1A	10	295	
SUM NITAG 1A Na	10	295	•
SUM NITAG 1B	10	350	
SUM NITAG 1C	20	350	
SUM NITAG 1D	20	400	
SUM NITAG 2A	10	295	
SUM NITAG 2A Na	10	295	•
SUM NITAG 2B	20	350	
SUM NITAG 2C	30	400	
SUM NITAG 3A	30	295	
SUM NITAG 3A Na	30	295	•
SUM NITAG 3B	30	350	
SUM NITAG 3C	30	400	
SUM NITAG EDTA 1	10	295	
SUM NITAG EDTA 2	20	295	
SUM NITAG CIST	10	295	
SUM NITAG CIST Na	10	295	•
SUM NITAG CIST 1	10	350	
SUM NITGAL 1	10	295	
SUM NITGAL 1 Na	10	295	•
SUM NITGAL 2	10	350	
SUM NITGAL 3	20	350	
SUM NITGAL 4	20	400	
SUM NITGAL EDTA 1	10	295	

SUM NITGAL EDTA 2	10	325	
SUM NITGAL CIST	10	295	
SUM NITGAL CIST Na	10	295	•
SUM NITGAL CIST 1	10	350	
SUM NITGAL OSS	10	325	
SUM NITGAL OSS Na	10	325	•
SUM NITGAL OSS 1	10	295	
SUM NITGAL OSS 2	10	350	

Tab. 2.5: Experimental matrix.

2.1.5 Choice of samples

The samples obtained by SUM Na, SUM NITAG CIST, SUM NITGAL CIST and SUM NITGAL OSS treatments were chosen for the morphological, physical, chemical and biological characterization. The preliminary screening was based on the results obtained by SEM and EDS analysis; the surface chosen have shown a surface morphology more uniform and repeatable and a chemical composition more suitable to reach the purpose of the work.

The SUM Na treatment, was used as control in all the characterizations. The table 2.6 shows the time in minutes necessary for the anodization process (average time ± standard deviation required to anodize 1 sample, n=30).

	SUM Na	SUM AgNPs	SUM NITAG CIST	SUM NITGAL CIST	SUM NITGAL OSS
ASD Duration [min]	12.86±1.92	10.94±0.81	11.50±0.47	11.66±0.23	10.1±1.10
Etching Duration [min]	120	-	-	-	-

Tab. 2.6: Time necessary to complete the treatments.

2.2 Methods

The chemical, physical and morphological characterizations of the surfaces obtained by ASD treatments were investigated by means of the following techniques:

- Scanning electron microscopy (SEM);
- Elemental dispersive X-ray spectrometry (EDS);
- X-ray diffractometry (XRD);
- Laser profilometry;
- Contact angle measurements;
- Glow discharge optical emission spectroscopy (GD-OES);
- Inductively coupled plasma optical emission spectrometry (ICP-OES);
- TiO_2 delamination tests

2.2.1 SEM and EDS

Scanning electron microscopy (SEM) is used to investigate the morphology of samples at high magnification (magnification ranging from 20X to approximately 30,000X, spatial resolution of 50 to 100 nm). The scanning electron microscope (SEM) uses a focused beam of high-energy electrons to generate a variety of signals at the surface of solid specimens. The signals that derive from electron-sample interactions reveal information about the sample including external morphology, chemical composition, crystalline structure and orientation of materials making up the sample.

The most common electron source is the tungsten filament. This consists of a bent piece of fine tungsten wire that is similar to the filament present in an incandescent lamp. The filament is connected to a source of current and electrons are passed through the wire. As this happens the filament heats up and electrons begin to be emitted from the tungsten atoms. In this type of gun the outside source of electrons and the heating source are one in the same. Electrons are preferentially emitted from the bent tip of the filament and produce a coherent source of electrons. Accelerated electrons in an SEM carry significant amounts of kinetic energy, and this energy is dissipated as a variety of signals produced by electron-sample interactions when the incident electrons are decelerated in the solid sample. These signals include secondary electrons (that produce SEM images), backscattered electrons

(BSE), diffracted backscattered electrons (EBSD, used to determine crystal structures and orientations of minerals), photons (characteristic X-rays that are used for elemental analysis and continuum X-rays), visible light (cathodoluminescence-CL), and heat. Secondary electrons and backscattered electrons are commonly used for imaging samples: secondary electrons are most valuable for showing morphology and topography on samples and backscattered electrons are most valuable for illustrating contrasts in composition in multiphase samples (i.e. for rapid phase discrimination). The X-rays detection is used by EDS to identify the chemical species present on surfaces. Every different element after being excited emits x-rays at particular frequencies. Each element emission depends on its atomic number. X-ray generation is produced by inelastic collisions of the incident electrons with electrons in discrete orbitals (shells) of atoms in the sample. As the excited electrons return to lower energy states, they yield X-rays that are of a fixed wavelength (that is related to the difference in energy levels of electrons in different shells for a given element). Thus, characteristic X-rays are produced for each element in a material that is "excited" by the electron beam. Although EDS is a qualitative chemical analysis and is not a true quantitative method, some semi-quantitative information can be obtained. Analysis can be performed at different voltage to obtain data at different degree of surface depth. For example, from the intensity of the emission it is possible to draw information about the percentage of a particular element within a heterogeneous sample. SEM and EDS analyses are considered to be "non-destructive"; that is, X-rays generated by electron interactions do not lead to volume loss of the sample, so it is possible to analyze the same materials repeatedly [86].

2.2.1.1 SEM and EDS analyses

Samples surfaces were analyzed by three different SEM, ZEISS-EVO 50 EP ables to work both in air and in high vacuum (10^{-6} mmHg), ZEISS-EVO LS-15 and Cambridge – Stereoscan 360 ables to work only in high vacuum (10^{-5} mmHg). The samples were analysed at different magnifications after the surface treatments, the TiO_2 delamination tests and after 48hours and 72hours of cell culture.

The EDS analysis was carried out on 500X and, in some cases, on 5kX magnification (Oxford, Inca energy 200, Politecnico di Milano) that correspond to micrometric surface

portions of about 170μm x 230μm and 17μm x 23μm respectively. The samples were analyzed with EDS after the surface treatments.

2.2.2 X-ray diffractometry (XRD)

XRD is an analysis instrument used to investigate the molecular composition of materials, in particular the crystalline materials. The analysis is performed hitting the surface of a sample with an X-rays beam and reading the diffraction pattern of the secondary beam. This analysis method was developed for assessing the composition of crystalline powders. Recently, it has been adapted to the analysis of solid surfaces and in particular of thin films (TF-XRD). However, the crystalline samples with small dimension crystallites are still the best type of samples to be investigated with this technique. Therefore, this technique is very useful to assess the different degree of crystallinity of a material. An X-ray beam with an established wave-length usually in the range of inter-atomic dimensions (0.1-100Å) is produced by an emitting source. This beam is shot on the surface to be analysed and hits the surface with several different incidence angles in a pre-established range. The diffracted beam is detected by a complicated system whose output is a diffraction pattern whose main features are the peak intensities and the diffraction angles. Diffraction angles and peak intensities give information about the chemical composition and the geometrical characteristics of the crystal. Many other factors contribute to the final spectrum and basically the analysis is achieved comparing unknown pattern to known spectra. Basically from a theoretical point the lattice properties (inter-planar distances d) can be assessed applying the law of Bragg:

Where d is the distance among crystallographic planes, is the incidence angle, is the reflection order and the wavelength of the incidence radiation. Peak intensities are plotted as function of the angle 2 [86].

2.2.2.1 XRD analyses

In the present study the parameters of the XRD diffractometer (Philips PW 1710) were set to 40KV of voltage and 40mA of current intensity. The angular range investigated was 20°-70° with a scanning speed of 2°/min. The analysis was performed at a source wavelength of 1.54056 Å using a Ni-filter Cu Kα1 radiation.

2.2.3 Laser profilometry

Investigating the morphology and in particular the roughness of materials is important to obtain information about the effect of the different degree of roughness and texture on the behaviour of the adhering cells. The laser profilometry technique gives information about the 'peaks' and 'valleys' present on the sample surface; is based on the signal produced by a spot laser beam released by a source and reflected by the material surface under a scanning mode. The reflected beam coming back to the source covers different optical paths according to the different morphology of the surface. The optical signals are processed by software and many different parameters related to different surface properties can be acquired and analysed in order to characterise accurately the surface texture, roughness and morphology. The limitations of this technique are the lateral resolution (1μm) due to the width of the laser beam, and the vertical resolution (50nm) due to the instrument precision.

The parameters used to quantify the surface roughness are (Fig 2.2) [87]:

- **Ra:** in a tract L of profile (base line), a mid line of profile is expressed by:

  Where y is the high of real profile and x is the orthogonal axis orientated along the direction of base line. Ra parameter represents arithmetical average of absolute values of real profile y deviation from base line and is expressed by:

  –

  Ra is expressed in micrometers.

- **Rt or Ry:** is the distance between the highest peak and the lowest valley along the entire sample. Is expressed in micrometers.
- **K:** is the Kurtosis and provides information about the profile morphology: K>3 means a sharp morphology of the surface profile; K<3 means a bevelled morphology of the surface profile.
- **Rmax:** distance in micrometres between two parallel lines tangent to the highest peak and the lowest valley within the base line.
- **Sk:** provide information on relative width of peaks and valleys; Sk=0 means a symmetric distribution of peaks and valleys, Sk>0 a ragged profile; sk<0 means a profile characterized by *Plateu* and depth valleys.

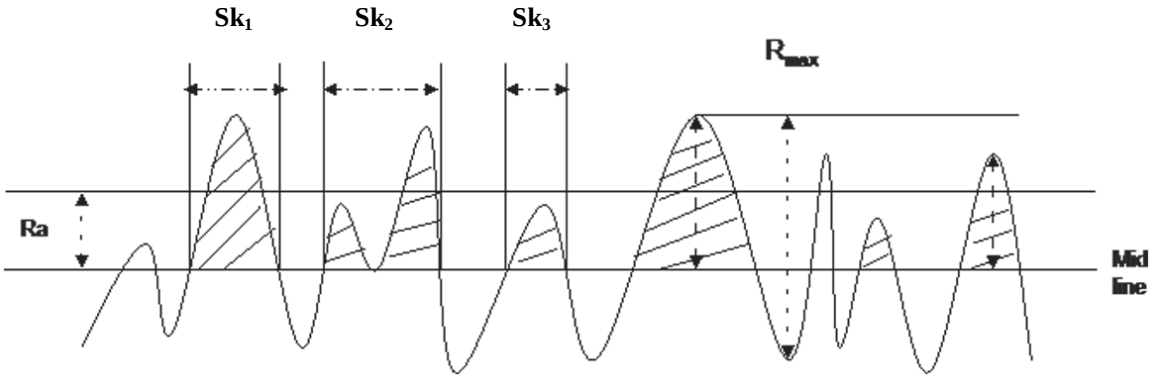

Fig. 2.2: Main Roughness Parameters [87]

2.2.3.1 Profilometric analyses on samples

The profilometric analyses were carried out with a laser profilometer (UBM Microfocus, 5600). Each sample underwent 3 measures on base lines of 4mm and points density of 500/mm.

2.2.4 Contact angle measurements

Measurements of contact angles permit to determine the wettability properties of surfaces. When a droplet of liquid is placed on a flat horizontal solid surface, the solid-air and liquid-air interfaces come together under the static contact angle (CA), θ (Fig. 2.3).

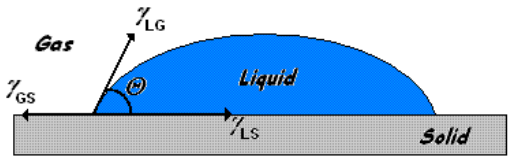

Fig. 2.3: liquid droplet in contact with a solid surface.

The surface is considered hydrophilic if $0<\theta<90°$ while is considered hydrophobic if $\theta>90°$. The value of θ can be determined from the Young's equation, which express the minimization of the total free energy of the system:

Where , and are respectively liquid-air, solid-air and solid-liquid interface free energies. Both surface chemistry (i.e. functional groups) and morphology contribute to determine the wetting behaviour of a material.

To measure the contact angle (static or dynamic) is used a device composed by an optic bench. A light source and an optical detector are used to take pictures of drops deposed on sample by a syringe perpendicular to the sample surface. Particular software elaborates the information from the picture and calculates the relative contact angle.

2.2.4.1 Samples surfaces analyses

The contact angle measurements were carried out by an optical device (Dataphysics Instruments Mod. OCA 15 plus) and a related software (32-bit software SCA20); was used a water drop of a 2µl of volume, deposed in 2µl/s on the samples surface. For each surface were performed 3 different water drop depositions at room temperature.

2.2.5 GD-OES

Glow discharge optical emission spectrometry (GDOES) is a method for elemental analysis of solids. Both the bulk analysis of homogeneous samples and the depth profile analysis of coating–substrate systems and surface-modified materials are possible. Positively charged argon ions from radio frequency plasma (adjacent to the sample

surface) are accelerated and bombard the surface of the negatively-polarized sample. When the argon-ions collide the surface, surface material is evaporated and emits light due to excitation by the surface near plasma condition. The emitted light is element-specific and used for semi-quantitative to quantitative elemental analysis as a function of time (depth). Sputtering rates are in the range of 10-50 nm/s. The analyses are carried out in vacuum environment and the detection limits are in the range of few ppm. Principal disadvantages are the high sample damaging and the low spatial resolution (few mm^2). The main advantage of this technique is the continuous profiling of chemical (elemental) composition as a function of depth up to 100 μm [88].

2.2.5.1 GDOES analyses

All the samples were analyzed after the anodizing treatments by Horiba Jobin-Yvon RF-GDOES (Politecnico di Milano). The analyses were carried out setting a voltage of 700 V, an argon pressure between 2.3 and 3.6 hPa and until a superficial depth of 20 μm.

2.2.6 ICP-OES

The ICP-OES analysis permits the simultaneous detection of many chemical elements (up to 70) even if in a very low concentration (under 1μg/L).

In the inductively coupled plasma optical emission spectrometry the sample to be analyzed is usually a liquid. Through a nebulisation process, usually carried out by pneumatic or ultrasonic nebulizers, the liquid sample is converted in aerosol phase (finely dispersed droplets). Afterwards the aerosol is injected in a plasma environment where atoms and ions are excited and emit their characteristic radiation in different wavelengths. The resultant polychromatic emission is scanned in individual wavelength voiding the detection and measure of each single emission without interference. The following conversion of the single detections in electrical signals allows the quantification of the relative concentrations (Fig. 2.4) [89].

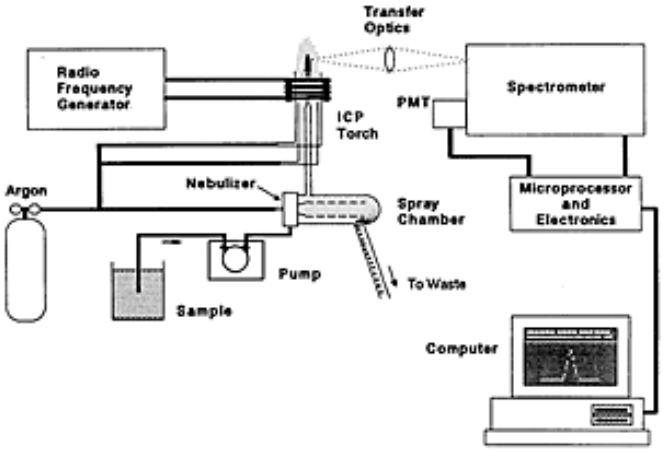

Fig. 2.4: ICP-OES working scheme.

2.2.6.1 ICP-OES analysis

The silver and silicon release from SUM Na, SUM AgNPs and SUM NITAG CIST surface were investigated by ICP-OES analysis. Five samples per each treatment were put in tubes containing 50 mL of PBS (phosphate buffered solution). The tubes were left at 37 °C for 7 days, in constant gentle shacking (Stuart Orbital Incubator SI150, T=37 °±1 °, rpm=40, University of Brighton) to avoid redeposit of silver and silicon eventually released. After 6 hours, 24 hours, 5 days and 7 days was taken a sample of 5 mL from each tube then analyzed with ICP-OES device (Perkin–Elmermodel ELAN-DRC-e, University of Brighton).

2.2.7 TiO_2 delamination tests

To analyze the oxides adhesion to the underlying substratum, all the samples were subjected to flexion stress of 30 °. To carry out these tests, was necessary apply the anodization treatments of interest on titanium grade 2 plates of rectangular shape (20mm x 50mm). Then, a 3-point flexure test was carried out on the treated rectangular plates; this experimental setup allowed the imposition of a 30 °flexion (Fig. 2.5, angle α=30 °) on the plates.

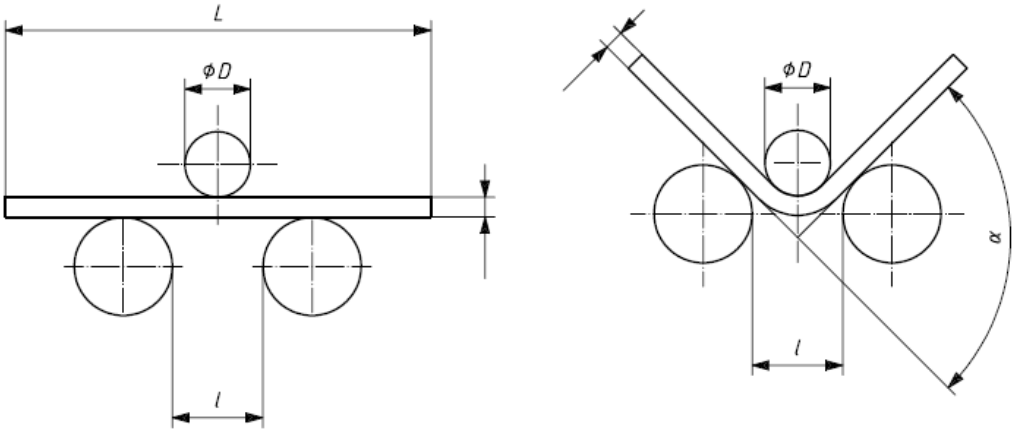

Fig. 2.5: 3-point flexion experimental setup.

2.3 *In vitro* Tests

In the next pages will be described all the procedures applied to perform the biological characterization of the samples chosen at par 2.1.5 (SUM Na, SUM AgNPs, SUM NITAG CIST, SUM NITGAL CIST and SUM NITGAL OSS) in order to assess their *in vitro* biocompatibility properties.

The *International Standard Organization* has defined some guidelines useful to define the biomaterials biocompatibility that consist in *in vitro* biological assay (cytocompatibility assays and protein adhesion), *in vitro* non-biological assays (mechanical characterization and corrosion) followed by *in vivo* assays (blood interactions, genotoxicity, systemic toxicity, etc.) [40]. Even if the *in vitro* tests provide information about the cell response to biomaterials, a complete biological characterization cannot neglect the *in vivo* tests that deepen the reaction of the body system. Information such as topical and systemic reactions, inflammatory response, and carcinogenicity cannot be obtained by in *vitro* tests that nevertheless represent the preliminary biological characterization. Indeed the cell cultures on a biomaterial provide important information about its cytotoxicity, and its capacity to favour the cells adhesion, proliferation and differentiation. Furthermore the *in vitro* techniques allow easy control of chemical-physical conditions, are more specifics and less expensive than the *in vivo* tests.

In this work, the *in vitro* tests carried out are where addressed to exclude the anodised material cytotoxicity on fibroblasts (3T3) and osteoblasts (Saos2) cells and the relative proliferation using HPI staining (Hoesch Propidium Iodide staining assay), evaluating the cell morphology by SEM (Saos2) and of the cytoscheleton conformation by phalloidin staining (Saos2). The biological characterization took place at the University of Brighton, School of Pharmacy and Biomolecular Science (Brighton, UK).

2.3.1 Samples sterilization

The samples, placed in a 24 wells tissue culture plate (TC) (Nunc Tm), were disinfected three times per each side with 1 ml of pure ethanol (Fisher); after the removal of ethanol with a sterile glass Pasteur (Nunc Tm) and total evaporation of residues, the samples were

sterilized using UV irradiation (235 nm; 30 minutes per side) in class II biological hood (Esco Air Strem, Class II BSC).

2.3.2 Cell cultures

The cell lines used to assess the biological characteristics were:

- **3T3** Murine Fibroblasts (Eurpoean Collection of Animal Cell Culture, ECACC);
- **Saos2** Osteoblasts, obtained by human osteosarcoma (ECACC).

2.3.2.1 Culture and seeding of 3T3 Fibroblasts

Culture

After thawing, the 3T3 cells were cultured in T75 flasks (Nunc Tm) with Dulbecco's Modified Eagle Medium DMEM low glucose (1g/L) with 584mg/L of L-Glutamine (PAA Cell Culture Company, E15-806), containing 15% of Fetal Bovine Serum (FBS) (PAA, A15-104) in a cell culture incubator (Heraeus, Hera Cell) set at 37 °C, 95% relative humidity and 5% V/V of CO_2.

Seeding on samples

When cells have reached the confluence, the culture medium was removed from the flask and replaced with 5 mL of Trypsin solution (Trypsin EDTA (1x) 0.05%/0.02% in DPBS, PAA, L11-OQ4); the flask was incubated for 4-5 minutes to allow the total detachment of cells. Afterwards was added 10 mL of medium to stop the trypsin action and the cell was transferred in a 30 mL tube (Corning) then centrifuge for 5 min at 2000 rpm. The result was a pellet of cells in the bottom of tube that, after the removal of the surnatant with a sterile glass Pasteur (Nunc Tm), was re-suspended in 1 mL of medium. 10 μL of the cell re-suspension were diluted in 90 μl of DMEM in an eppendorf in order to make a dilution 1:10; 10 μL of the diluted suspension were loaded onto a Neubauer haemocytometer to perform the cell counting. Was then calculated the amount of cell suspension containing the number of cells necessary for the seeding: 6.1μL of cell suspension containing $3*10^4$ cells were transfer on the surfaces of samples sterilized (2 samples per each treatment in 2

plates). 1mL of warm DMEM was added to all the wells containing cells avoiding shear stress on the adhering cells and the TC-plates were finally incubated.

2.3.2.2 Culture and seeding of Saos2 Osteoblasts

Culture

After thawing, the Saos2 cells were cultured in T75 flasks (Nunc Tm) with McCoys 5A Medium with 219.2mg/L of L-Glutamine (PAA Cell Culture Company, E15-823), containing 10% of Fetal Bovine Serum (FBS) (PAA, A15-104) in a cell culture incubator (Heraeus, Hera Cell) set at 37 °C, 95% relative humidity and 5% V/V of CO_2.

Seeding on samples

When cells have reached the confluence, the culture medium was removed from the flask and, after a washing with 5 ml of sterile PBS solution (Dulbecco's phosphate buffered solution, PAA, H15-01), replaced with 6 mL of Trypsin solution (Trypsin EDTA (1x) 0.05%/0.02% in DPBS, PAA, L11-OQ4); the flask was incubated for 8-9 minutes to allow the total detachment of cells. Afterwards was added 12 mL of medium to stop the trypsin action and the cell was transferred in a 30 mL tube (Corning) then centrifuge for 5 min at 1500 rpm. The result was a pellet of cells in the bottom of tube that, after the removal of the surnatant with a sterile glass Pasteur (Nunc Tm), was re-suspended in 1 mL of medium. 10 μL of the cell re-suspension were diluted in 90 μl of medium in an eppendorf in order to make a dilution 1:10; 10 μL of the diluted suspension were loaded onto a Neubauer haemocytometer to perform the cell counting. Was then calculated the amount of cell suspension containing the number of cells necessary for the seeding: 20μL of cell suspension containing $1.5*10^4$ cells were transfer on the surfaces of samples sterilized (3 samples per each treatment placed in 2 plates). The samples supporting a drop of cell suspension were then incubated for 30 min at room temperature to allow the cells to adhere on the surface before adding the growth medium to the wells. After 30 min, 1 mL of warmed media was added in each well avoiding shear stress on the adhering cells. Finally the plates were incubated at 37 °C, 95% relative humidity and 5% V/V of CO_2.

2.3.3 Cell viability and proliferation assessment with HPI

Hoesch Propidium Iodide (HPI) staining was used to study the effect of all the different samples on cell proliferation and viability.
In particular, after the direct cell seeding on the samples, were assessed the behaviour of:

- **3T3** Fibroblasts after 24h and 72h of cell culture
- **Saos2** Osteoblasts after 48h and 72h of cell culture

HPI is a staining technique performed combining the staining capability of Hoesht 33342 (Sigma) and Propidium iodide dyes (Sigma). The DNA binding dye Hoechst 33342 is able to permeate freely the membrane of normal and apoptotic cells and stain their DNA with an intense blue colour detectable by fluorescent microscope. In this method the apoptotic cells are distinguished from the living ones by their characteristic chromatin condensation and nuclear fragmentation which induce the formation of a pink staining. Indeed, Propidium iodide (red dye) does not enter the intact plasma membranes of the living cells but penetrates damaged apoptotic or dead cells labelling their DNA with a pink or reddish colour, respectively.

2.3.3.1 HPI staining procedure

Half millilitre of HPI staining was prepared mixing 50 µl of Hoechst 33342 solution with 50 µl of Propidium iodide solution (10µg/ml) in 900 µl of media used for cell culture (DMEM for fibroblast and McCoy's 5A for osteoblasts). The media contained in the wells was removed and the samples were washed with 1 ml of sterile phosphate buffered solution (PBS) for three times by gentle suction/pipetting action. Clean samples were then stained with 10µl of HPI staining and incubated for 2-3 min to favour the binding action of

dyes. Samples were observed quickly since cells rapidly die in these conditions and the assessment of their viability can be compromised by artefacts due to long permanence of cells in dry environment. Stained samples were analysed under fluorescent microscope using a broad band filter at an excitation wavelength of 365 nm and an emission wavelength of 397 nm. An experiment was considered inconsistent if cell control has shown necrosis rate over 5 %. Apoptosis was determined by visual evidence of nuclear fragmentation.

2.3.3.2 Counting method

Living, apoptotic and dead cells were counted on each sample. Microscope magnification was kept constant for all the investigated samples at 40x. On each samples 6 counts were performed on 6 different areas chosen randomly, starting form the centre of the sample where the cell suspension drop was originally pipetted. Starting from the centre of the sample the microscope ocular was moved upward to another field corresponding to an entire turn of the microscope stage knob. Similarly, the successive counting fields were reached moving rightward and downward the stage following the same procedure.
Two samples for each treatment, comprise the control, and for each cell line were investigated at the relative time points (24h and 48h for fibroblasts, 48h and 72h for osteoblasts). Results were expressed as average value ± standard deviation (n=12).

2.3.4 Saos2 adhesion assessment with SEM

Scanning electron microscopy was used to evaluate Saos2 morphology and adhesion on all the surfaces after 48h and 72h of cell culture.
After supernatant removal, samples were washed gently with sterile PBS and incubated in 1 ml of 2.5% glutaraldehyde in PBS for 45min. The incubation in glutaraldehyde fixed the cells by cross-linking proteins present on their cell membranes. The cells were then gently washed three times in sterile distilled water in order to remove any trace of glutaraldehyde. Cleaned samples were dehydrated in ethanol solution of increasing concentrations (25%, 50%, 75%, and 90% for two times). Each step lasted 15 min at room temperature. After dehydration, the samples were freeze dried overnight, mounted on SEM stabs, sputter-coated by platinum (Quorum QT 150TS) and analysed with SEM.

2.3.5 Saos2 spreading assessment with Phalloidin staining

Phalloidin-Rhodamine (Sigma, TRITC P1951) was used to evaluate osteoblasts spreading on all the surfaces after 48 h and 72 h of culture. The phalloidin staining was used to analyse the disposition of the actin filaments inside the cell. Phalloidin is a fungal toxin isolated from the poisonous mushroom *Amanita phalloides*. Phalloidin toxicity is attributed to its ability to bind F-actin in liver and muscle cells. After binding with the toxin, actin filaments become strongly stabilised. Indeed, Phalloidin is able to bind the polymeric and oligomeric forms of actin and dissociation constant of the actin–phalloidin complex is in the order of $38*10^{-8}$M.

To obtain 2 ml of fluorescent phalloidin conjugated solution in PBS at the concentration of 50μg/mL, 1.9 mL of PBS were added to 0.1 mg of phalloidin dissolved in 0.1 mL of pure methanol (Sigma).

2.3.5.1 Staining procedure

Supernatants were removed from wells and samples were washed with sterile PBS three times. Cells were fixed for five minutes in 3.7% (w/v) formaldehyde in PBS and then washed again three times in PBS. On the surface of each sample were transferred 20 μL of fluorescent Phalloidin conjugate solution in PBS. Samples were stored in a dark condition for 1 hour (stain fluorescence was visible at the microscope even after several days); to remove unbound Phalloidin conjugate and reduce background signal disturbing analysis the samples were washing several times with PBS. Finally the stained cells on the samples surfaces were analysed by fluorescence microscope using a red filter (540 nm).

2.3.5.2 DAPI staining

DAPI (4’6-diaminido-2-phenylindole) is a popular DNA stain for use in fluorescent techniques; as it can pass thought an intact cell membrane is use to stain both live and fixed cells. In this work, a drop of DAPI solution (Sigma) was added on the samples surface just covered with phalloidin staining. The aim of the DAPI staining in conjunction with Phalloidin staining is to assess the nucleus belonging to skeleton-stained cells.

3. Results

3.1 Physicochemical and morphological characterizations

3.1.1 Surface morphology (SEM)

Pictures 3.1-3.5 show the surface morphology of the samples surface after the ASD treatment. Picture 3.5 shows the surface of the SUM Na sample.

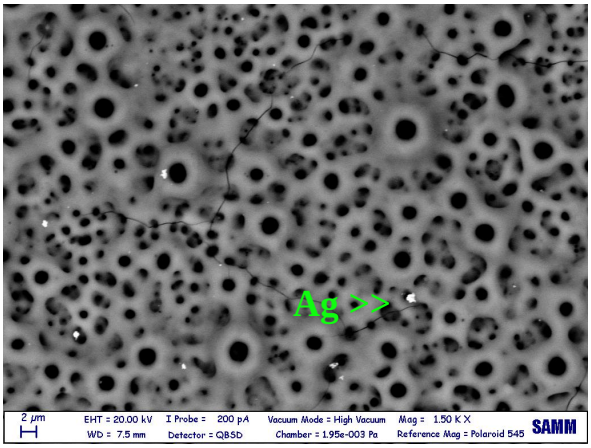

Fig. 3.1: SEM pictures of SUM AgNPs surface

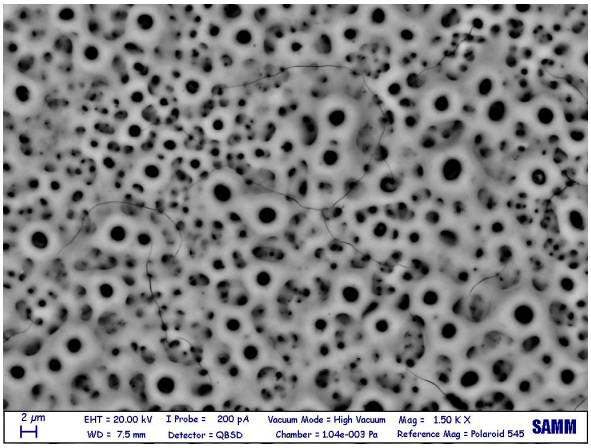

Fig. 3.2: SEM pictures of SUM NITAG CIST surface

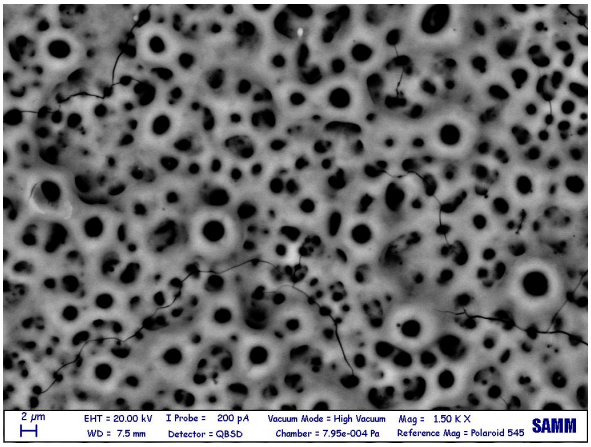

Fig. 3.3: SEM pictures of SUM NIGAL CIST surface

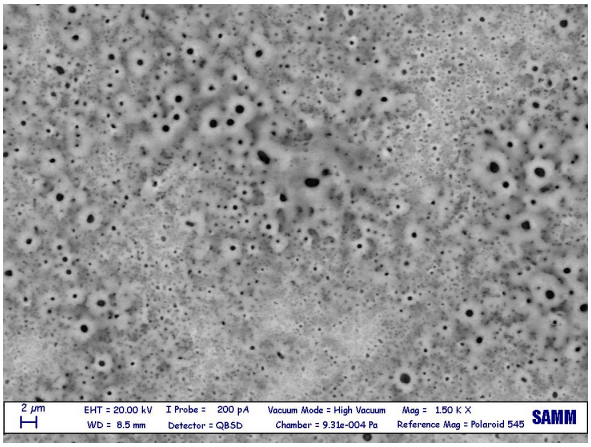

Fig. 3.4: SEM pictures of SUM NITGAL OSS surface

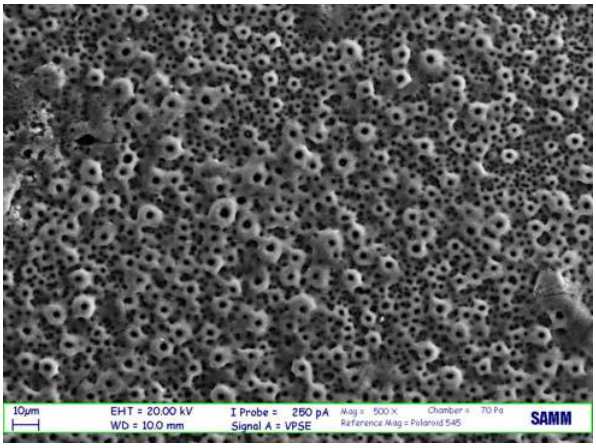

Fig. 3.5: SEM pictures of SUM Na surface

The surfaces with gallium (Fig. 3.3 and 3.4) show a different morphology in comparison to both the SUM Na surface (Fig. 3.5) and the silver-enriched surfaces (Fig. 3.1 e 3.2). SUM NITGAL OSS has a completely different morphology for pores distribution, density and shape in comparison to all the others surfaces. SUM NITGAL CIST instead shows a different morphology for pores shapes that are less regular and, like SUM AgNPs and SUM NITAG CIST, shows zones with large pores emerging from an underlying substrate that was characterised by pores of smaller diameter. In comparison to all the other surfaces, SUM Na shows a more uniform morphology both in terms of distribution and average size of the pores.

3.1.2 Chemical composition (EDS)

The EDS analyses are shown in Fig. 3.6-3.10. Silicon, calcium and phosphorus are present on all the surfaces except on SUM NITGAL OSS (Fig 3.9), where the calcium presence is not detected and the silicon/phosphorus ratio is different; the silicon levels exceeding those of the phosphorus.

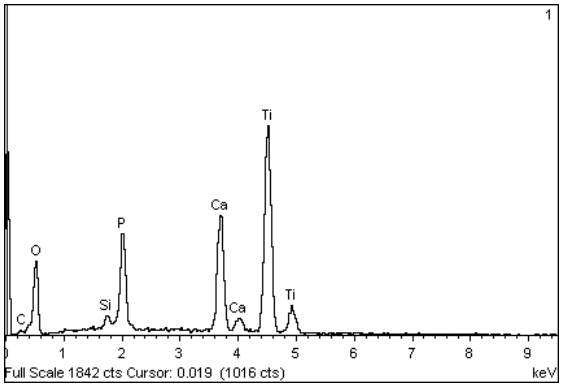

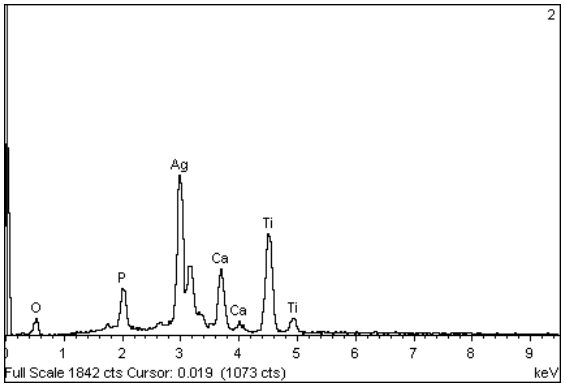

Fig. 3.6: EDS analysis of AgNPs **1.**Surface average; **2.**Particle.

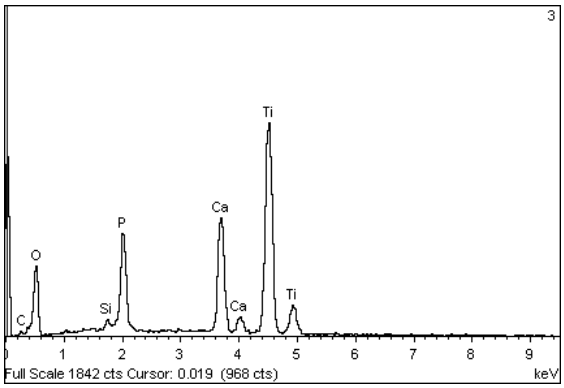

Fig. 3.7: EDS analysis of SUM NITAG CIST

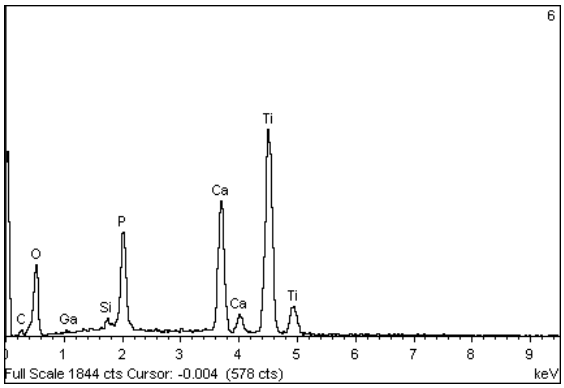

Fig. 3.8: EDS analysis of SUM NITGAL CIST

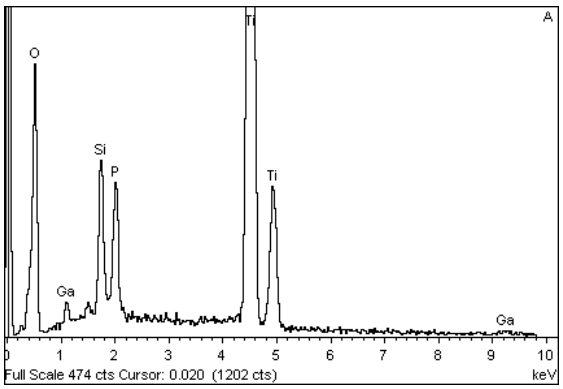

Fig. 3.9: EDS analysis of SUM NITGAL OSS

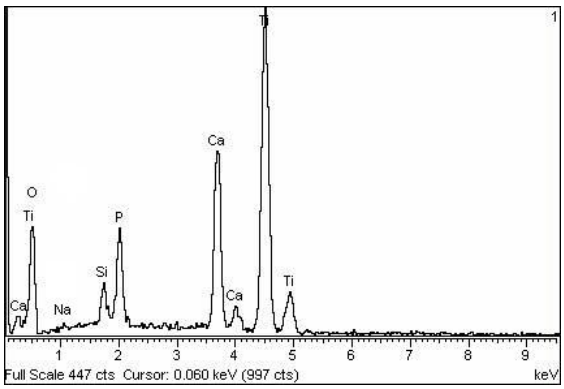

Fig. 3.10: EDS analysis of SUM Na

Gallium is present in both the SUM NITGAL CIST and SUM NITGAL OSS samples (Fig. 3.8-3.9). Fig 3.6.2 confirms the integration of the silver nanoparticles within the SUM AgNPs surface. Instead, silver was not detected by EDS in SUM NITAG CIST samples (Fig. 3.7). In the case of the SUM Na (Fig. 3.10), unlikely the remainder of the samples, the presence of sodium was ascribed to the post-treatment with NaOH.

3.1.3 XRD analysis

The XRD analyses are shown in Fig. 3.11-3.15. In all the surfaces, in addition to titanium, the titanium oxide (TiO_2) in its anatase form was detected. In the SUM NITAG CIST and SUM NITGAL CIST sample, the anatase peaks ($2\theta = 25°$) are 2-fold higher than the titanium peaks ($2\theta = 38°$ or $2\theta = 40°$) probably due to thickness differences in the oxide layers. The same behaviour, but less accentuated, is visible in the SUM Na sample where the rutile form is also present. The SUM NITGAL OSS sample shows the lower anatase peaks in comparison with all other samples suggesting the presence of a reduced thickness of the oxide layer. SUM AgNPs sample shows comparable anatase and titanium peaks suggesting an intermediate thickness of the oxide layer.

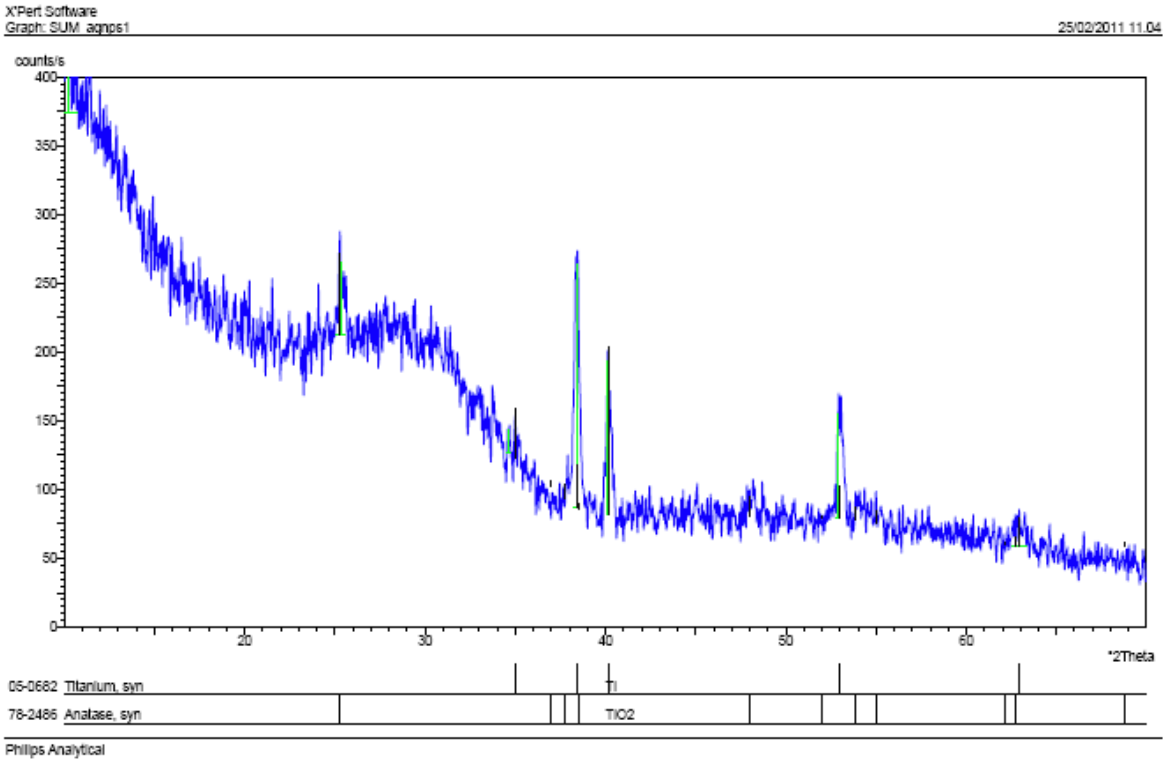

Fig. 3.11: XRD analysis of SUM AgNPs sample

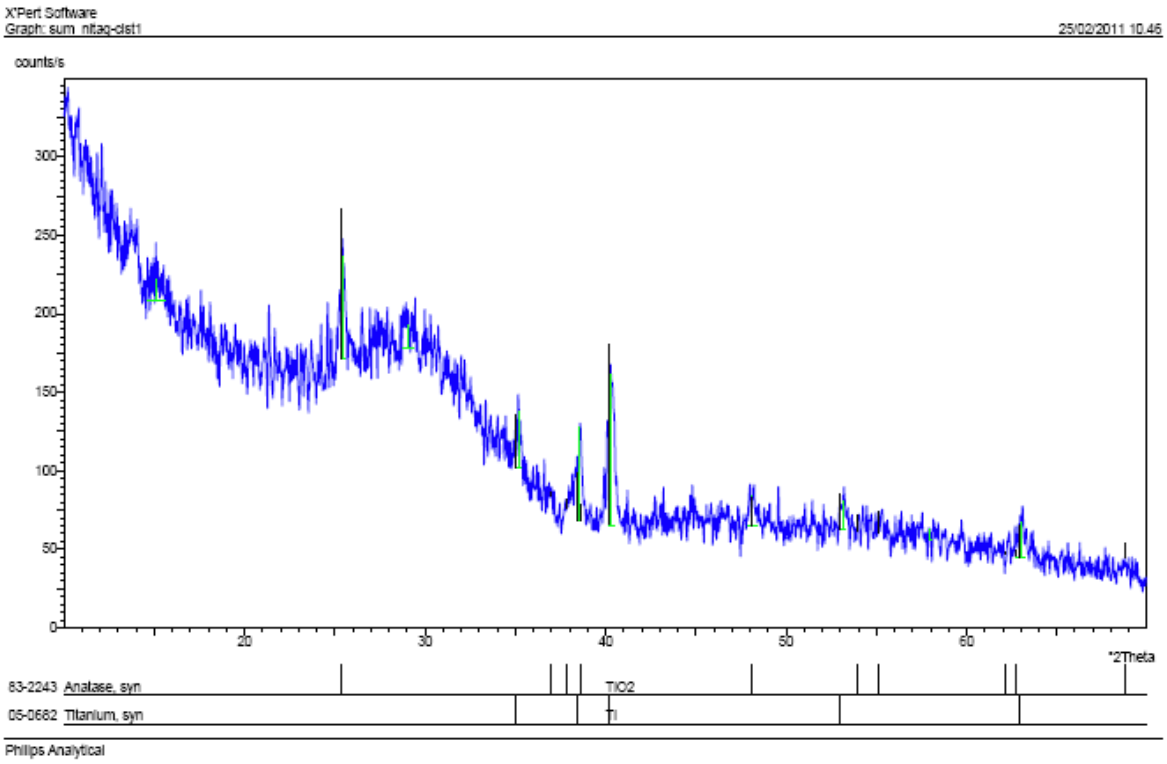

Fig. 3.12: XRD analysis of SUM NITAG CIST sample

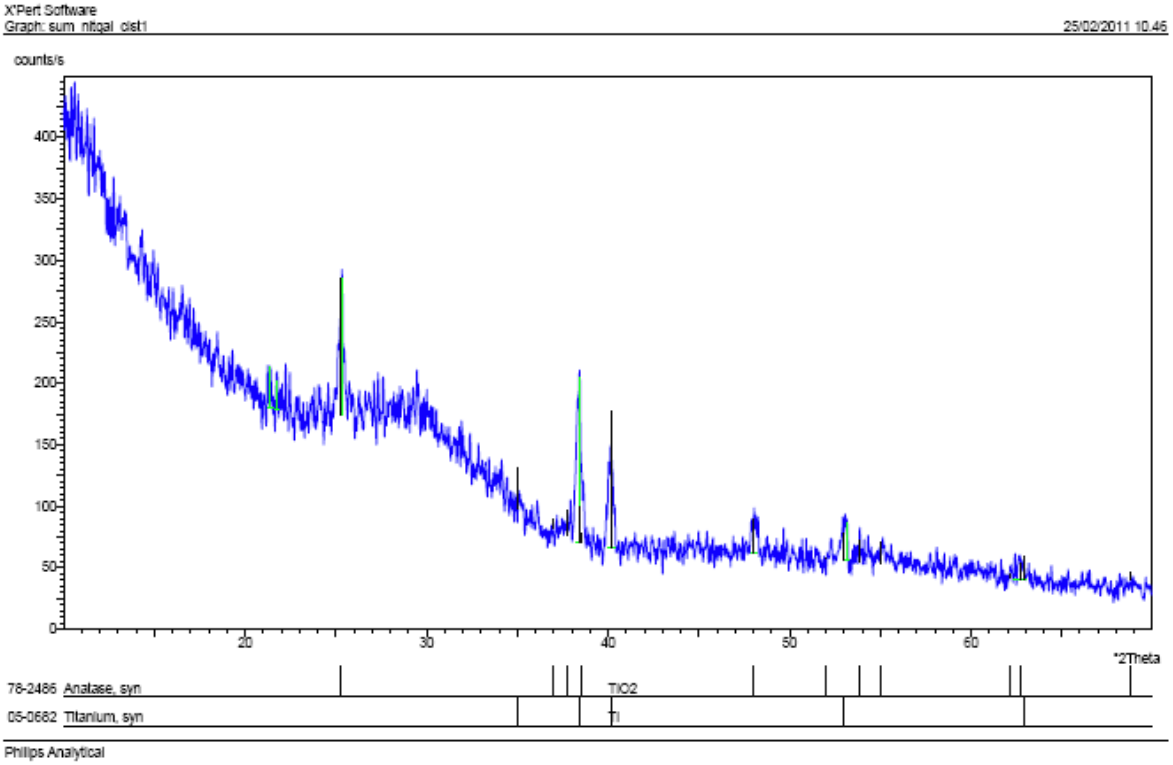

Fig. 3.13: XRD analysis of SUM NITGAL CIST sample

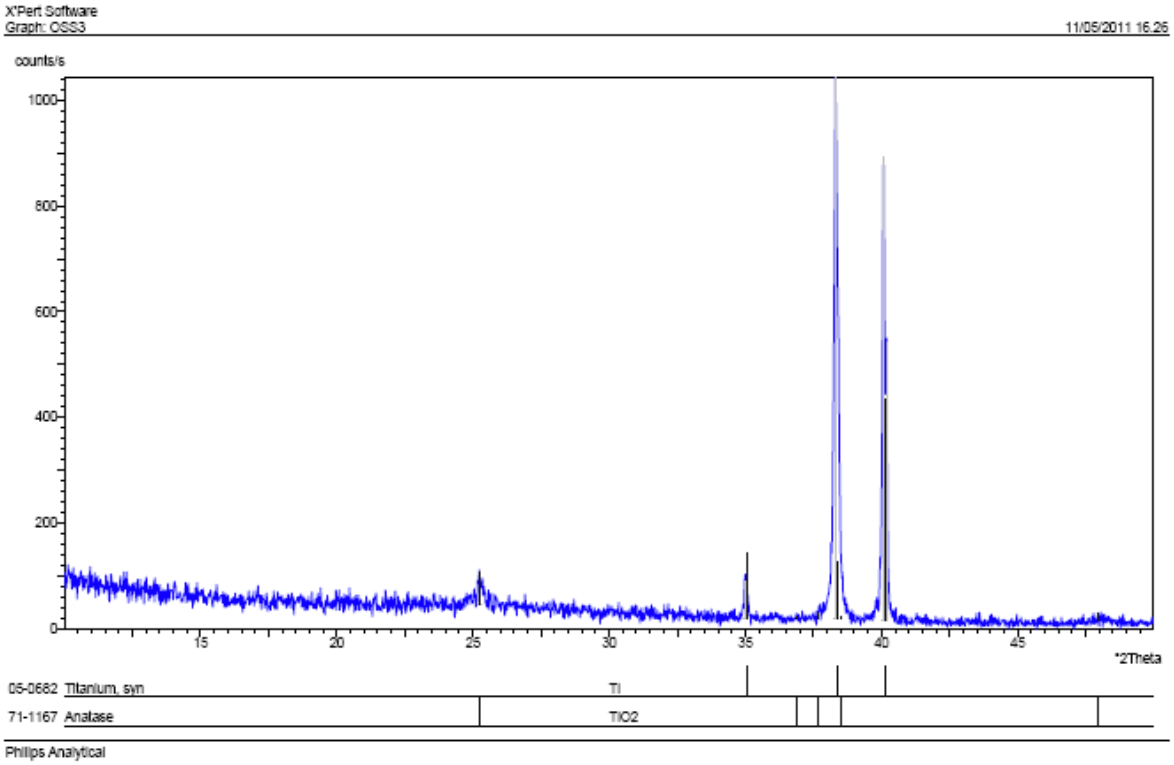

Fig. 3.14: XRD analysis of SUM NITGAL OSS sample

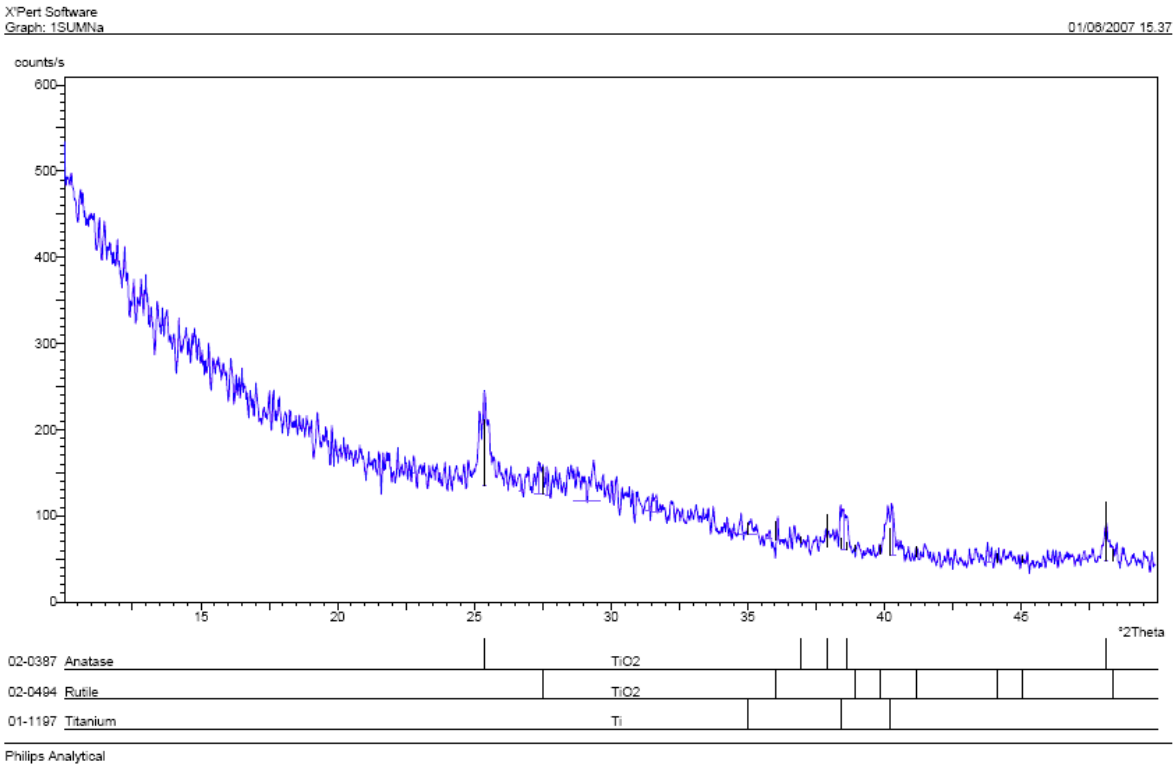

Fig. 3.14: XRD analysis of SUM Na sample

3.1.4 Profilometry

Figures 3.15-3.19 show the chats of parameters Ra, RMax, Ry, K and Sk of profilometry analysis.

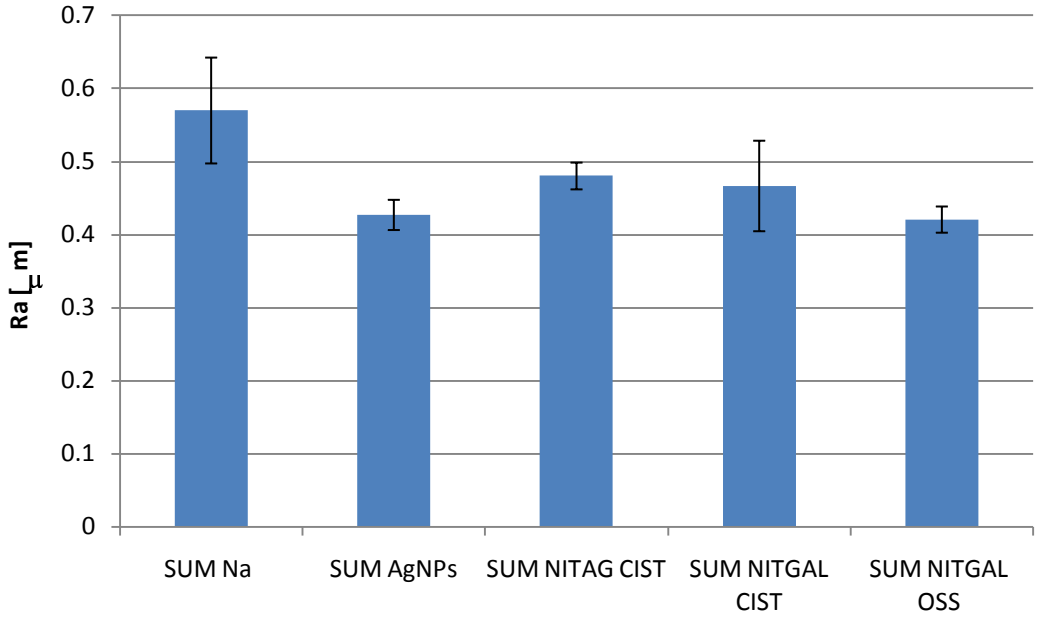

Fig. 3.15: Ra parameter of samples

All the samples have a Ra parameter lower than the SUM Na samples undergoing post-treatment etching by NaOH; Ra variations in the range 90-150nm making their values not significantly different from the SUM Na (Fig. 3.15). All the remaining surfaces showed significantly lower roughness values. The surfaces obtained by integration of cysteine (SUM NITAG CIST and SUM NITGAL CIST) showed similar Ra values and slightly higher (of about 40-60nm) than SUM AgNPs and SUM NITGAL OSS. SUM Na and SUM NITAG CIST show the higher RMax parameter (Fig. 3.16) but both with relatively large standard deviations. The same considerations are also valid for the Ry parameter (Fig. 3.17) but in this case SUM Na shows a smaller standard deviation.

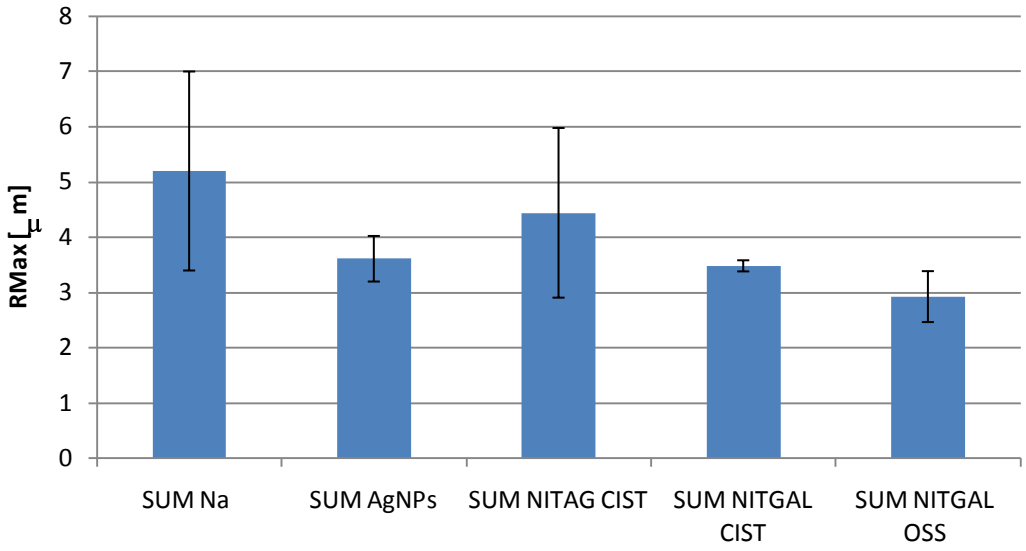

Fig. 3.16: RMax parameter of samples

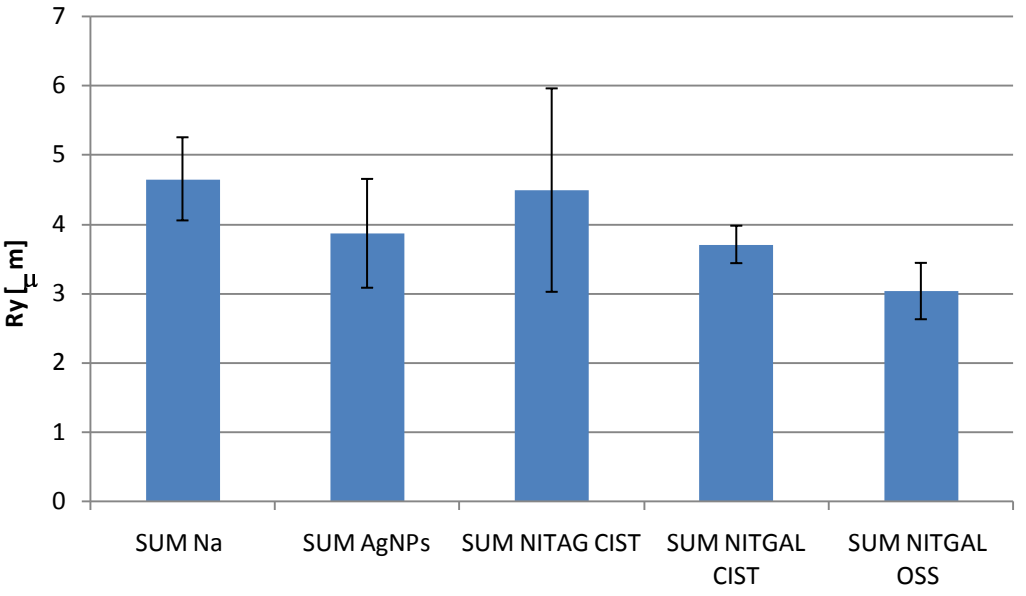

Fig. 3.17: Ry parameter of samples

The presence of gallium nitrate during treatments has a decreasing effect on kurtosis values (Fig. 3.18). Indeed, both the SUM NITGAL CIST and SUM NITGAL OSS show lower K values (variation in the range 2-3µm) than the other samples; their k values were lower than 3µm suggesting bevelled morphologies of the surface profiles. Differently, SUM Na, SUM AgNPS and SUM NITAG CIST have k values higher than 3µm indicating sharp morphologies of the surface profiles. Even if more dispersed, SUM AgNPS sample has a K

value very close to the SUM Na. SUM NITAG CIST has a K value higher than the SUM Na of about 1μm and moreover relatively inconsistent.

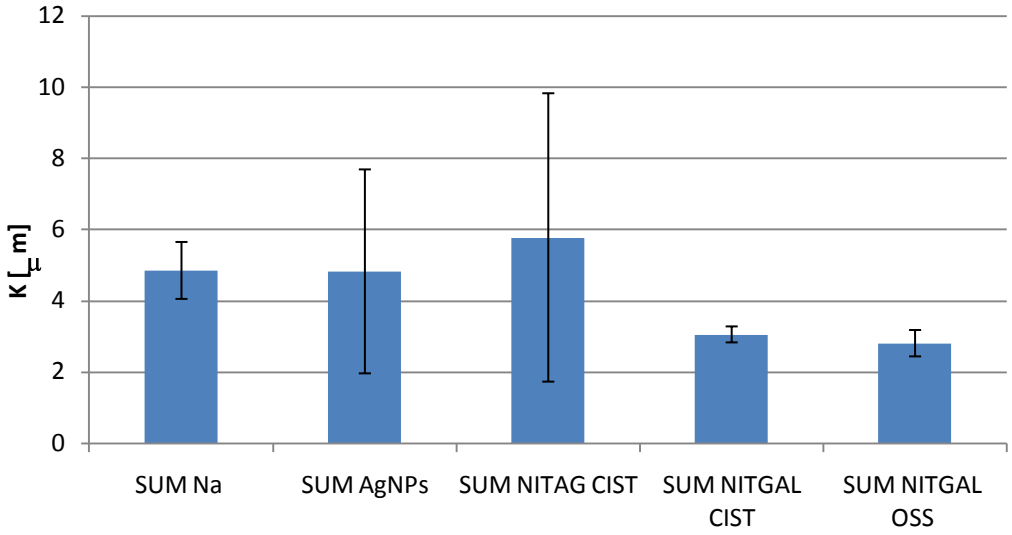

Fig. 3.18: K parameter of samples

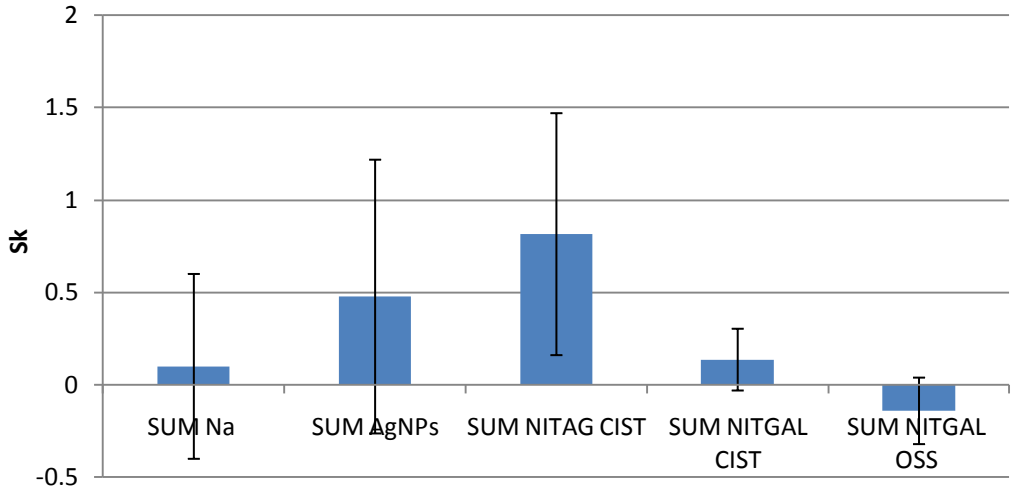

Fig. 3.19: Sk parameter of samples

The Sk values (Fig. 3.19), within the experimental errors, are in a range including 0 for all the samples except SUM NITAG CIST that, like SUM Na and SUM AgNPs, is characterized by a relatively high standard deviation. This suggests a relative uniform distribution of peaks and valleys in all samples except SUM NITAG CIST which has a positive Sk value.

3.1.5 Surface wettability tests

The average values of water contact angle are shown in figure 3.20. SUM Na contact angle is under the analysis detection limit as it has a very hydrophilic surface (Fig 3.21B) contrary to the titanium grade II that is relatively more hydrophobic (Fig. 3.21A). More importantly, all the treated surfaces have contact angle values lower than the so-called Berg's threshold (50-55^{o}) which is considered to limit the denaturation of adsorbed plasma proteins.

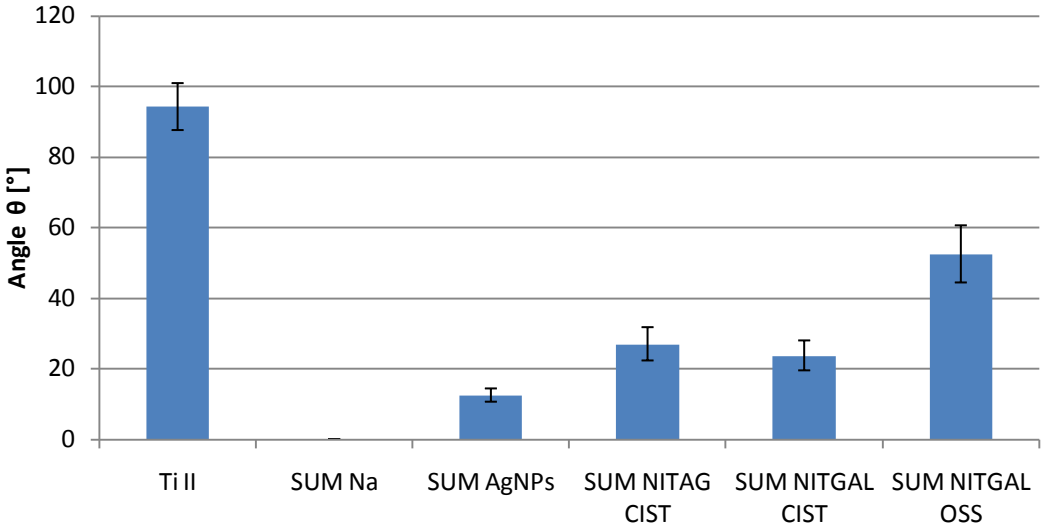

Fig. 3.20: Average values of static water contact angle.

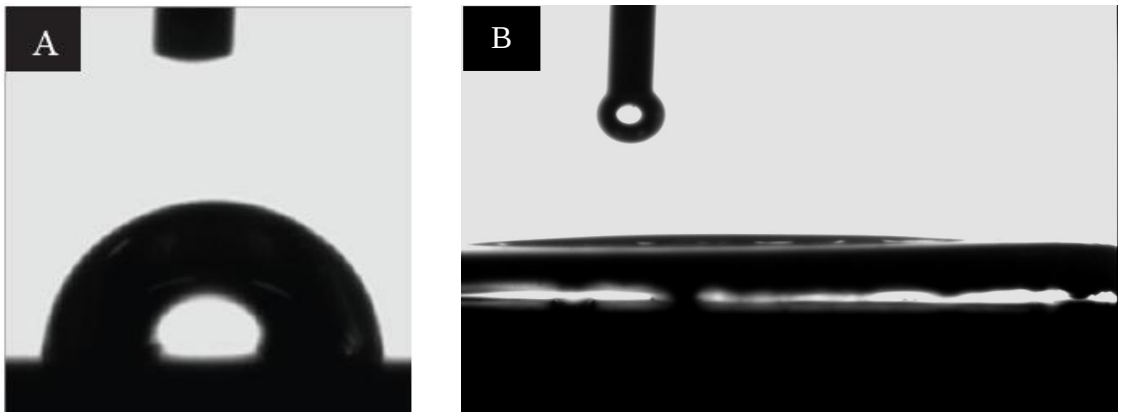

Fig. 3.21: Water drop morphology on: **A.** Titanium grade II surface; **B.** SUM Na surface;

Indeed, the samples with cysteine (SUM NITAG CIST and SUM NITGAL CIST) have contact angles values of around 20°, slightly higher than the SUM AgNPs value (around 15°).

All the surfaces have a contact angles lower than Ti II, included SUM NITGAL OSS (around 50°). The low standard deviation values suggest a relative homogeneity of the surface features and preparation reproducibility for all the samples.

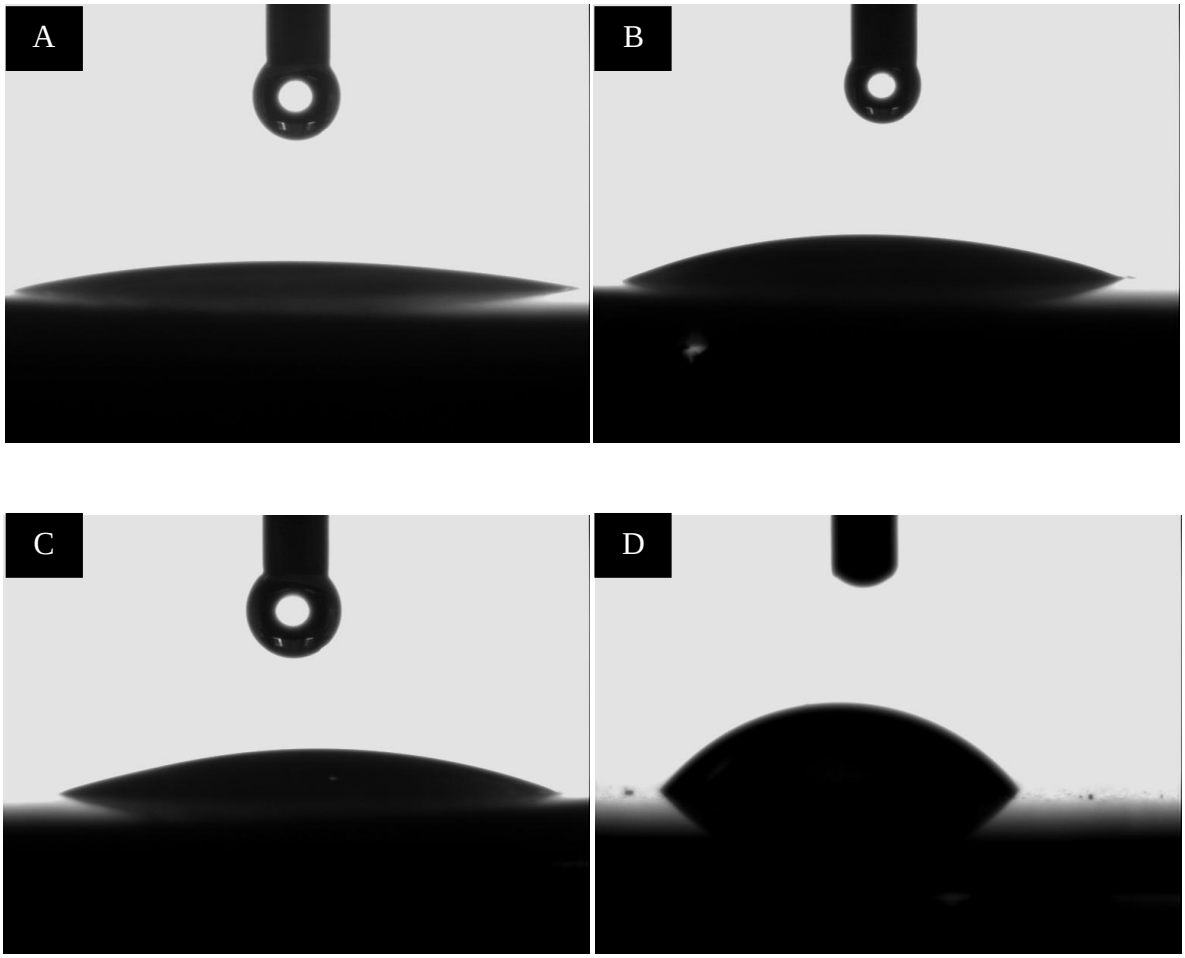

Fig. 3.22: Water drop morphology on: **A.** SUM AgNPs; **B.** SUM NITAG CIST; **C.** SUM NITGAL CIST; **D.** SUM NITGAL OSS

3.1.6 GDOES

The GDOES analysis evaluates the mass concentration of chemical species at different substratum depths. Figure 3.23 shows the result of GDOES analysis on SUM AgNPs as an example. From the GDOES analyses it was possible to quantify the thickness of the oxide layers present on the samples (Fig 3.24) that is represented by the depth correspondent to the 99.2% of titanium mass concentration (titanium grade II concentration).

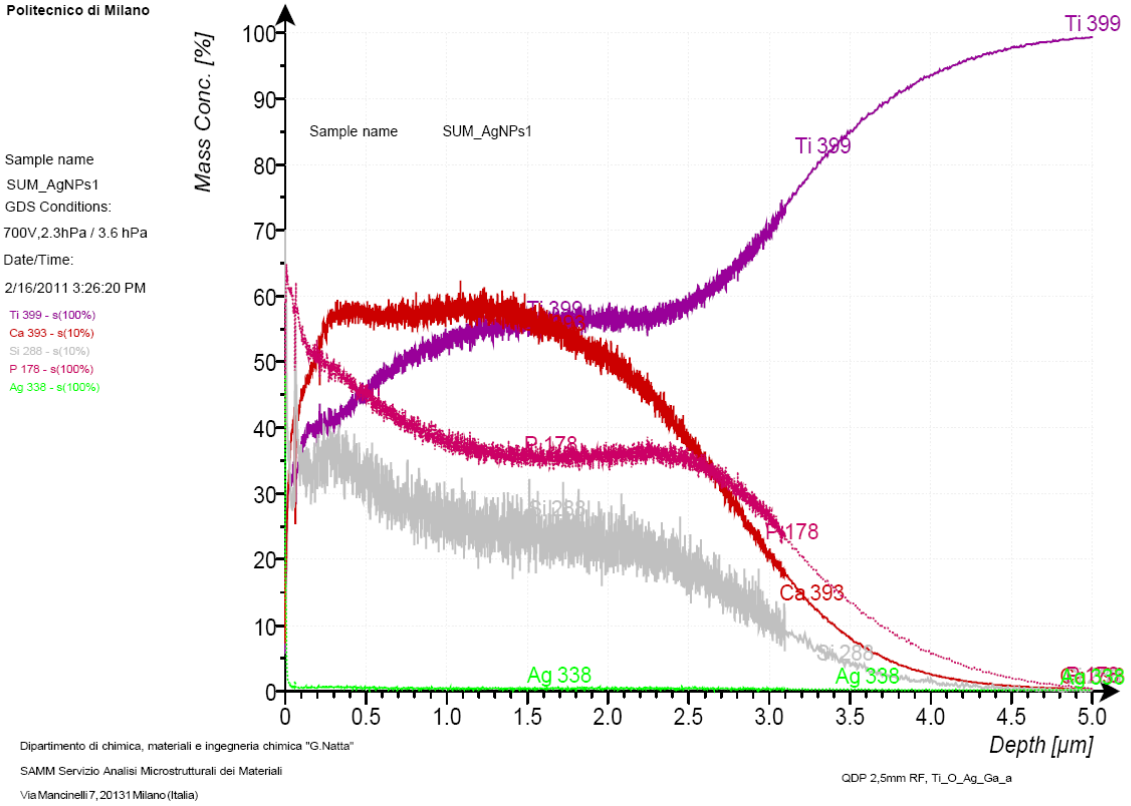

Fig. 3.23: GDOES analysis on SUM AgNPs sample.

Sample	Oxide Layer Thickness [µm]
SUM AgNPs	4.95
SUM NITAG CIST	5.44
SUM NITGAL CIST	5.80
SUM NITGAL OSS	1.05
SUM Na	4.41

Fig. 3.24: Thickness of oxide layers for all the samples

The GDOES analysis clearly shows the effect of cystein and oxalate in their opposite effects on the formation of a titanium layer. The presence of cysteine appears to increase the oxide layer thickness, while the ossalate leads to its sharp reduction. Indeed, both the samples including cysteine in their surface treatments (SUM NITAG CIST and SUM NITGAL CIST) have oxide layers thicker than all the other samples.

Otherwise, the presence of oxalic acid during the anodization treatment has a strong inhibiting action on the growth of oxide layer on the substratum. The oxide layer of SUM NITGAL OSS is indeed 5 fold thinner than all the other layers.

Pictures 3.25 show the silver mass concentration in function of depth in SUM AgNPs and SUM NITAG CIST samples. In both the samples the entire silver amount is contained in the first 20nm of depth. Comparing the superficial concentration, SUM AgNPs sample shows a silver concentration (32%) higher than SUM NITAG CIST (9%).

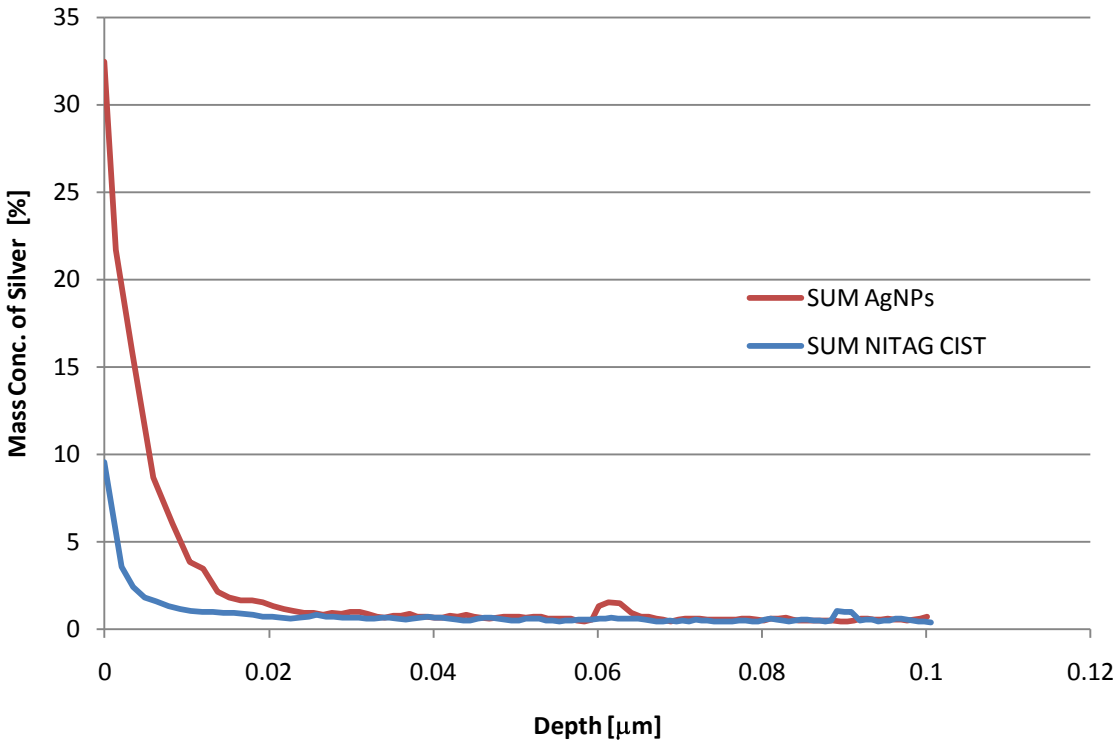

Fig. 3.25: Silver Mass Concentration [%] vs Depth [μm].

Figure 3.26 shows the ualitative trend of gallium mass concentration in the gallium-containing samples (SUM NITGAL CIST e SUM NITGAL OSS).

Unlike the silver-containing samples, the gallium amount is detectable over the first 50nm of depth in both the samples. This behaviour suggests that gallium is incorporating in the inner oxide matrix and not only in the superficial layer where the SUM NITGAL OSS sample has a gallium concentration higher than SUM NITGAL CIST sample.

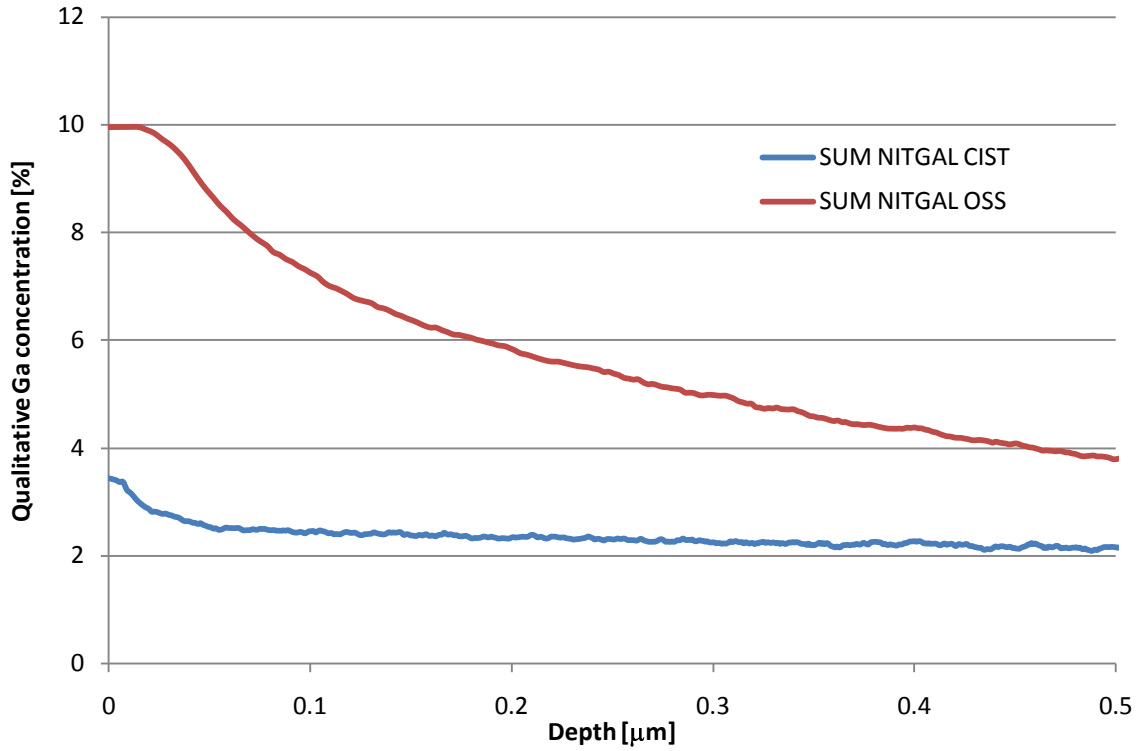

Fig. 3.26: Thickness of oxide layers for all the samples

3.1.7 ICP-OES

The ICP-OES tests was carried out to evaluate the silicon and silver release in PBS at 37 ° from the surfaces of the samples containing silver (SUM AgNPs and SUM NITAG CIST) and material control SUM Na (Fig. 3.27). As expected, no silver release was detected in the case of SUM Na. Silver release from SUM AgNPs surface slightly increases after 24 hours and remains at similar levels at later experimental points (around 0.06μg/L*cm^{-2}). SUM NITAG CIST silver release (around 0.01μg/L*cm^{-2}) is about 5-fold less than SUM AgNPs still remaining at constant levels in all the time points.

The silicon release from SUM AgNPS is remarkable already after 6h and is 2-fold higher than the material control SUM Na; after 7days is still higher than SUM Na. SUM NITAG CIST show a silicon release lower than both SUM Na and SUM NITAG CIST but nevertheless increases during the time points. The negligible titanium release for all the surfaces at all the time points suggests that the titanium oxide in all the surfaces is not reactive and does not undergo degradation or corrosion.

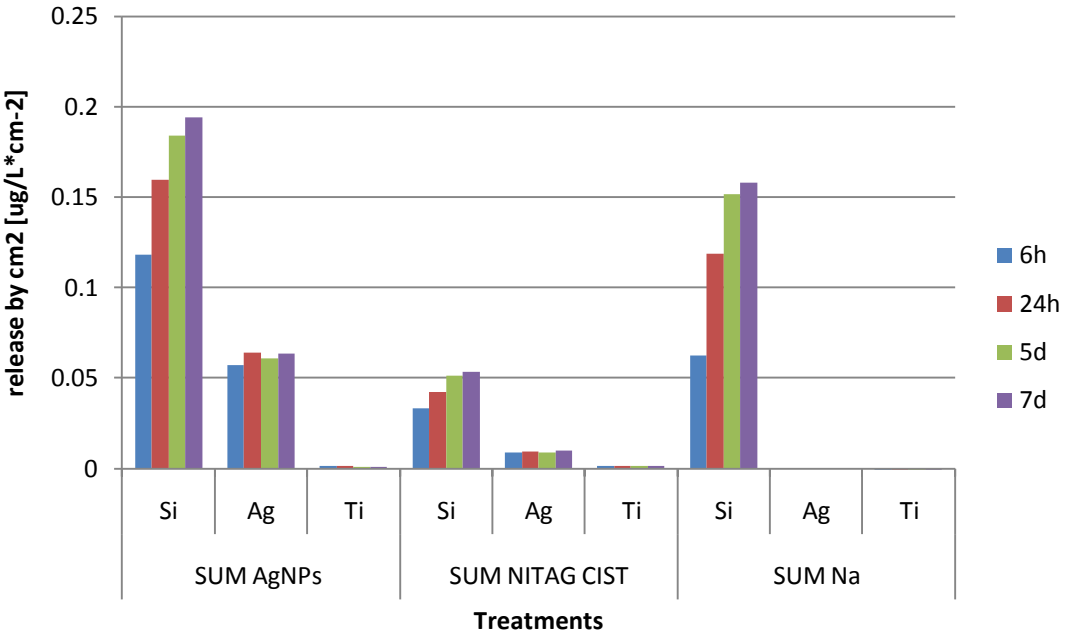

Fig. 3.27: Si, Ag and Ti release after 6h, 24h, 5days and 7 days in PBS at 37° degrees.

3.1.8 TiO_2 delamination tests

Figures from 3.28 to 3.30 show the surface morphology after flexion of 30°of all the samples. Although as a consequence of flexion some cracks are visible, especially on the SUM AgNPs (Fig. 3.28) and SUM NITGAL CIST (Fig. 3.29) surfaces, all the coatings adhere perfectly on the substrata since there is no detectable oxide layer delaminations.

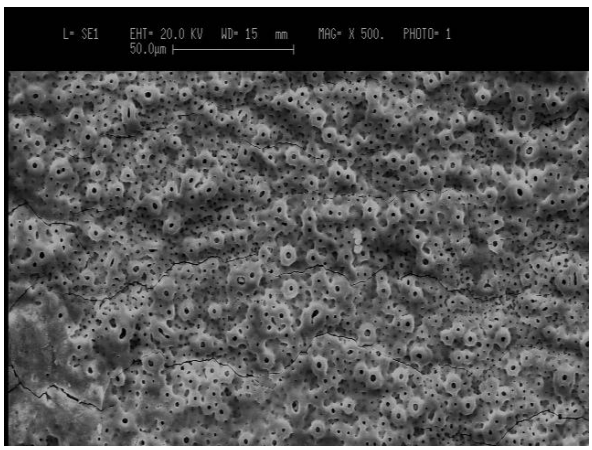

Fig. 3.28: SEM pictures of SUM AgNPs sample after flexion of 30°.

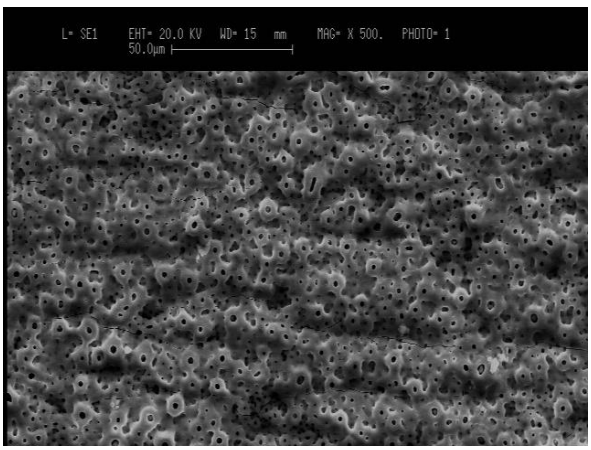

Fig. 3.29: SEM pictures of SUM NITAG CIST sample after flexion of 30°.

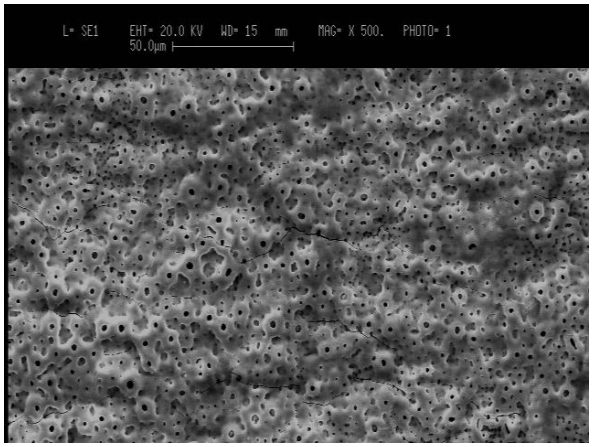

Fig. 3.30: SEM pictures of SUM NITGAL CIST sample after flexion of 30°.

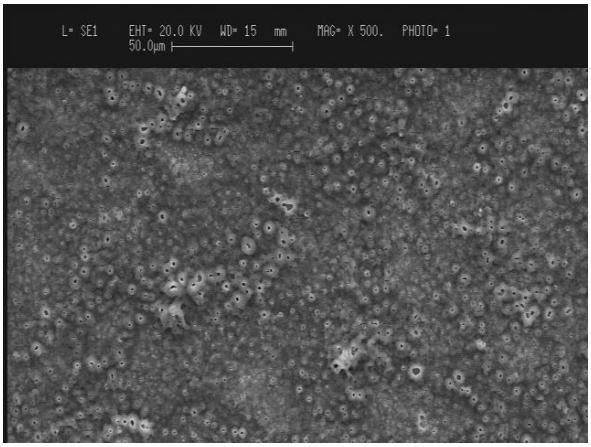

Fig. 3.31: SEM pictures of SUM NITGAL OSS sample after flexion of 30°.

3.2 *In vitro* biocompatibility tests

3.2.1 Assessment of the material cytotoxicity by murine 3T3 fibroblast direct contact tests

3.2.1.1 Viability and proliferation assessment with HPI test

All the samples have shown a considerable cell proliferation rate in comparison with the control tissue culture plate. Indeed, the number of viable cells on all the tested surfaces after 48 hours of cell culture is higher than the number of viable cells on tissue culture plate (cell control). In comparison with the material control SUM Na, all the surfaces have shown a similar proliferation after 48 hours except for SUM NITGAL CIST where the viable cells proliferation increases of about 25% (Fig. 3.32).

The viable cell rate after 24h (Fig. 3.33) is higher than 90% in all samples except in SUM AgNPs (74.31%). The relatively lower numbers of viable cell in the tissue culture plate and in all the surfaces except SUM AgNPs may be ascribed to a relatively fast rate of cell confluence caused by the relatively high cell seeding density adopted in the experimental model. Regardless of any experimental artefact of the tissue culture plate control cells, these results clearly demonstrate that all the tested surfaces had no cyto-toxic potential on fibroblasts.

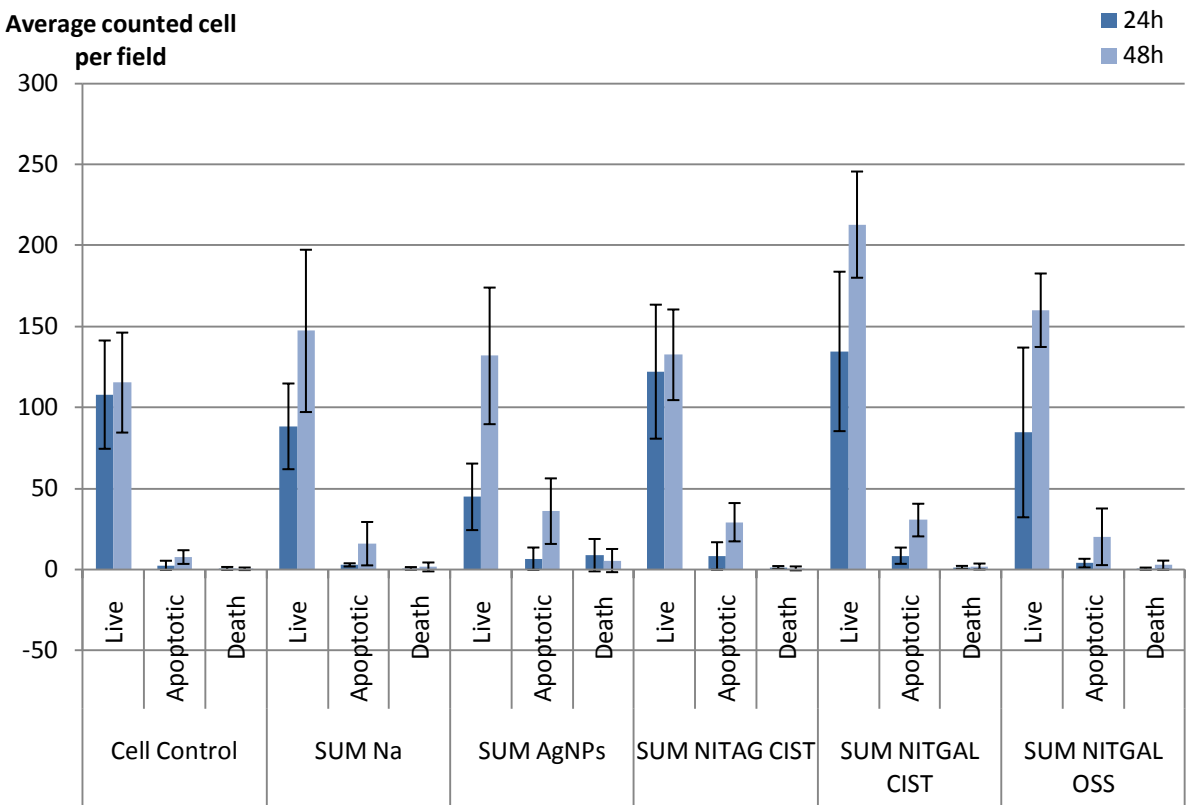

Fig. 3.32: Direct contact proliferation test on 3T3 fibroblasts performed with HPI staining allowing evaluation of viable, apoptotic and death cells after 24h and 48h.

	24h			48h		
Sample	**Live [%]**	**Apoptotic [%]**	**Dead [%]**	**Live [%]**	**Apoptotic [%]**	**Dead [%]**
Cell Control	97.08	2.32	0.60	93.45	6.21	0.34
SUM Na	96.19	3.09	0.73	89.38	9.66	0.96
SUM AgNPs	74.31	11.05	14.64	76.06	20.77	3.17
SUM NITAG CIST	92.72	6.33	0.95	81.62	17.97	0.41
SUM NITGAL CIST	93.19	5.89	0.92	81.62	17.97	0.41
SUM NITGAL OSS	95.04	4.40	0.56	87.51	11.03	1.46

Fig. 3.33: Percent of proliferation rate of live, apoptotic and dead cells valuated at 24-48 hours

3.2.2 Saos2 Osteoblast-like cell activity on tested materials

3.2.2.1 Viability and proliferation assessment with HPI test

Pictures 3.34-3.35 show the cell viability and proliferation with HPI staining after 48hours and 72hours of culture.

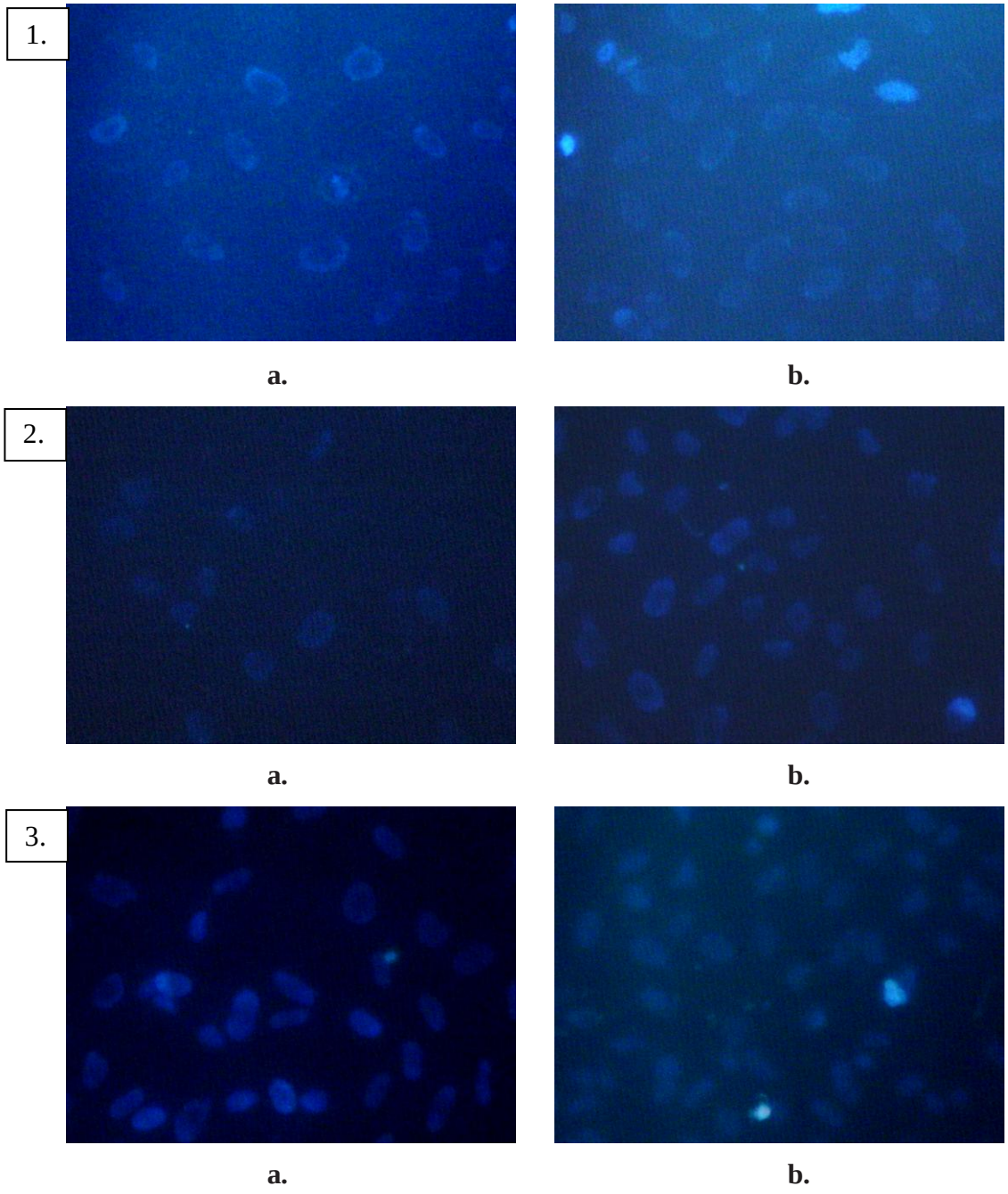

Fig. 3.34: 1. Saos2 viability on tested surfaces. Cell control after 48hours (**a.**) and 72hours (**b.**); **2. SUM Na** after 48hours (**a.**) and 72hours (**b.**); **3. SUM AgNPs** after 48hours (**a.**) and 72hours (**b.**).

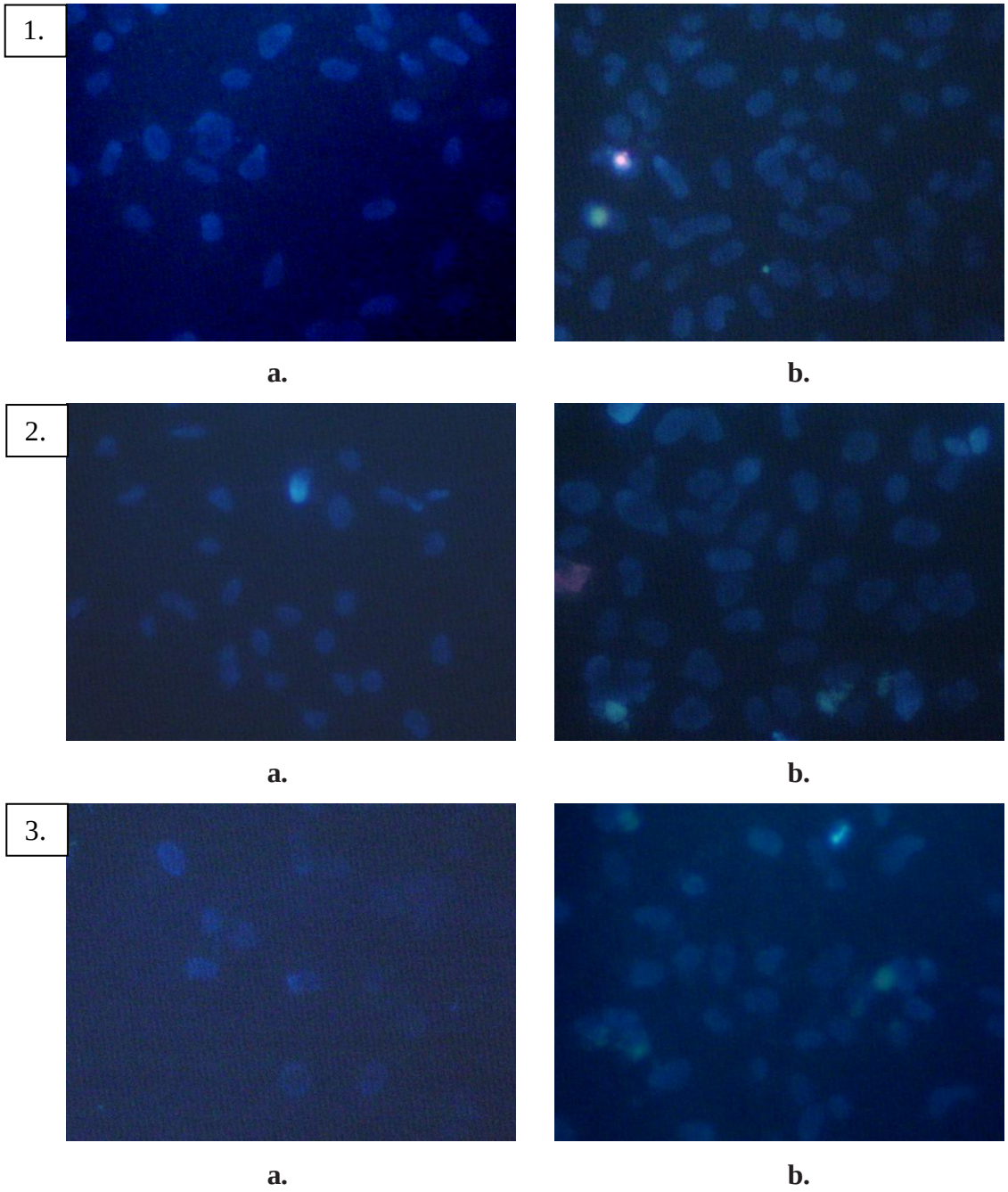

Fig. 3.35: 1. Saos-2 viability tests on tested surfaces. SUM NITAG CIST after 48hours (**a.**) and 72hours (**b.**); **2. SUM NITGAL CIST** after 48hours (**a.**) and 72hours (**b.**); **3. SUM NITGAL OSS** after 48hours (**a.**) and 72hours (**b.**);

After 48hours of culture all the samples have shown to support an osteoblast proliferation rate slightly higher than both the control cells and the osteoblasts growing on the SUM Na in which a rate of proliferation similar to the tissue culture plate control was observed (Fig 3.36). After 72 hours of culture, while SUM Na showed a cell proliferation rate slightly higher than the control, all the other samples have shown an increased cell proliferation in comparison with both cells in the control plate and on the SUM Na surface. Particularly, SUM AgNPs and SUM NITAG CIST surfaces have a proliferation increment in the range of 50-60% in comparison to the material control SUM Na rate. After 48 hours of cell culture, all the samples had a viable cell percentage higher than 90% and particularly, about 4-7% higher than SUM Na (Fig. 3.37). After 72 hours, only SUM NITGAL CIST and SUM NITGAL OSS show a slightly reduction of viable cell rate. The dead rates ranged between 0-1% for all the samples both at 48 hours and 72 hours of culture. These results suggest that the surfaces with antibacterial properties not only have no cytotoxicity, but they also favour the proliferation of osteoblasts at a rate higher than the control SUM Na material.

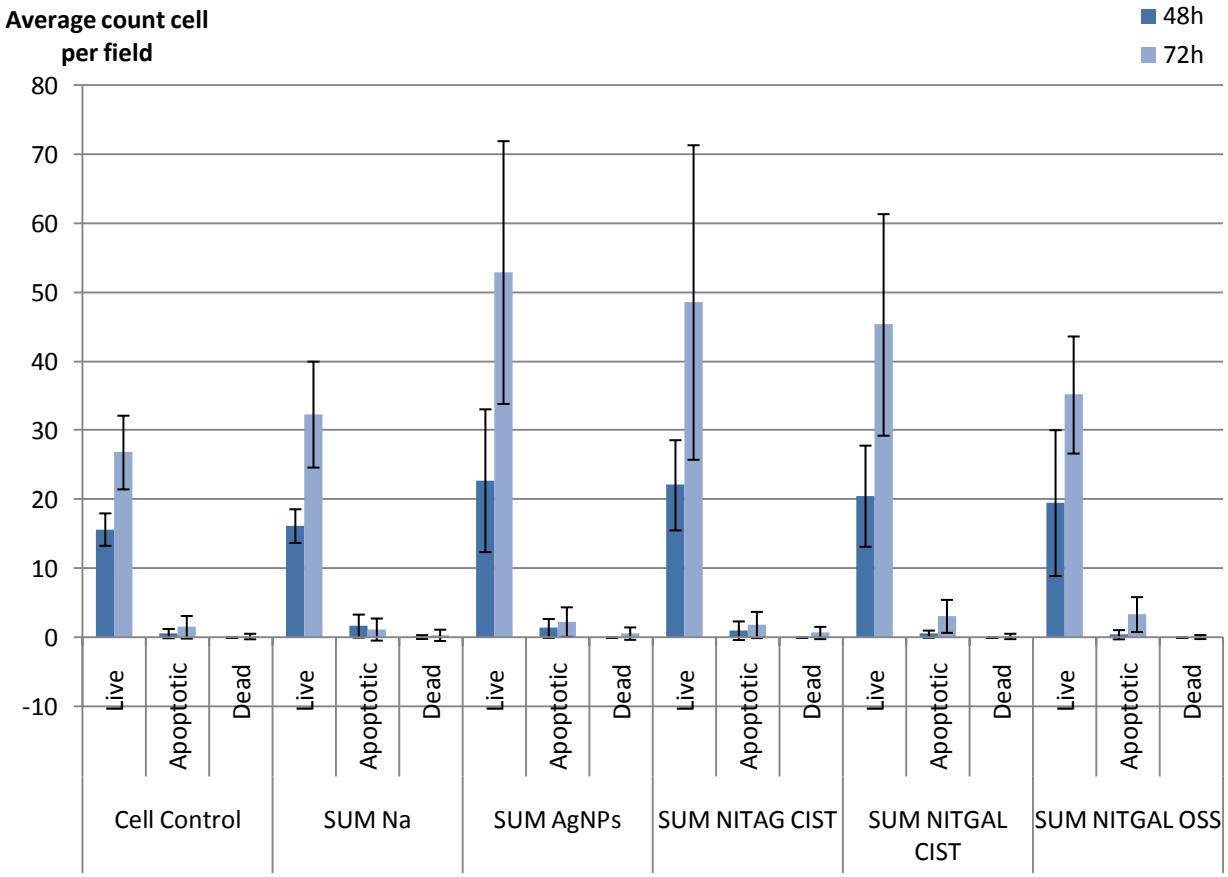

Fig. 3.36: Proliferation tests on Saos2 osteobalsts performed by HPI staining assessing viable, apoptotic and death cells after 48h and 72h of direct culture on samples.

	48h			72h		
Sample	**Live [%]**	**Apoptotic [%]**	**Dead [%]**	**Live [%]**	**Apoptotic [%]**	**Dead [%]**
Cell Control	96.41	3.59	0.00	94.15	5.26	0.58
SUM Na	90.23	9.30	0.47	95.57	3.45	0.99
SUM AgNPs	94.46	5.54	0.00	94.92	4.04	1.05
SUM NITAG CIST	95.67	4.33	0.00	95.11	3.59	1.31
SUM NITGAL CIST	97.62	2.38	0.00	93.31	6.35	0.34
SUM NITGAL OSS	97.91	2.09	0.00	91.14	8.64	0.22

Fig. 3.37: Percentage of live, apoptotic and dead cells valuated at 48 and 72 hours on tested surfaces.

3.2.2.2 SEM Analysis

Figures 3.38-3.42 show the morphology of cells adhering on the sample surfaces after 48 hours and 72 hours of culture. At 72 hours, the cells on AgNPs, SUM NITAG CIST and SUM NITGAL CIST surfaces (Fig. 3.39b-40b-41b) appeared to acquire a more spread morphology than the cells at 48h; at 72 hours the level of cell spreading is very pronounced and their bodies is difficult to distinguish from the material surface.

This phenomenon, more marked on SUM AgNPs, SUM NITAG CIST and SUM NITGAL CIST surfaces (Fig. 3.39b-40b-41b) than on the material control SUM Na (Fig. 3.38b), suggests that the cells are involved in the adhesion process and that, on the sample surfaces, they find a favourable substratum. Therefore, the typical surface morphology of anodized titanium provides a sort of anchorage sites to the cells. Indeed, the external profile of the cells at both 48 hours and 72 hours often coincides with the external edge of the doughnut-like structure surrounding the pores. This behaviour appeared to be favoured especially on those surfaces where the pores structure is larger. Here, the doughnut-like structure more clearly emerge from the underlying substrate offering anchorage points to the cell plasmalemma. This was a constant feature in the case of SUM AgNPs, SUM NITAG CIST, SUM NITGAL CIST (yellow arrow on Fig. 3.39, 3.40a, 3.41 and 3.43). Surfaces with smaller pores diameter and doughnut-like structures showed a relatively lower degree of protrusion of their features; this is the case of SUM Na (Fig. 3.38) and SUM NITGAL OSS (Fig. 3.42) showing a cell

morphology less spread. This Saos2 morphology well relates to their improved proliferation rate on SUM AgNPs, SUM NITAG CIST and SUM NITGAL CIST samples (Fig. 3.36). However, on all the surfaces, but especially on the antibacterial coatings, at 72h cells tend to form gap junctions that are likely to improve their autocrine biochemical signalling.

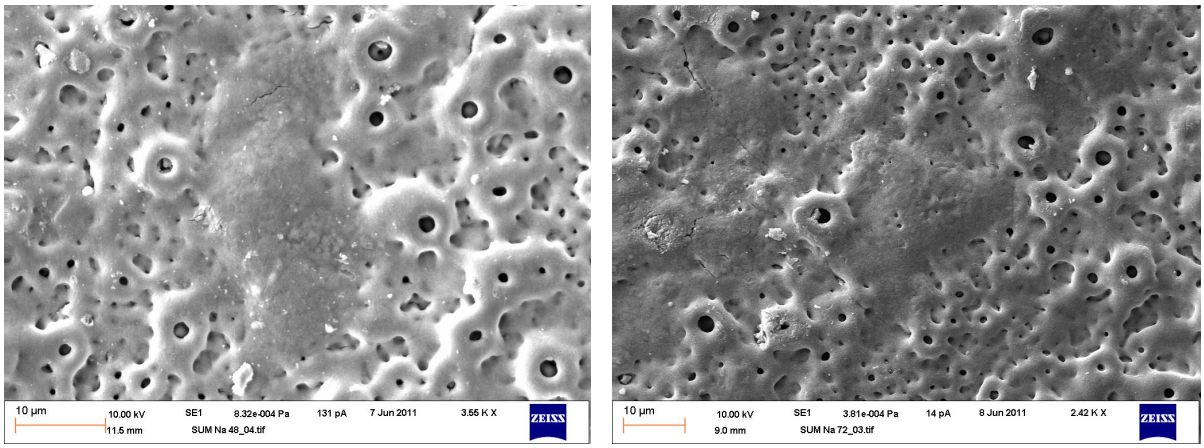

a. **b.**

Fig. 3.38: Saos2 on SUM Na surface at: **a.** 48h of culture; **b.** 72h of culture

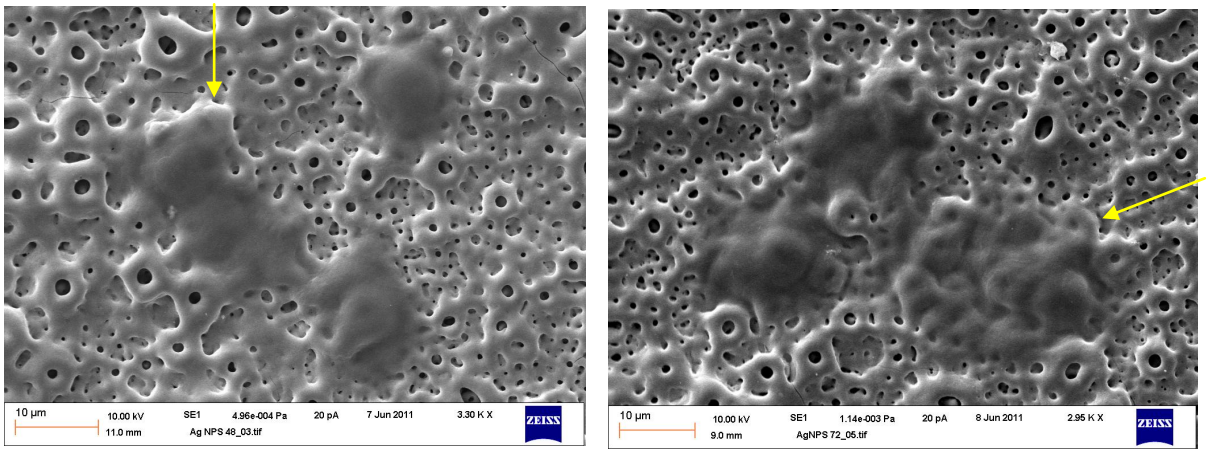

a. **b.**

Fig. 3.39: Saos2 on SUM AgNPs surface at: **a.** 48h of culture; **b.** 72h of culture

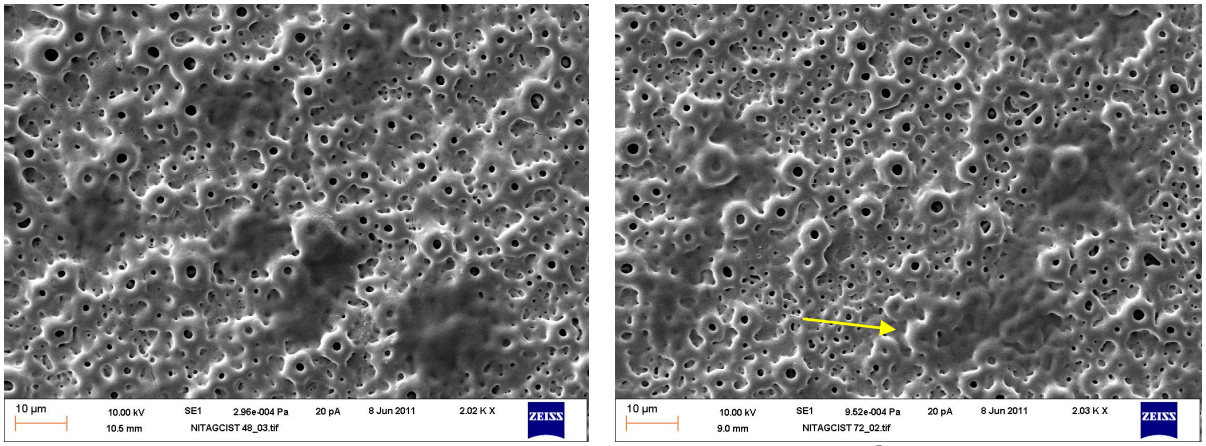

a. **b.**

Fig. 3.40: Saos2 on SUM NITAG CIST surface at: **a.** 48h of culture; **b.** 72h of culture

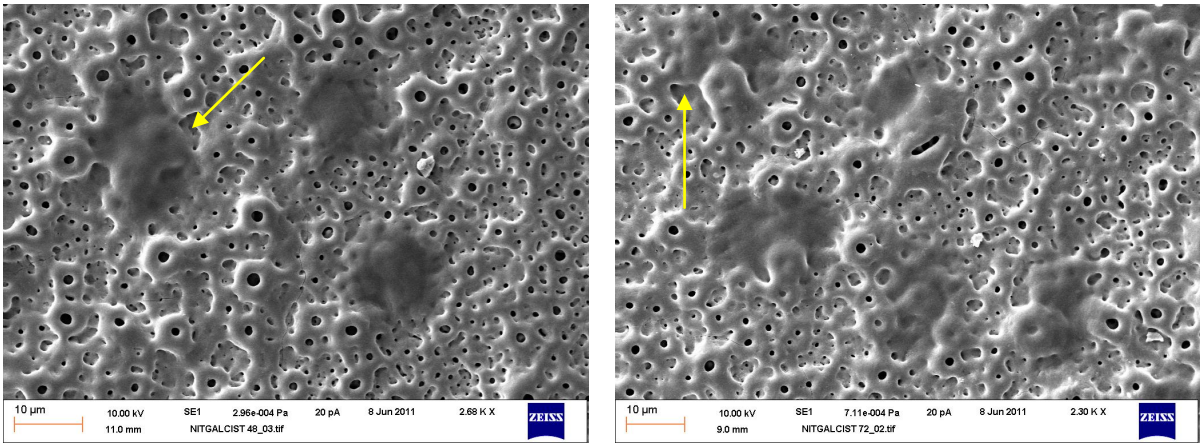

a. **b.**

Fig. 3.41: Saos2 on SUM NITGAL CIST surface at: **a.** 48h of culture; **b.** 72h of culture

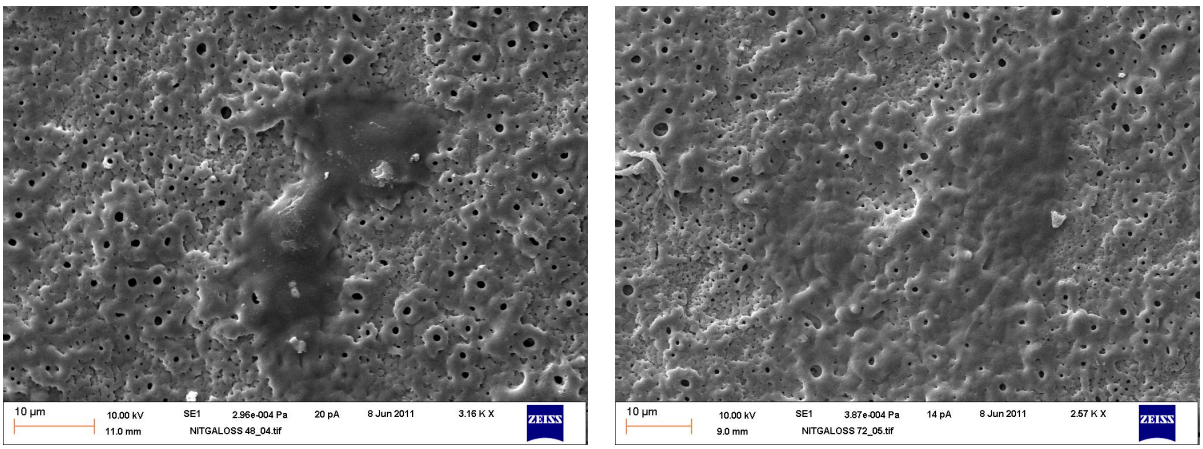

a. **b.**

Fig. 3.42: Saos2 on SUM NITGAL OSS surface at: **a.** 48h of culture; **b.** 72h of culture

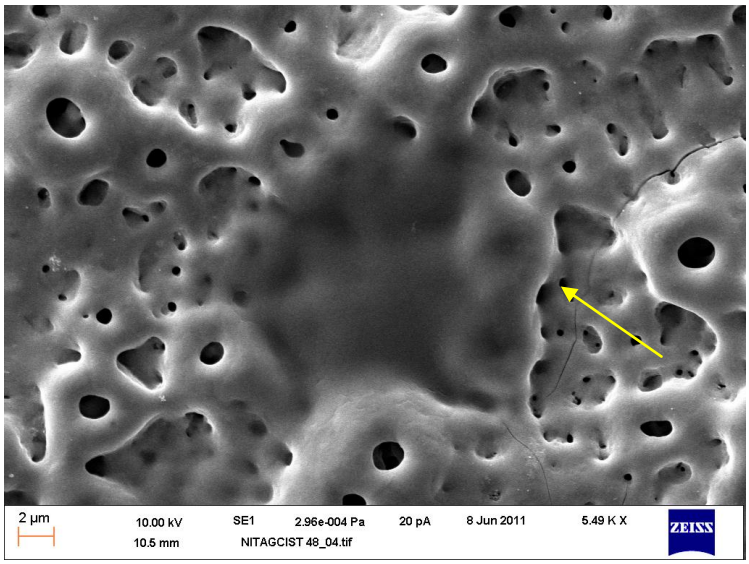

Fig. 3.43: Saos2 adhesion on SUM NITAG CIST surface at 48h of culture.

3.2.2.3 Phalloidin actin filaments staining and DAPI staining

Figures from 3.44 to 3.48 show the Phalloidin staining (red) and DAPI staining (blue) of Saos2 cells on the surface of all the tested samples after 48 hours and 72 hours of cell culture. The DAPI staining shows the nucleus of cells, while the phalloidin provides a detailed profile of their morphology.

On all the surfaces analyzed, the phallodin staining shows that most of the cells acquired the polarised morphology typical of the osteoblasts with an eccentric nucleous leaving large areas of cytoplasms where the cytoskeleton was either organised in oriented actin filaments or in focal points following the contour of the surface doughnut-like structures. Even after 48 hours of culture, the osteoblasts on all the surfaces have a stretched out morphology and, especially on SUM NITAG CIST, SUM NITGAL CIST and SUM NITGAL OSS, begin to protrude into filopodia establishing connection with both the material surface and other cells (white arrows in Fig. 3.46-47-48). In particular, the combined formation of focal points and filopodia was more evident after 72 hours of culture on SUM AgNPs, followed by the SUM NITGAL CIST and by the SUM NTIGAL OSS (white arrows in Fig. 3.45 and 3.47) thus providing a possible link with the various level of cell proliferation observed by HPI tests.

The cytoscheleton edge of several cells adhering on all the surfaces tested followed the underlying substrata and in many cases is so thin that is possible identify the pores profiles (yellow arrows in all the pictures). This behaviour confirms that the porous surface

morphology resulting by ASD treatment offers anchorage sites used by the osteoblasts to adhere more tenaciously on the material surface.

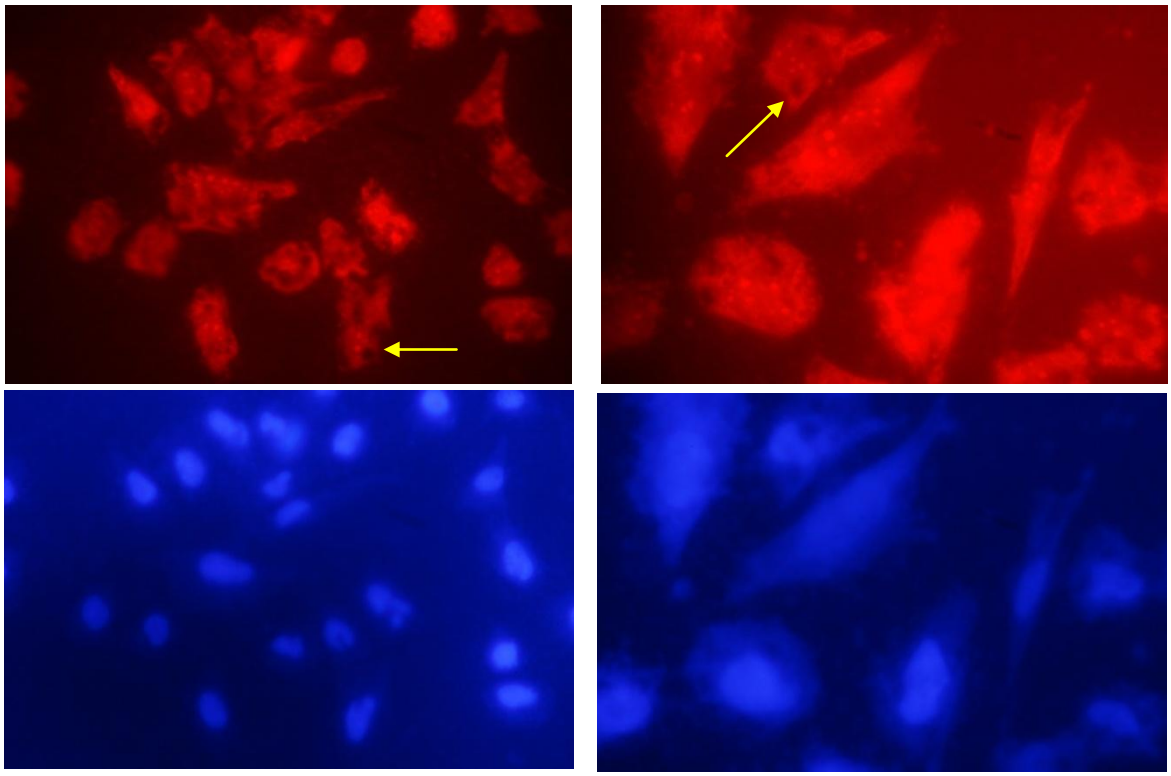

a. **b.**

Fig. 3.44: Phalloidin and DAPI staining of Saos2 on SUM Na surface at: **a.** 48h of culture; **b.** 72h of culture

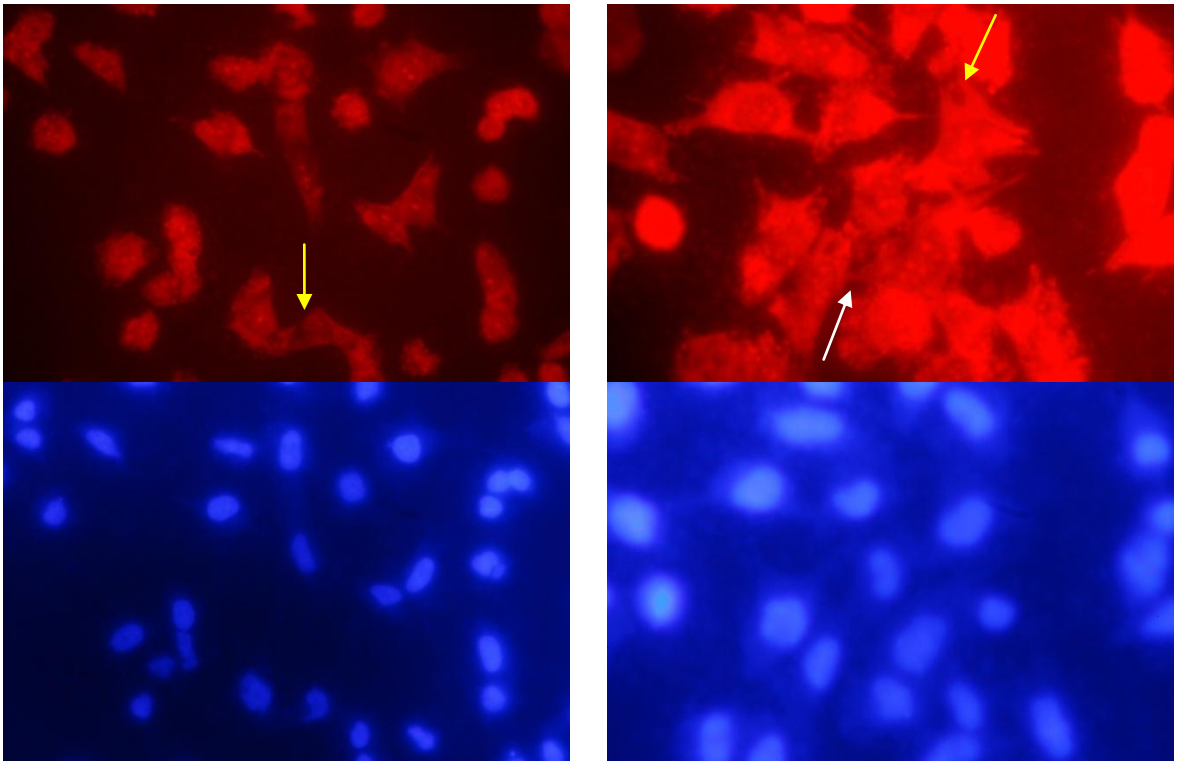

a. **b.**

Fig. 3.45: Phalloidin and DAPI staining of Saos2 on SUM AgNPs surface at: **a.** 48h of culture; **b.** 72h of culture

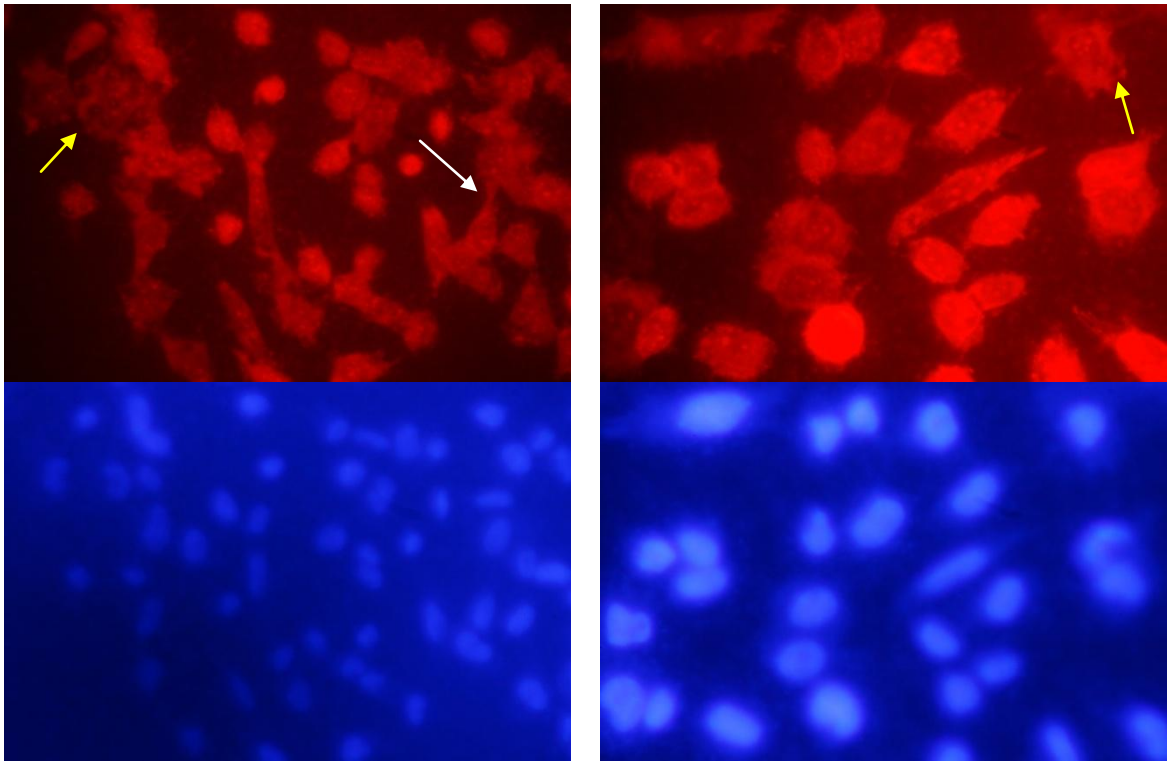

a. **b.**

Fig. 3.46: Phalloidin and DAPI staining of Saos2 on SUM NITAG CIST surface at: **a.** 48h of culture; **b.** 72h of culture.

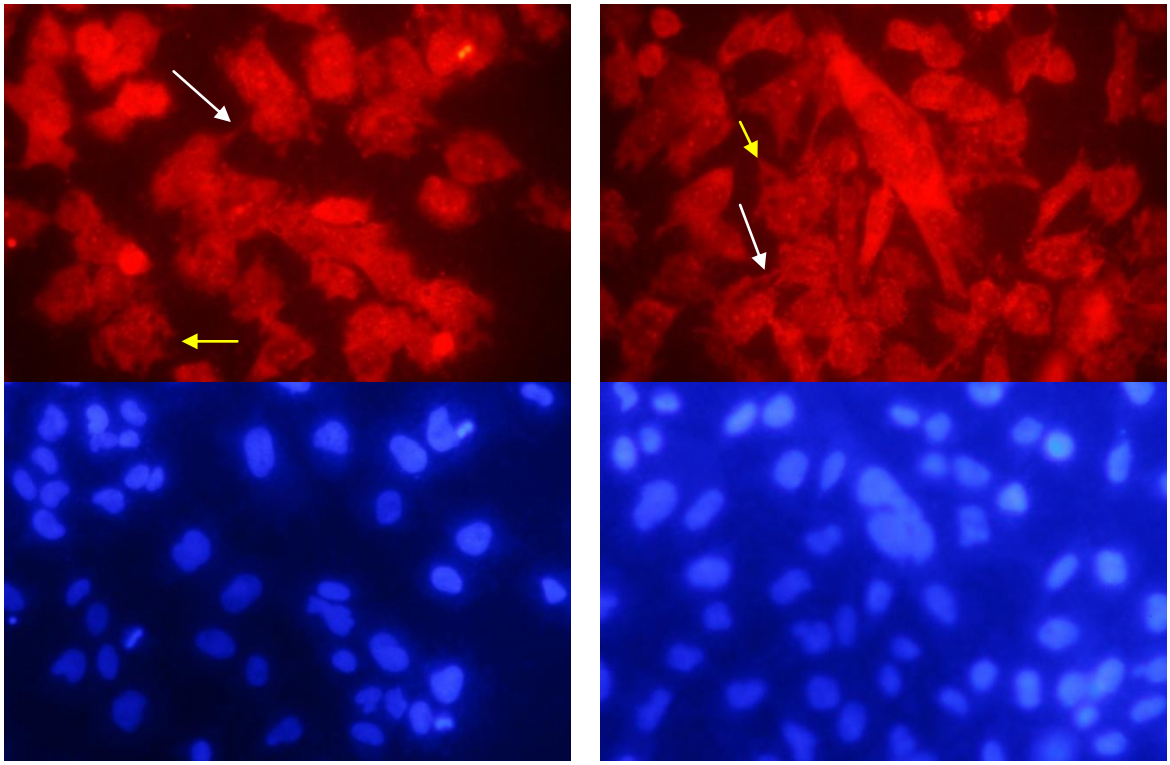

a. **b.**

Fig. 3.47: Phalloidin and DAPI staining of Saos2 on SUM NITGAL CIST surface at: **a.** 48h of culture; **b.** 72h of culture.

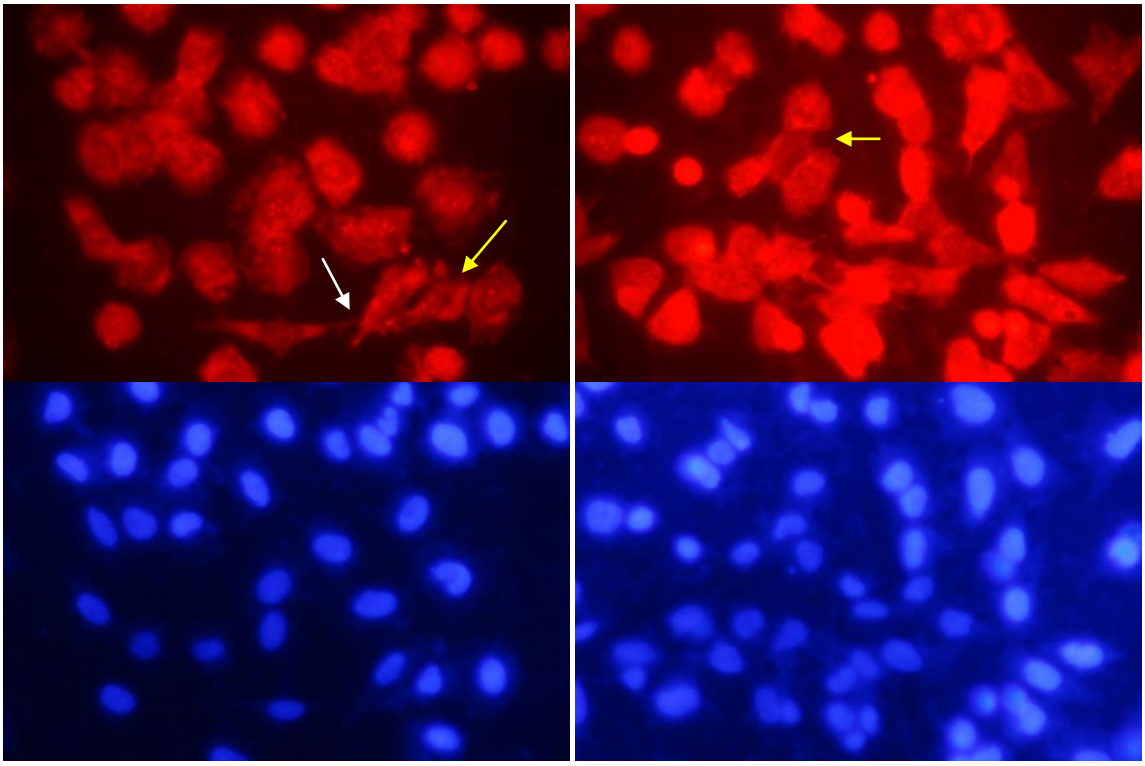

a. **b.**

Fig. 3.48: Phalloidin and DAPI staining of Saos2 on SUM NITGAL OSS surface at: **a.** 48h of culture; **b.** 72h of culture.

4. Discussion

The use of titanium and titanium alloys as first choice biomaterials for the majority of clinical treatments for hard tissues replacement has been expanding in the last few decades because of the unique combination of high mechanical properties, weightlessness, good workability and excellent resistance to corrosion. The clinical performance of titanium implants also depends on their surface characteristics. Untreated titanium is indeed known to have relatively poor properties of cell adhesion that is the first step in the osteointegration process. In applications such as dental implants and orthopaedics prostheses (i.e. hip joint replacement and knee arthroplasty), achieving a better osteointegration allows not only a faster patient's rehabilitation, but also a long-term stable fixation of the biomaterial surface to the surrounding bone thus improving implant longevity. Such an improved clinical outcome is particularly important in joint replacements where an early loading of the device has great significance in terms of decreased patients' morbidity, and of improved patients' psychology and where a long-term stability decreased the incidence of health care costs related to re-hospitalisation, revision surgery and impaired quality of life.

Since the lack of osteointegration is strongly related to loosening and failure of the titanium implants, researchers and companies have developed several surface modification methods (i.e. chemical-elechtrochemical, physical and biological treatments) to respond to the needs of enhanced osteointegrative potential. Among these, the 'biomimetic' treatments confer to the surface functional groups or bio-molecules using biological or chemical and electrochemical treatments with the aim of 'mimicking' the biological characteristics of the bone tissue and, consequently, to promote the cell recognition and to stimulate an effective regeneration process *in vivo*. The Anodic Spark Deposition method (ASD) is one of the most effective techniques to obtain surfaces with biomimetic characteristics since it allows the fine modification of surface morphology, roughness, microporosity, hydrophilicity and at the same time the incorporation of particular chemical agents (i.e. Ca, P, Si, and Na). Indeed, when compared with conventional hydroxyapatite

plasma spray coatings, the ASD allows the intimate bonding of a thin ceramic layer to the oxide gel of the titanium surface. This leads to a significant clinical advantage as the known delamination occurring in the case of the plasma-sprayed hydroxyapatite are ruled out. Furthermore, the fine regulation of the surface physic-chemical properties has clearly shown to enhance cell substrate properties and consequently osteointegration.

Despite these remarkable steps forward in terms of biocompatibility and osteointegrative potential of these kinds of coatings, a risk still remains of loosening and failing of the implant caused by bacterial infection, the so-called septic loosening. In the case of joint replacements, the septic loosening represents the second main cause of failure after aseptic implant loosening [15] and often leads to revision surgery with the prosthesis replacement significantly impacting on the patient's prolonged hospitalisation, health and social costs and impaired quality of life.

The aim of the present study was to confer antibacterial properties to ASD coatings obtained by means of a silicon-based ASD treatment on titanium substratum as patented by the Politecnico di Milano in 2010 [83]. To confer antibacterial properties, the surfaces of materials undergoing ASD were enriched with well-known inorganic antimicrobial agents and, particularly, with silver nanoparticles (SUM AgNPs sample) or silver nitrate or gallium nitrate that were added in the electrolytic solutions used for the treatment. To avoid the precipitation of silver nitrate and gallium nitrate, chelating agents were also added in the electrolytic solutions including L-cysteine (SUM NITAG CIST and SUM NITGA CIST samples) and oxalic acid (SUM NITGAL OSS sample). The surfaces were characterised both physico-chemically and for their biocompatibility properties. The sample labelled SUM Na has been obtained by the patented silicon-based ASD treatment and has been used as a control material.

SEM analyses show that the addition of antimicrobial and chelating agents in the electrolytic solution has an effect on the surface morphology of all the samples. SUM NITGAL OSS shows a morphology completely different in comparison with all the other surfaces suggesting that the presence of oxalic acid in the ASD electrolytic solution has a strong effect on the surface topography. In comparison with SUM Na (material control), SUM AgNPS, SUM NITAG CIST and SUM NITGAL CIST show surface morphologies with different size and structure of pores. Generally, in these surfaces the size of the pores is not uniform and the structures embedding the larger pores are deeper. Hence, the edge of

the larger pores emerges more markedly from the underlying layer thus offering anchorage sites to the osteoblasts. Indeed, analysing the SEM micrographs of the osteoblasts cultures on SUM AgNPS, SUM NITAG CIST and SUM NITGAL CIST surfaces, it is clearly visible that the cells adhere strongly onto the surface by projecting their membranes towards and around the donught-like structures delimiting the pores. The alignment of osteoblasts cytoscheleton on microstructures appears to have an increasing effect on profileration [90].

Like the presence of microstructures, the overall surface topography has an effect on the osteoblasts adhesion. The profilometric tests have showed Ra values for the antimicrobial coatings minor than the material control SUM Na value. However, the Ra values of antimicrobial coatings, especially in samples treated with cysteine, are close to the threshold of roughness (0.5μm) suggested by Wennerberg & Albrektsson as the minimum value required to favour osteoblast adhesion [91].

Several researchers have found that titanium roughness surfaces have a better osteointegration and mechanical stability in comparison with smooth surfaces [92]. Furthermore, surfaces with micro-roughness favours the bone tissue synthesis in the peri-implant region and a faster healing process *in vivo* [93].

The kurtosis values suggest that the presence of gallium nitrate in electrolytic solution has a decreasing effect on k values. Both SUM NITGAL CIST and SUM NITGAL OSS sample have a k value minor than 3μm indicating a bevelled morphology of the profile. Oppositely, the k value of SUM Na, SUM AgNPs and SUM NITAG CIST is higher than 3μm indicating a sharp morphology of the profile. Recent *in vivo* studies show that kurtosis values higher than 3μm positively affect osteoblasts anchorage and bone retention of implants [94].

The surfaces of all the samples tested have water contact angle values lower than untreated titanium grade 2 indicating that the ASD treatment leads to a considerable increase of surface hydrophilicity. The material control SUM Na has a surface markedly hydrophilic indicating that the post-treatment with NaOH has an additional reducing effect on water contact angle. Even if all the antimicrobial surfaces have contact angles higher than the material control SUM Na, they have a remarkable hydrophilic character as well especially in the case of SUM AgNPs sample. Hydrophilic surfaces enhance interactions with biological fluids, cells and tissues [95] and are more resistant to bacterial adhesion [28].

Another important factor enhancing surface performances *in vivo* is the crystallographic form of the titanium oxide. Particularly, the anatase crystallographic form catalyzes the enucleation of hydroxyapatite crystals improving the surface mineralization [96]. The XRD analyses have shown the presence of titanium oxide in the form of anatase on the surfaces of all the samples. The samples anodized in presence of cysteine (SUM NITAG CIST and SUM NITGAL CIST) have a remarkable amount of anatase suggesting a role of cysteine in the formation of crystalline titanium oxide during ASD.

The crystalline oxide layers on all the samples strongly adhere to the substrata since they do not undergo delaminations after a mechanical flexion of 30° (higher than the solicitations in the body environment). These results show that the incorporation of antimicrobial agents and chelants in electrolytic solution used for ASD treatments does not affect the mechanical properties of the resultant oxide layers.

EDS analyses demonstrate that the chemical species present on sample surface are related to the species present in the electrolytic solutions. All the samples except SUM NITGAL OSS have an amount of calcium, phosphorus and silicon on their surfaces comparable with SUM Na. It was widely demonstrated that calcium, phosphorus and silicon favour a direct connection between implant surface and surrounding bone matrix and, furthermore, promote cell activation and the expression of osteogenic phenotype [77,97,98]. The lack of calcium on the surface on SUM NITGAL OSS sample is reasonably due to the great affinity of oxalic acid for calcium. However, SUM NIGAL OSS has a great superficial amount of silicon and phosphorus that could compensate the lack of calcium in terms of cell osteogenic stimulation. EDS analyses also confirm the presence of gallium on both the samples treated with gallium nitrate (SUM NITGAL CIST e OSS) and the presence of silver nanoparticles in SUM AgNPS sample; on SUM NITAG CIST sample the silver is not detected.

In order to demonstrate and compare the presence of antimicrobial agents in the superficial layers of the samples GDOES analyses were performed. Gallium is more abundant on the SUM NITGAL OSS surface than on SUM NITAG CIST surface and in both the samples is contained also in deeper layers of the oxides. Silver is more abundant on the SUM AgNPS surface than on SUM NITAG CIST surface; in both the sample silver is concentrated in the uppermost 20nm of the deposited film. The presence of silver in SUM NITAG CIST sample seems to contradict the EDS analysis. However, it is necessary to highlight that

EDS, contrary to GDOES, is not able to provide an accurate analysis of the very superficial layers, the electron beam usually penetrating the surface of approximately 1 μm in a drop-like shape. The different distribution of gallium and silver in the oxide section may cause different dynamic of release. The silver amount concentrated in the more superficial layers of SUM AgNPS and SUM NITAG CIST might imply a fast and concentrated release whereas the gallium release could be slower but more durable since is present in deeper layers of SUM NITGAL CIST and SUM NITGAL OSS sample.

The ICP analyses on silver-containing samples show that silver is effectively released from the samples surface and that the released amount in PBS at 37 °C is more or less the same at different time points. This behaviour may confirm the previous hypotheses but further studies will be necessary to better define the release profiles. However, the amount of silver present on both the silver-containing surfaces and the amount of release are in the range recognised as sufficient to produce an antibacterial effect [54,99]. However, microbiological tests will be required to confirm the bacteriostatic/bactericidal potential of these novel ASD surfaces. Recent studies have demonstrated the antibacterial potential of gallium [60,100] but currently there is no investigation on its use as an antimicrobial agent when deposited on titanium. Consequently, microbiological tests are also necessary to assess the effect of gallium-enriched coatings on bacteria. In comparison with SUM Na, the SUM AgNPs samples have shown a higher silicon release suggesting a stronger effect on cell activation and differentiation towards osteogenic phenotype. Since the HPI tests both with fibroblasts (3T3) and osteoblasts (Saos2) have demonstrated excellent cell viability upon contact with the silver-containing surfaces (SUM AgNPs and SUM NITAG CIST), the silver presence and release from surfaces is under the cytoxicity detection limit. An excellent viability was also found on the gallium-containing surfaces confirming that the gallium presence and release is also not toxic.

Focusing on Saos2 osteoblasts cell cultures, the proliferation rate after 72 hours is higher on all the antibacterial surfaces in comparison with SUM Na. Particularly, between the silver-containing samples, SUM AgNPs surface has allowed the highest Saos2 proliferation; between the gallium-containing samples, SUM NITGAL CIST shows the higher proliferation rate. SEM images of Saos2 on the antibacterial surface show their tendency to establish anchorage sites with the surfaces protruding features to spread on the surface. Indeed rhodamine-phalloidin staining and SEM clearly show that the osteoblasts

cytoscheletons bind the edge of pores and, especially after 72 hours of culture on SUM AgNPS and SUM NITGAL CIST samples, cell-material and cell-to-cell interactions are established through filopodia and well defined focoal points. The interaction among osteoblasts can also be associated to an increased proliferative behaviour [101]. The proliferative behaviour has direct consequences in terms of osteointegration since it permits a faster colonization of implants and a deposition of a mineralized extracellular matrix with consequent enhancement of implant osteoconduction [102].

5. Conclusions and future work

5.1 Conclusions

The aim of this work was to confer antimicrobial properties to titanium coatings obtained through a silicon-based ASD treatment patented by Politecnico di Milano and characterized by excellent osteointegration potential. To achieve the purpose of producing stable titanium coatings with both osteointegration and antibacterial properties, the electrolytic solution used in the silicon-based ASD treatment was enriched with inorganic antibacterial agents such as silver nanoparticles, silver nitrate and gallium nitrate. In light of the biological characterization, the antibacterial surfaces not only are not toxic but have also showed better osteoblast response in terms of adhesion and proliferation in comparison to the sample obtained by the original silicon-based ASD treatment (SUM Na). The osteointegration potential of coatings carried out by silicon-based treatments was improved especially in the case of SUM AgNPs, SUM NITAG CIST and SUM NITGAL CIST samples. Indeed, the electrolytic solutions modified with antibacterial agents and used in the ASD treatment have modified the resultant morphology and chemical content of the coatings. The physical and morphological characterizations of SUM AgNPs, SUM NITAG CIST and SUM NITGAL CIST have showed a surface morphology with pores larger than the control materials and protruding more sharply from the underlying substrates thus allowing a better osteoblasts adhesion and, consequently, proliferation. The chemical characterization have showed that on SUM AgNPs, SUM NITAG CIST and SUM NITGAL CIST surfaces are present the chemical species typical of the silicon-based ASD treatment (i.e. Ca, P, Si) and, furthermore, the antimicrobial agents (Ag or Ga).

In conclusion, the silicon-based ASD treatment modified with antibacterial agents has allowed the production of titanium coatings characterized by enhanced osteintegrative potential and potential antimicrobial properties. The anti-bacterial silicon-based ASD treatment is industrially-feasible as it is achievable by a one-step process that is completed in a relatively short time. Like the original silicon-based ASD treatment, these characteristics represent an obvious advantage for industrial manufacturing.

5.2 Future work

Microbiological tests performed with the bacterial species more relevant to the septic loosening of dental and orthopaedic implants (e.g. *Staphylococcus Aureus, Stroptococcus mutans, Pseudomonas Aeruginosa*) will be necessary to confirm the antibacterial potential of the coatings developed in this work.

Furthermore, to complete the biological characterization it would be interested evaluate the differentiation factors expressed by osteoblasts (e.g. Collagen I, alkaline phosphatise activity, osteonectin, osteocalcin) *in vitro* and the mineralization potential of the colonised surfaces. The further *in vivo* characterization would allow the evaluation of possible systemic and topical reactions not determinable *in vitro*.

References

[1] MarketsAndMarkets, *Global Biomaterial Market 2009-2014*, 2009.

[2] B.M. Research, "Geographic analysis of biomaterial market," 2009.

[3] "http://www.datamonitor.com/."

[4] "http://www.orthoinfo.aaos.org/."

[5] S. Kurtz, K. Ong, E. Lau, F. Mowat, and M. Halpern, "Projections of Primary and Revision Hip and Knee Arthroplasty in the United States from 2005 to 2030," *The Journal of Bone and Joint Surgery*, 2007, pp. 780-785.

[6] J. Park and R.S. Lakes, *Biomaterials: An introduction*, Springer, 2007.

[7] M. Geetha, A.K. Singh, R. Asokamani, and A.K. Gogia, "Ti based biomaterials, the ultimate choice for orthopaedic implants – A review," *Progress in Materials Science*, vol. 54, 2009, pp. 397-425.

[8] D.F. Williams, "On the nature of biomaterials," *Biomaterials*, vol. 30, Oct. 2009, pp. 5897-909.

[9] R. Pietrabissa, *Biomateriali per protesi e organi artificiali*, Bologna: Pàtron, 1996.

[10] G.A. Borelli, "Reazione biologica e biocompatibilità."

[11] J.M. Anderson, "Biological responses to materials," *Annual Review of Materials Research*, vol. 31, 2001, p. 81–110.

[12] D. a Puleo and A. Nanci, "Understanding and controlling the bone-implant interface," *Biomaterials*, vol. 20, Dec. 1999, pp. 2311-21.

[13] B. Gottenbos, H.J. Busscher, H.C. Van Der Mei, and P. Nieuwenhuis, "Pathogenesis and prevention of biomaterial centered infections," *Journal of materials science. Materials in medicine*, vol. 13, Aug. 2002, pp. 717-22.

[14] B. Costerton, G. Cook, M. Shirtliff, P. Stoodley, and M. Pasmore, "Biofilms, Biomaterials, and Device-Related Infections," *Biomaterials Science: An Introduction to Materials in Medicine*, B.D. Ratner, A.S. Hoffman, F.J. Schoen, and J.E. Lemons, eds., Elsevier Academic Press, 2004, pp. 345-353.

[15] D. Campoccia, L. Montanaro, and C.R. Arciola, “The significance of infection related to orthopedic devices and issues of antibiotic resistance,” *Biomaterials*, vol. 27, Apr. 2006, pp. 2331-9.

[16] E.F. Berbari, A.D. Hanssen, and M.C. Duffy, “Risk Factors for Prosthetic Joint Infection: Case-Control Study,” *Clinical Infection Disease*, vol. 27, 1998, pp. 1247-1254.

[17] C.E. Zobell, “The effect of solid surfaces upon bacterial activity,” *Journal of Bacteriology*, 1943.

[18] M. Katsikogianni and Y.F. Missirlis, “Concise review of mechanisms of bacterial adhesion to biomaterials and of techniques used in estimating bacteria-material interactions,” *European cells & materials*, vol. 8, Dec. 2004, pp. 37-57.

[19] Y.H. An, R.B. Dickinson, and R.J. Doyle, “Mechanisms of Bacterial Adhesion and Pathogenesis of Implant and Tissue Infections,” *Handbook of Bacterial Adhesion: Principles, Methods, and Applications*, Y.H. An and R.J. Friedman, eds., Totowa, NJ, USA: Humana Press Inc., 2000.

[20] K. Hori and S. Matsumoto, “Bacterial adhesion: From mechanism to control,” *Biochemical Engineering Journal*, vol. 48, 2010, pp. 424-434.

[21] E.J.W. Verwey and J.T.D. Overbeek, *Theory of the stability of lyophobic colloids: the interaction of sol particles having an electric double layer*, London: Elsevier Inc., 1948.

[22] B.V. Derjanguin and L.D. Landau, “A theory of the stability of strongly charged lyophobic sols and the coalescence of strongly charged particles in electrolytic solution,” *Acta Physicochimica*, vol. 14, 1941, p. 633.

[23] M. Katsikogianni and Y.F. Missirlis, “Concise review of mechanisms of bacterial adhesion to biomaterials and of techniques used in estimating bacteria-material interactions,” *European cells & materials*, vol. 8, Dec. 2004, pp. 37-57.

[24] F. Ming, W. Whish, J. Hubble, and R. Eisenthal, “Estimation of parameters for cell-surface interactions: maximum binding force and detachment constant,” *Enzyme Microbiological Technolgy*, vol. 22, 1998, pp. 94-99.

[25] C.R. Bunt, D.S. Jones, and I.G. Tucker, “The effects of pH, ionic strength and polyvalent ions on the cell surface hydrophobicity of Escherichia coli evaluated by the BATH and HIC methods,” *International Journal of Pharmacy*, vol. 113, 1995, pp. 257-261.

[26] C. León, S. Ruiz-Santana, J. Rello, and M.V. De la Torre, “Benefits of minocycline and rifampin-impregnated central venous catheters. A prospective, randomized, double-blind, controlled, multicenter trial,” *Intensive Care Medical*, vol. 30, 2004, pp. 1891-9.

[27] C.R. Arciola, D. Campoccia, and L. Montanaro, "Effects of antibiotic resistance of Staphylococcus epidermidis following adhesion to polymethylmethacrylate and to silicone surfaces," *Biomaterials*, vol. 23, 2002, pp. 1945-1502.

[28] Y.H. An and R.J. Friedman, "Concise review of mechanisms of bacterial adhesion to biomaterial surfaces," *Journal of biomedical materials research*, vol. 43, Jan. 1998, pp. 338-48.

[29] N. Satou, J. Satou, H. Shintani, and K. Okuda, "Adherence of streptococci to surface-modified glass," *Journal of General Microbiology*, vol. 134, 1988.

[30] K. Merrit and Y.H. An, "Factors Influencing Bacterial Adhesion," *Handbook of Bacterial Adhesion: Principles, Methods, and Applications*, Y.H. An and R.J. Friedman, eds., Totowa, NJ, USA: Humana Press Inc., 2000.

[31] C.C. Chu and D.F. Williams, "Effects of physical configuration and chemical structure of suture materials on bacterial adhesion," *The American Journal of Surgery*, vol. 147, 1987, pp. 197-204.

[32] A.G. Gristina, C.D. Hobgood, and E. Barth, "Biomaterial specificity, molecular mechanisms, and clinical relevance of S. epidermidis and S. aureus infections in surgery," *Fisher Verlag*, 1987, pp. 143-157.

[33] V.A. Tegoulia and S.L. Cooper, "Staphylococcus aureus adhesion to self-assembled monolayers: effect of surface chemistry and fibrinogen presence," *Colloids and surfaces. B, Biointerfaces*, vol. 24, 2002, pp. 217-228.

[34] M. Kiremitci-Gumustedereliogl u and A. Pesmen, "Microbial adhesion to ionogenic PHEMA, PU and PP implants," *Biomaterials*, vol. 17, 1996, pp. 443-449.

[35] S.D. Puckett, E. Taylor, T. Raimondo, and T.J. Webster, "The relationship between the nanostructure of titanium surfaces and bacterial attachment," *Biomaterials*, vol. 31, 2010, pp. 706-713.

[36] T. Haiying, T. Cao, X. Liang, A. Wang, S.O. Salley, J. McAllister, and K.Y.S. Ng, "Influence of silicone surface roughness and hydrophobicity on adhesion and colonization of Staphylococcus epidermidis," *Journal of Biomedical Research Part A*, vol. 88A, 2008, pp. 454-463.

[37] R.L. Taylor, J. Verran, G.C. Lees, and A.J.P. Ward, "The influence of substratum topography on bacterial adhesion to polymethyl methacrylate," *Journal of materials science. Materials in medicine*, vol. 9, 1998, pp. 17-22.

[38] R.B. Dickinson, J.A. Nagel, R.A. Proctor, and S.L. Cooper, "Quantitative comparison of shear-dependent Staphylococcus aureus adhesion to three polyurethane ionomer analogs with distinct surface properties," *Journal of Biomedical Materials Research*, vol. 36, 1997, pp. 152-162.

[39] J.N. Baumgartner and S.L. Cooper, “Influence of thrombus components in mediating staphylococcus aureus adhesion to polyurethane surfaces,” *Journal of Biomedical Materials Research 1998*, vol. 40, 1998, pp. 660-670.

[40] B.D. Ratner, A.S. Hoffman, F.J. Schoen, and J.E. Lemons, *Biomaterials Science: An Introduction to Materials in Medicine*, Elsevier Academic Press, 2004.

[41] A. Di Martino, M. Sittinger, and M.V. Risbud, “Chitosan: a versatile biopolymer for orthopaedic tissue-engineering,” *Biomaterials*, vol. 26, 2005, pp. 5983-90.

[42] J.D. Bumgardner, R. Wiser, P.D. Gerard, P. Bergin, B. Chestnutt, and M. Marin, “Chitosan: potential use as a bioactive coating for orthopaedic and craniofacial/dental implants,” *Journal of Biomaterial Science Polymer Edition*, vol. 14, 2003, pp. 423-38.

[43] Z. Shi, K.G. Neoh, E.T. Kang, and W. Wang, “Antibacterial and mechanical properties of bone cement impregnated with chitosan nanoparticles,” *Biomaterials*, vol. 27, 2006, pp. 2440-9.

[44] N.M. Milovic, J. Wang, K. Lewis, and A.M. Klibanov, “Immobilized N-alkylated polyethylenimine avidly kills bacteria by rupturing cell membranes with no resistance developed,” *Biotechnology and bioengineering*, vol. 90, 2005, pp. 715-22.

[45] L.G. Harris, S. Tosatti, M. Wieland, M. Textor, and R.G. Richards, “Staphylococcus aureus adhesion to titanium oxide surfaces coated with non-functionalized and peptide-functionalized poly(L-lysine)-grafted-poly(ethylene glycol) copolymers,” *Biomaterials*, vol. 25, 2004, pp. 4135-48.

[46] B. Del Curto, M.F. Brunella, C. Giordano, P. M.P., V. Valtulina, and L. Visai, “Decreased bacterial adhesion to surface-treated titanium,” *International Journal of Artificial Organs*, vol. 28, 2005, pp. 718-30.

[47] M.E. Rupp, S.J. Lisco, P.A. Lipsett, and T.M. Perl, “Effect of a Second-Generation Venous Catheter Impregnated with Chloroexidine and Silver Sulphadiazine on Central Catheter-Related Infections,” *Annals of Internal Medicine*, vol. 143, 2005, pp. 570-580.

[48] L. Zhao, P.K. Chu, Y. Zhang, and Z. Wu, “Antibacterial coatings on titanium implants,” *Journal of biomedical materials research. Part B, Applied biomaterials*, vol. 91, Oct. 2009, pp. 470-80.

[49] A.B.G. Lansdown, “Silver in health care: antimicrobial effects and safety in use,” *Biofunctional textiles and the skin*, vol. 33, 2006, p. 17–34.

[50] M. Rai, A. Yadav, and A. Gade, “Silver nanoparticles as a new generation of antimicrobials,” *Biotechnology advances*, vol. 27, 2009, pp. 76-83.

[51] Y. Matsumura, K. Yoshikata, S.-ichi Kunisaki, and E. Tsuchido, “Mode of Bactericidal Action of Silver Zeolite and Its Comparison with That of Silver Nitrate,” *Applied and Environmental Microbiology*, vol. 69, 2003, pp. 4278-81.

[52] Q.L. Feng, J. Wu, G.Q. Chen, F.Z. Cui, T.N. Kim, and J.O. Kim, “A mechanistic study of the antibacterial effect of silver ions on Escherichia coli and Staphylococcus aureus,” *Journal of biomedical materials research*, vol. 52, Dec. 2000, pp. 662-8.

[53] D.J. Balazs, K. Triandafillu, P. Wood, and Y. Chevolot, “Inhibition of bacterial adhesion on PVC endotracheal tubes by RF-oxygen glow discharge, sodium hydroxide and silver nitrate treatments,” *Biomaterials*, vol. 25, 2004, pp. 2139-2151.

[54] W.-H. Song, H.S. Ryu, and S.-H. Hong, “Antibacterial properties of Ag (or Pt)-containing calcium phosphate coatings formed by micro-arc oxidation,” *Journal of biomedical materials research. Part A*, vol. 88, Jan. 2009, pp. 246-54.

[55] C.-N. Lok, C.-M. Ho, R. Chen, Q.-Y. He, W.-Y. Yu, H. Sun, P.K.-H. Tam, J.-F. Chiu, and C.-M. Che, “Silver nanoparticles: partial oxidation and antibacterial activities,” *Journal of biological inorganic chemistry : JBIC : a publication of the Society of Biological Inorganic Chemistry*, vol. 12, May. 2007, pp. 527-34.

[56] L. Juan, Z. Zhimin, M. Anchun, L. Lei, and Z. Jingchao, “Deposition of silver nanoparticles on titanium surface for antibacterial effect,” *International journal of nanomedicine*, vol. 5, Jan. 2010, pp. 261-7.

[57] H.H.L.N.V. Ayala-nu, C. Ixtepan, and C. Rodrı, “Bactericidal effect of silver nanoparticles against multidrug-resistant bacteria,” *Journal of Microbiology*, 2010, pp. 615-621.

[58] A.B.G. Lansdown, “A pharmacological and toxicological profile of silver as an antimicrobial agent in medical devices,” *Advances in pharmacological sciences*, vol. 2010, Jan. 2010, p. 910686.

[59] O. Olakanmi, B.E. Britigan, and L.S. Schlesinger, “Gallium disrupts iron metabolism of mycobacteria residing within human macrophages,” *Infection and immunity*, vol. 68, Oct. 2000, pp. 5619-27.

[60] Y. Kaneko, M. Thoendel, O. Olakanmi, B.E. Britigan, and P.K. Singh, “The transition metal gallium disrupts Pseudomonas aeruginosa iron metabolism and has antimicrobial and antibiofilm activity,” *The Journal of Clinical Investigation*, vol. 117, 2007, pp. 877-888.

[61] L.R. Bernstein, “Mechanisms of therapeutic activity for gallium,” *Pharmacological reviews*, vol. 50, Dec. 1998, pp. 665-82.

[62] N.L. Eigler, M.J. Khorsandi, J.F. Forrester, M.C. Fishbein, and F. Litvack, "Implantation and recovery of temporary metallic stents in canine coronary," *Journal of the American College of Cardiology*, vol. 22, 1993, pp. 1207-1213.

[63] A.F. Mavrogenis, R. Dimitriou, J. Parvizi, and G.C. Babis, "Biology of implant osseointegration," *Muscoloskelet Neuronal Interact*, vol. 9, 2009, pp. 61-71.

[64] J. Lausmaa, L. Mattson, U. Rolander, and B. Kasemo, "Chemical composition and morphology of titanium surface oxides," *Materials Research Society Symposium Proceedings*, vol. 55, 1986, pp. 351-359.

[65] M.J. Donachie, *Titanium: a technical guide*, ASM International, 2000.

[66] "http://www.astm.org/."

[67] R. Chiesa, "Handouts of the course Biomateriali," 2008.

[68] S.G. Steinemann, "Titanium-the material of choice?," *Periodontology*, vol. 17, 1998, pp. 7-21.

[69] G.C.F. Clark and D.F. William, "The effects of proteins on metallic corrosion," *Journal of Biomedical Materials Research*, vol. 16, 1998, pp. 125-134.

[70] T. Hanawa, "In vivo metallic biomaterials and surface modification," *Materials Science and Engineering A*, vol. 267, Jul. 1999, pp. 260-266.

[71] X. Liu, "Surface modification of titanium, titanium alloys, and related materials for biomedical applications," *Materials Science and Engineering: R: Reports*, vol. 47, Dec. 2004, pp. 49-121.

[72] C.L. Tisel, V.M. Goldberg, and J.A. Parr, "The influence of hydroxyapatite and tricalcium phosphate coating on bone growth into titanium fiber-metal implants," *Journal of Bone Joint Surgery*, vol. 76, 1994, pp. 139-171.

[73] K. De Groot, R. Geesink, C.P. Klein, and P. Serekian, "Plasma sprayed coating of hydroxilapatite," *Journal of Biomedical Materials Research*, vol. 21, 1987, pp. 1375-1381.

[74] R. Chiesa, E. Sandrini, M. Santin, G. Rondelli, and A. Cigada, "Osteointegration of titanium and its alloys by anodic spark deposition and other electrochemical techniques : A review," *Journal of Applied Biomaterials & Biomechanics*, vol. 1, 2003, pp. 91-107.

[75] J. Redepenning and J.P. McIsaac, "Electrocrystallization of Brushite Coatings on Prosthetic Alloys," *Chemistry of Materials*, vol. 2, 1990, pp. 625-627.

[76] T. Kokubo, F. Miyaji, and H.M. Kim, “Spontaneus formation of bonelike apatite layer on chemically treated titanium metals,” *Journal of American Ceramic Society*, vol. 79, 1996, pp. 1127-1129.

[77] E. Sandrini, C. Morris, R. Chiesa, A. Cigada, and M. Santin, “In vitro assessment of the osteointegrative potential of a novel multiphase anodic spark deposition coating for orthopaedic and dental implants,” *Journal of biomedical materials research. Part B, Applied biomaterials*, vol. 73, May. 2005, pp. 392-9.

[78] T. Bao Van, S.D. Brown, and G.P. Wirtz, “Mechanism of anodic spark deposition,” *Ceramic Bulletin*, vol. 56, 1977.

[79] R. Winand and J.L. Delplancke, “Galvanostatic Anodization of Titanium - Structures and Compositions of the Anodic Film,” *Electrochimica Acta*, vol. 33, 1988, pp. 1539-1549.

[80] X. Lu, B. Zhang, Y. Wang, X. Zhou, J. Weng, S. Qu, B. Feng, F. Watari, Y. Ding, and Y. Leng, “Nano-Ag-loaded hydroxyapatite coatings on titanium surfaces by electrochemical deposition,” *Journal of the Royal Society, Interface / the Royal Society*, vol. 8, Apr. 2011, pp. 529-39.

[81] X. Zhu, K.H. Kim, J.L. Ong, and S. Kim, “Surface characteristics and structure of anodic oxide films containing Ca e P on a titanium implant material,” *Journal of Biomedical Materials Research*, vol. 60, 2002, pp. 333-338.

[82] H. Ishizawa and M. Ogino, “Formation and characterization of anodic titanium oxide films containing Ca e O,” *Journal of Biomedical Materials Research*, vol. 29, 1995, pp. 65-72.

[83] R. Chiesa, A. Cigada, C. Della Valle, G. Rondelli, G. Candiani, and C. Giordano, “Silicon-based biomimetic treatment for the osteointegration of metal substrates,” *WO/2010/013120*, 2010.

[84] C. Della Valle, “Sviluppo di Trattamenti Biomimetici a base di Silicio per l osteointegrazione del Titanio,” Politecnico di Milano Thesis, 2007.

[85] X.X. Wang, S. Hayakawa, K. Tsuru, and A. Osaka, “Improvement of bioactivity of H2O2/TaCl5 treated titanium after subsequent heat treatment,” *Journal of biomedical materials research*, vol. 52, 2000, pp. 171-176.

[86] J. Goldstein, D. Newbury, D. Joy, C. Lyman, P. Echlin, and E. Lifshin, *Scanning Electron Microscopy and X-Ray Microanalysis*, Springer, 2003.

[87] H.Y. Marghalani, “Effect of filler particles on surface roughness of experimental composite series,” *Journal of applied oral science : revista FOB*, vol. 18, 2010, pp. 59-67.

[88] J. Voros, M. Wieland, L. Ruiz-Taylor, M. Textor, and D.M. Brunette, "Characterization of Titanium Surfaces," *Titanium in Medicine*, D.M. Brunette, P. Tengvall, M. Textor, and P. Thomsen, eds., Springer, 2001.

[89] A. Sliepcevich, "Spettrometria ottica di emissione al plasma," *http://www.chem.polimi.it/lac/spettro_plasma.php*.

[90] J. Qu, B. Chehroudi, and D.M. Brunette, "The use of micromachined surfaces to investigate the cell behavioral factors essential to osseintegration," *Oral Desease*, vol. 2, 1996, pp. 102-115.

[91] A. Wennerberg and T. Albrektsson, "Effects of titanium surface topography on bone integration : a systematic review," *Clinical Oral Implant Research*, vol. 20, 2009, pp. 172-184.

[92] I. Degasne, M.F. Basle□ , G. Hure□ , M. Lesourd, and B. Grolleau, "Effects of roughness, fibronectin and vitronectin on attachment, spreading, and proliferation of human osteoblast-like cells (Saos-2) on titanium surfaces," *Calcified Tissue International*, vol. 64, 1999, pp. 449-507.

[93] J.W. Park, I.S. Janng, and J.Y. Suh, "Bone response to endosseouns titanium implants surface modified by blasting and chemical treatment: A histomorphometric study in rabbit femur," *Journal of Biomedical Materials Research*, vol. 84B, 2007, pp. 400-407.

[94] S. Lamolle, M. Monjo, P. Lyngstadaas, J. Ellingsen, and H. Haugen, "Titanium implant surface modification by cathodic reduction in hydrofluoric acid: Surface characterization and in vivo performance," *Journal of Biomedical Materials Research Part A*, vol. 88A, 2009, pp. 581-588.

[95] G. Zhao, Z. Schwartz, M. Wieland, F. Rupp, J. Geis-Gerstorfer, and D.L. Cochran, "High surface energy enhances cell response to titanium substrate microstructure," *Journal of Biomedical Materials Research*, vol. 74, 2005, pp. 49-58.

[96] X.X. Wang, S. Hayakawa, K. Tsuru, and A. Osaka, "Improvement of bioactivity of H2O2/TaCl5 treated titanium after subsequent heat treatment," *Journal of Biomedical Materials Research*, vol. 52, 2000, pp. 171-176.

[97] X. Zhu, K.H. Kim, and Y. Jeong, "Anodic oxide film containing Ca and P of titanium biomaterial," *Biomaterials*, vol. 22, 2001, pp. 2199-2206.

[98] K.A. Hing, P. Revell, N. Smith, and T. Buckland, "Effect of silicon level on rate,quality and progression of bone healing within silicate-substituted porous hydroxyapatite scaffolds," *Biomaterials 2006*, vol. 27, 2006, pp. 5014-5026.

[99] B.S. Necula, L.E. Fratila-Apachitei, S. a J. Zaat, I. Apachitei, and J. Duszczyk, "In vitro antibacterial activity of porous TiO2-Ag composite layers against methicillin-

resistant Staphylococcus aureus," *Acta biomaterialia*, vol. 5, Nov. 2009, pp. 3573-80.

[100] S.P. Valappil, D. Ready, E. a Abou Neel, D.M. Pickup, L. a O□ Dell, W. Chrzanowski, J. Pratten, R.J. Newport, M.E. Smith, M. Wilson, and J.C. Knowles, "Controlled delivery of antimicrobial gallium ions from phosphate-based glasses," *Acta biomaterialia*, vol. 5, May. 2009, pp. 1198-210.

[101] W. Singhatanadgit, "Biological Responses to New Advanced Surface Modifications of Endosseous Medical Implants," *Bone and Tissue Regeneration Insights*, vol. 2, 2009, pp. 1-11.

[102] L.F. Cooper, "Biologic determinants of bone formation for osseointegration: clues for future clinical improvements," *The Journal of prosthetic dentistry*, vol. 80, Oct. 1998, pp. 439-49.